1-Dimensional Nanostructures

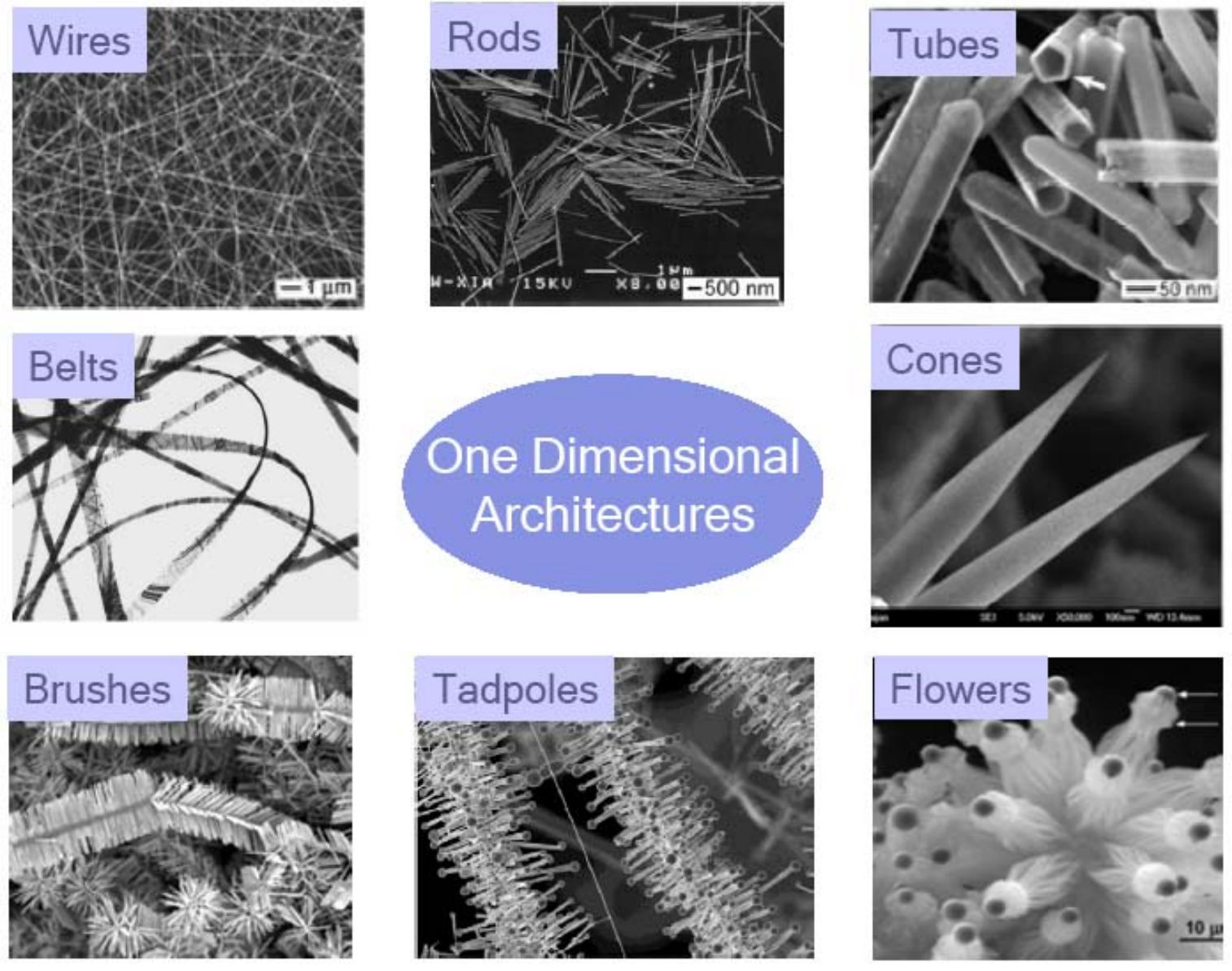

1-Dimensional Nanostructures

Aspect ratio (AR) = the ratio of length to diameter
Cross section
Internal twin structure
Straight, wavy (worm-like), branched (dendritic)
Solid or hollow
Monocomponent, bicomponent, multicomponent
Homogeneously mixed, spatially segregated
Monocrystalline, twinned (1 or 5 twin planes), polycrystalline

Nanorod (NR)

(AR < 30)

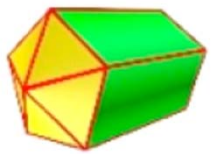

No widely accepted cutoff

Nanowire (NW)

(AR > 100)

1-Dimensional Nanostructures

Core−Satellite
Core−Sheath
Hollow
Branched (dendritic)

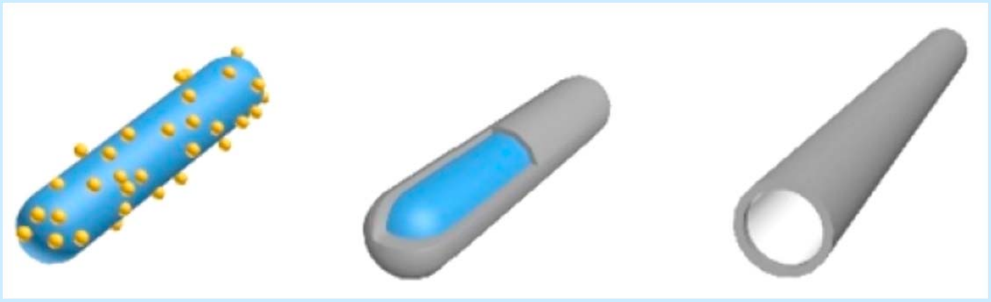

Dimension-Properties Interplay

Carbon allotropes

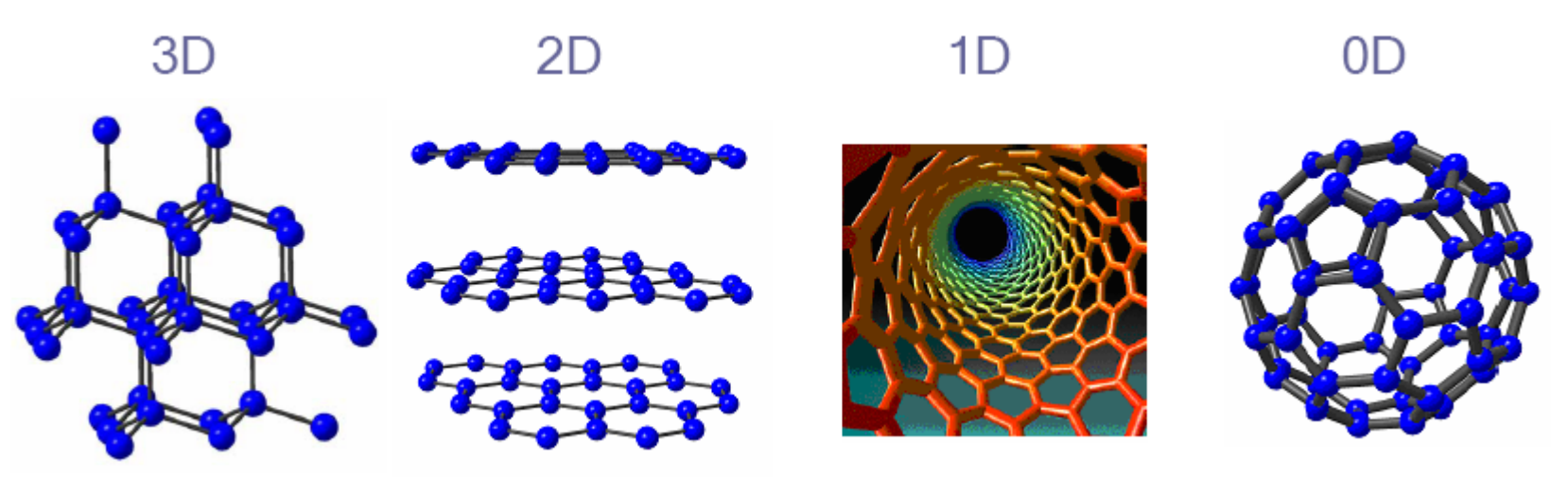

Brilliant, Transparent	Metallic lusture, Opaque	Black, Fibrous	Black Shiny Crystals
Mohs Hardness 10	1-2	1-1.2	-
20 W/cmK	25	6000	-
High Melting point	Lubricant	Unusual Electrical Behaviour	Superconductor (10-40 K)

Role of Dimensionality

Dimensionality influences electronic structure
From continuous bands to discrete energy levels
Changes in electrical, optical, magnetic,….properties

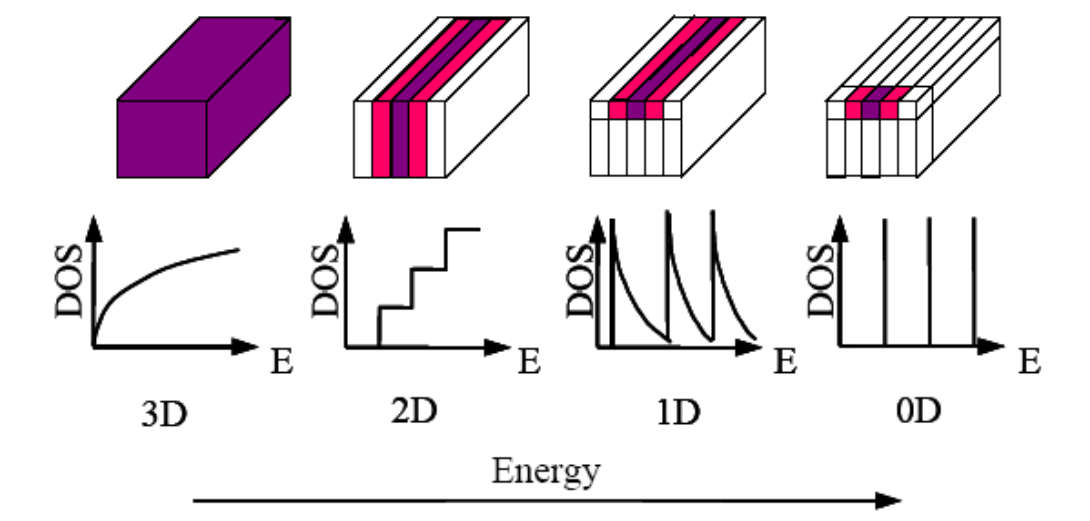

3 D: $E = \frac{\hbar^2}{2m}\left[k_x^{\,2} + k_y^{\,2} + k_z^{\,2}\right]$

2 D: $E = \frac{\hbar^2}{2m}\left[k_x^{\,2} + k_y^{\,2} + \left(n_z \frac{\pi}{L}\right)^2\right]$ $\quad n_z = 1,2,3\ldots$

1 D: $E = \frac{\hbar^2}{2m}\left[k_x^{\,2} + \left(n_y \frac{\pi}{L}\right)^2 + \left(n_z \frac{\pi}{L}\right)^2\right]$ $\quad n_y, n_z = 1,2,3\ldots$

0 D: $E = \frac{\hbar^2}{2m}\left[\left(n_x \frac{\pi}{L}\right)^2 + \left(n_y \frac{\pi}{L}\right)^2 + \left(n_z \frac{\pi}{L}\right)^2\right]$ $\quad n_x, n_y, n_z = 1,2,3\ldots$

1D Nanostructures

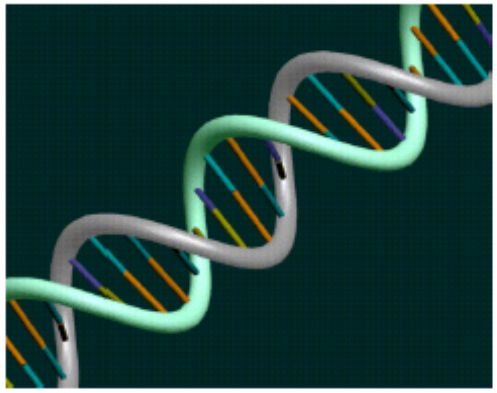

DNA

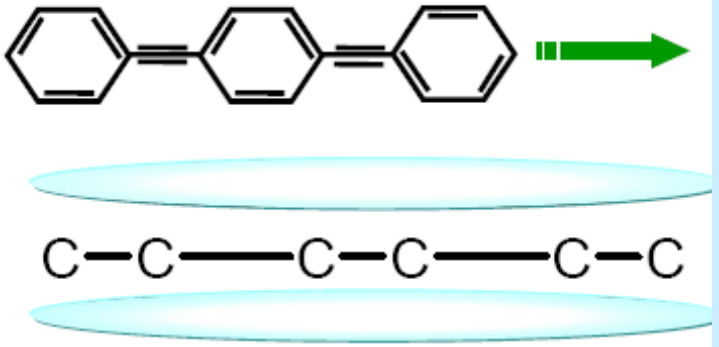

Molecular Wire

The Nano World

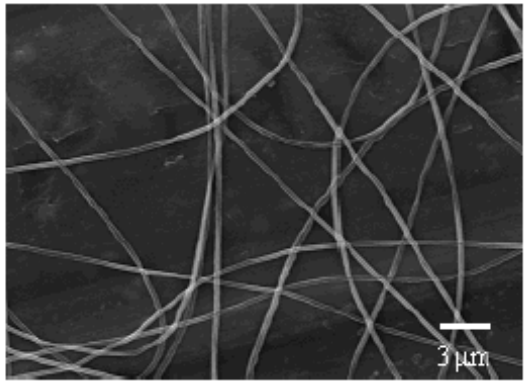

Poly (ethylene oxide)

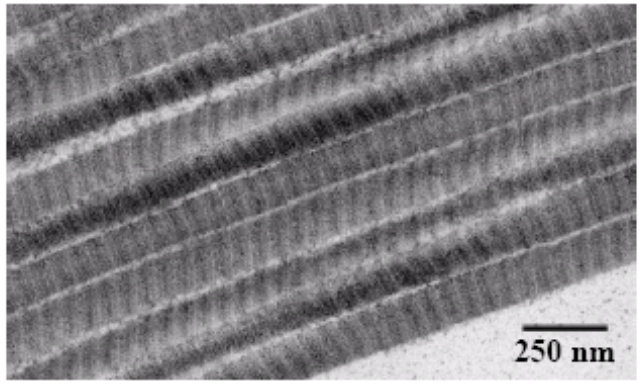

Collagen Fibrils

Potential Applications of Nanowires

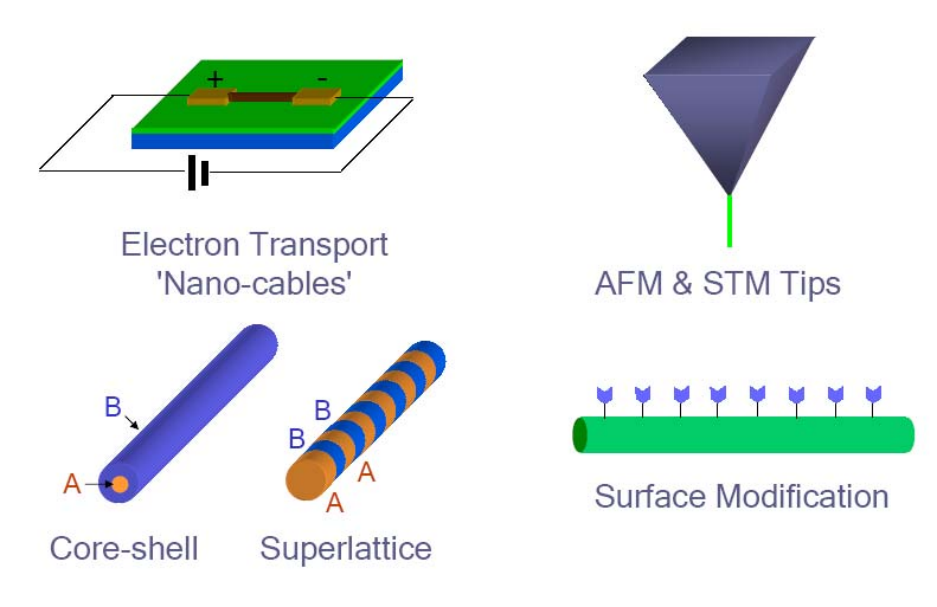

Interconnects
Novel probes
Multifunctional
Hierarchical alignment
Building blocks for devices

Quantum Confinement Effect

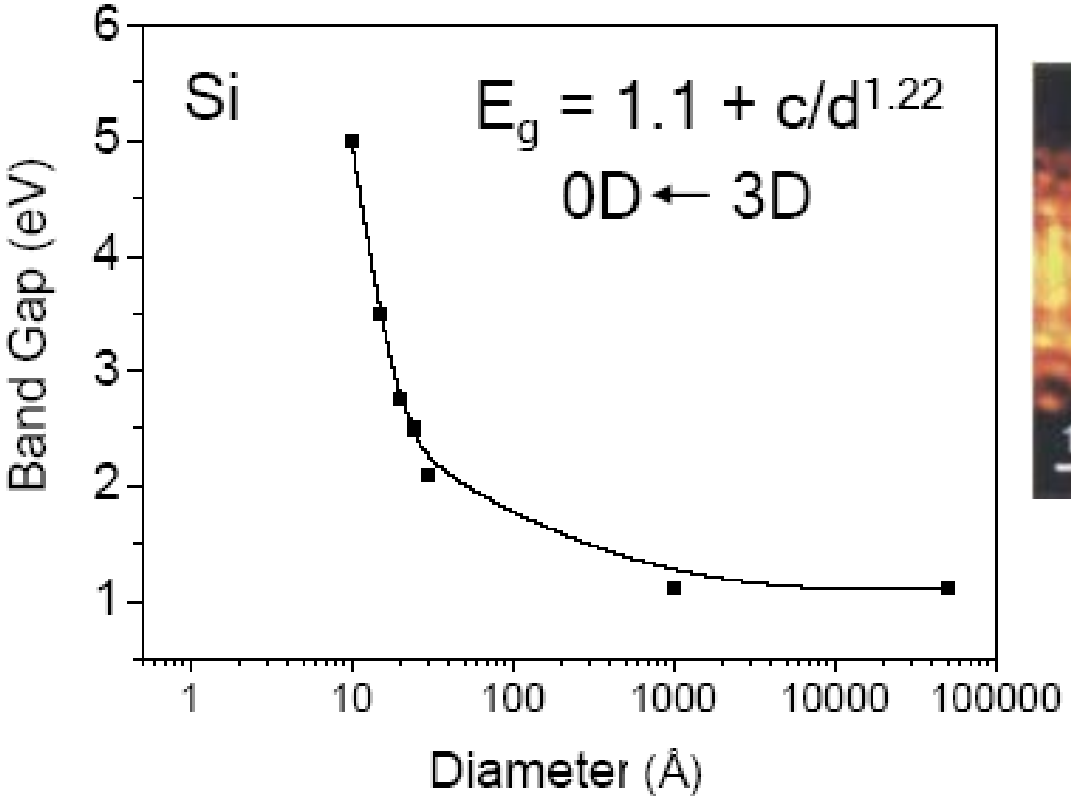

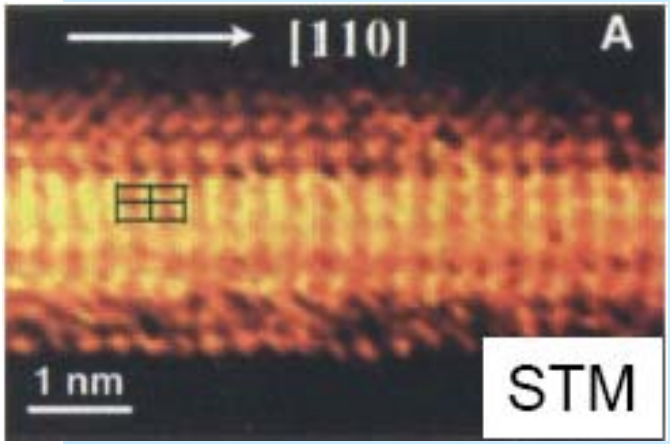

The band gap increases with decreasing diameter (quantum confinement)

Mechanical Properties

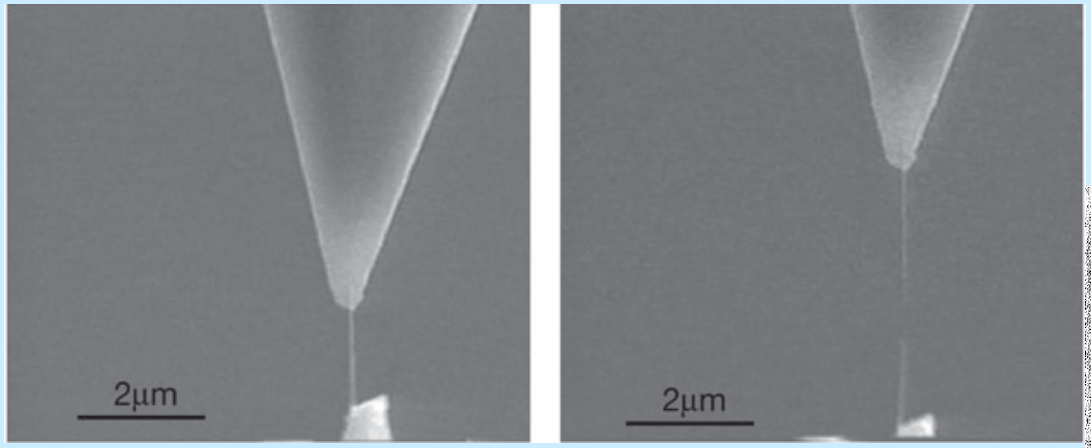

WS_2 nanotube during a tensile test before (left) and after (right) failure

WS_2 nanotube

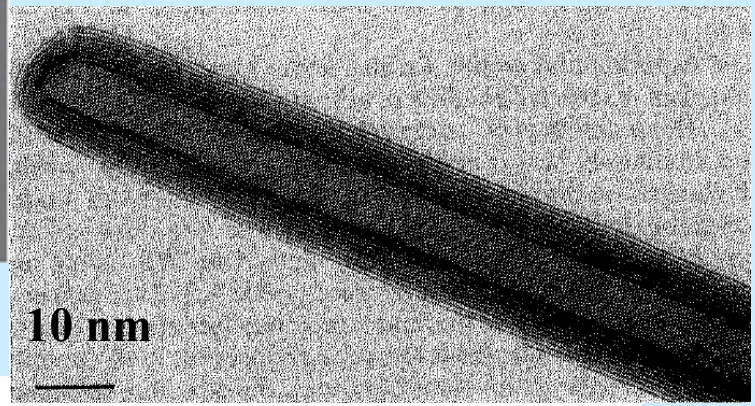

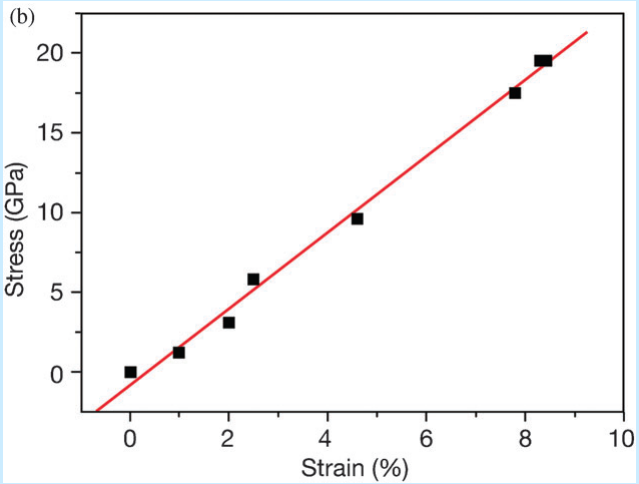

Strain–stress curve of a nanotube

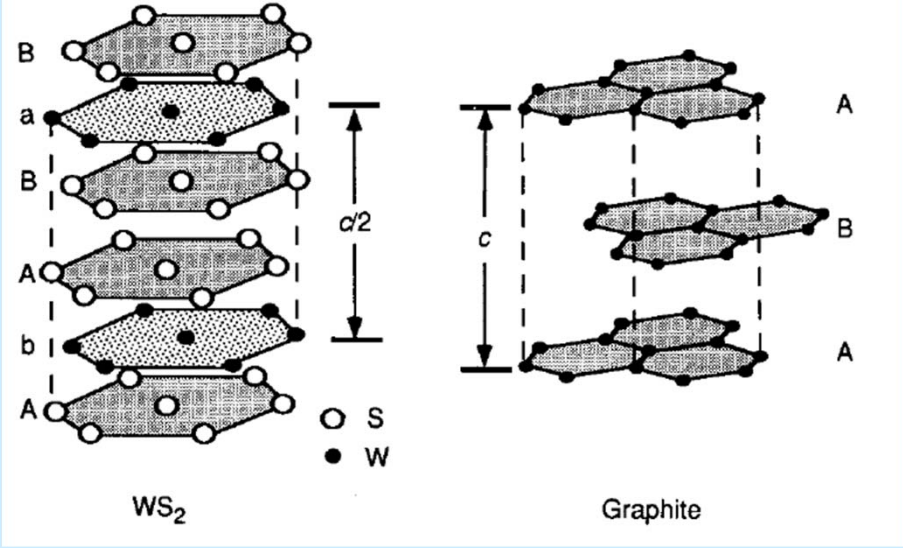

Carbon Nanotubes

- (Re)discovered by Iijima (1991, NEC)
- 1952 Russians (CO + Fe hot, SEM)
- Rolled up sheet of graphene
- Capped at the ends with half a fullerene

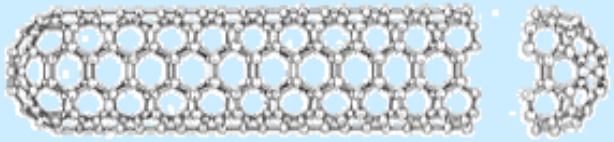

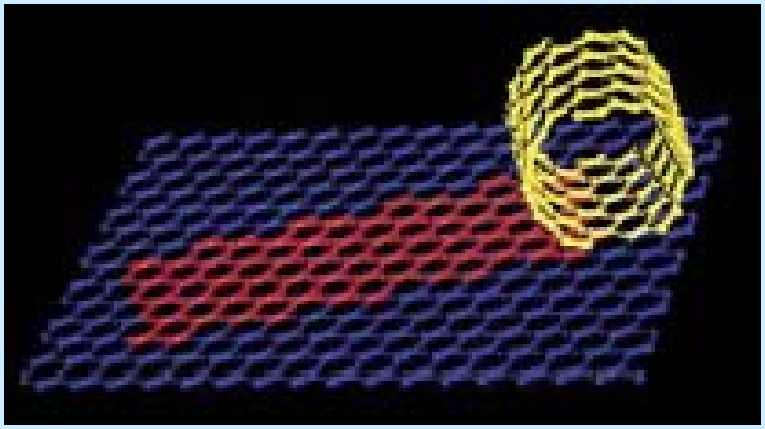

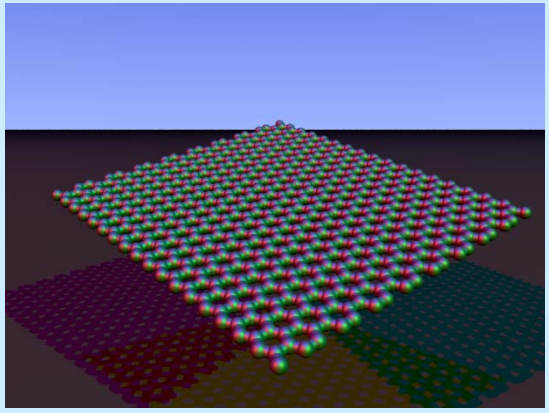

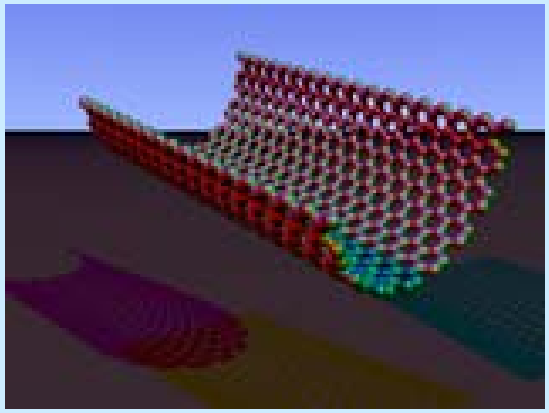

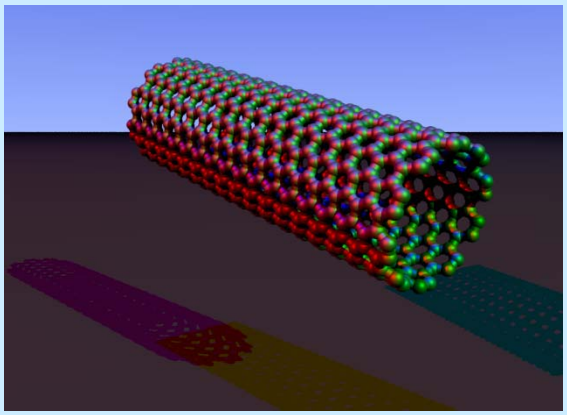

Carbon Nanotubes

Bulk graphite - molecular slabs (graphene) stacked together via weak van der Waals interactions

The rim atoms of graphite (sp^2) are only two-fold bonded - a dangling bond pointing outward, but the number of surface atoms is outnumbered by the three-fold-bonded “bulk” atoms

The relative chemical energy stored by the rim atoms is negligibly small

Flat graphite nanoclusters cannot tolerate the **large chemical energy** stored in **the dangling bonds** of the rim atoms of a small graphene sheet:

- rolling to nanotubes
- curling to fullerenes

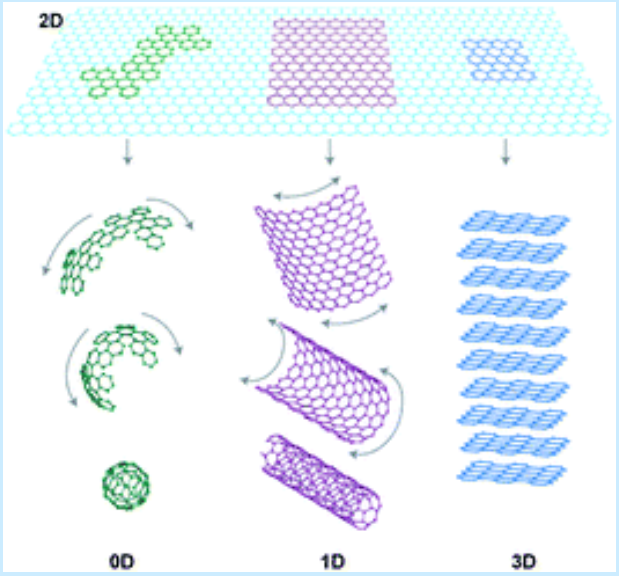

Carbon Nanotubes

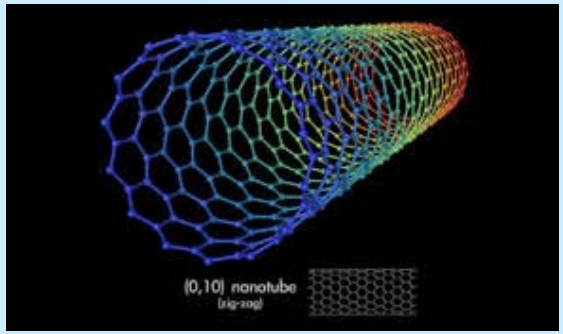

Single Walled Nanotubes (SWNT)

- Single atomic layer wall
- Diameter of 0.7 – 5 nm
- Length several microns to centimeters

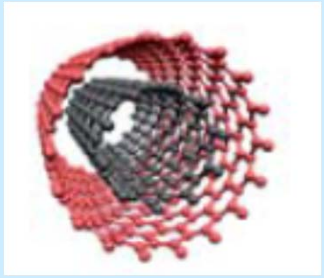

Double Walled Nanotubes (DWNT)

- exactly two concentric CNT
- the outer wall selectively functionalized while maintaining an intact inner-tube

Multi Walled Nanotubes (MWNT)

- Concentric tubes ca. 50 in number, separation 0.34 nm
- Inner diameters : 1.5 – 15 nm
- Outer diameters : 2.5 – 150 nm

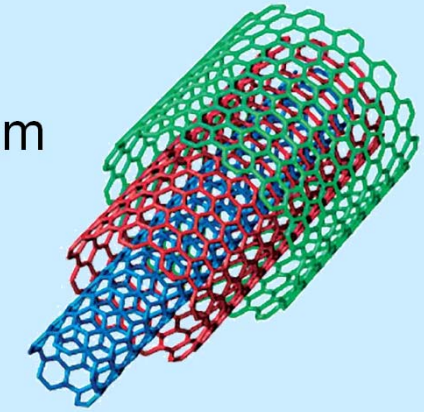

Lengths: micrometers to centimeters
Aspect Ratio: up to 10^7

SWCNT Diameter from Raman Spectroscopy

- **RBM** (Radial Breathing Mode): 100 to 300 cm^{-1}, vibration at which the nanotube diameter contracts and expands
- D-band: vicinity of 1350 cm^{-1}, defect-derived peak
- G-band: vicinity of 1550 -1605 cm^{-1}, in-plane vibration of graphite
- G'-band: 2700 cm^{-1}, overtone of D-band

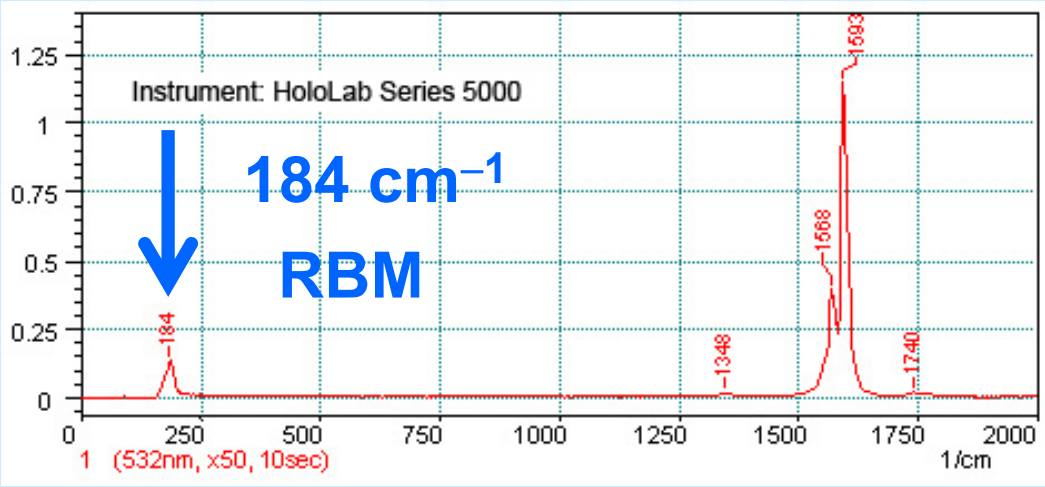

The wavenumber of RBM is inversely proportional to the tube diameter D

$D\ (nm) = 248/\omega$ = 248/184 = 1.3 (nm)

Raman Spectroscopy

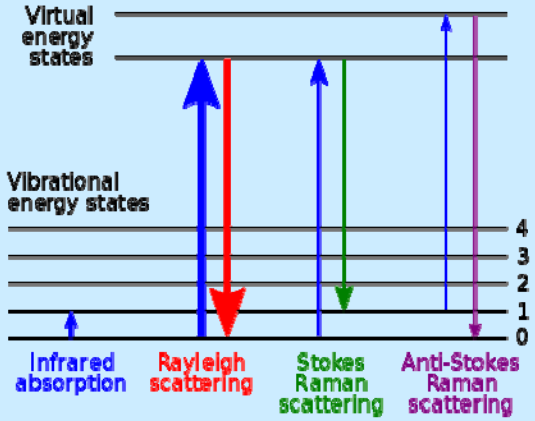

Raman scattering is an extremely weak process - only one in every 10^6 - 10^8 photons scatters

Raman effect

- interaction between the electron cloud of a molecule and the external electrical field of the monochromatic light
- a change in **polarizability** with respect to the vibrational coordinate

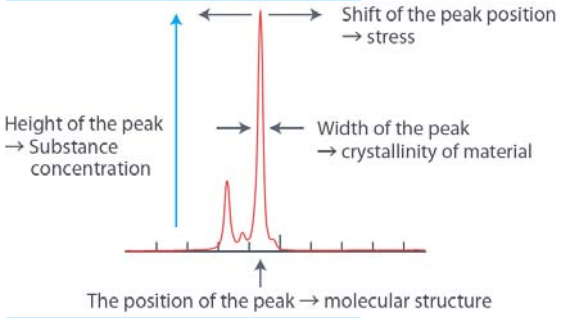

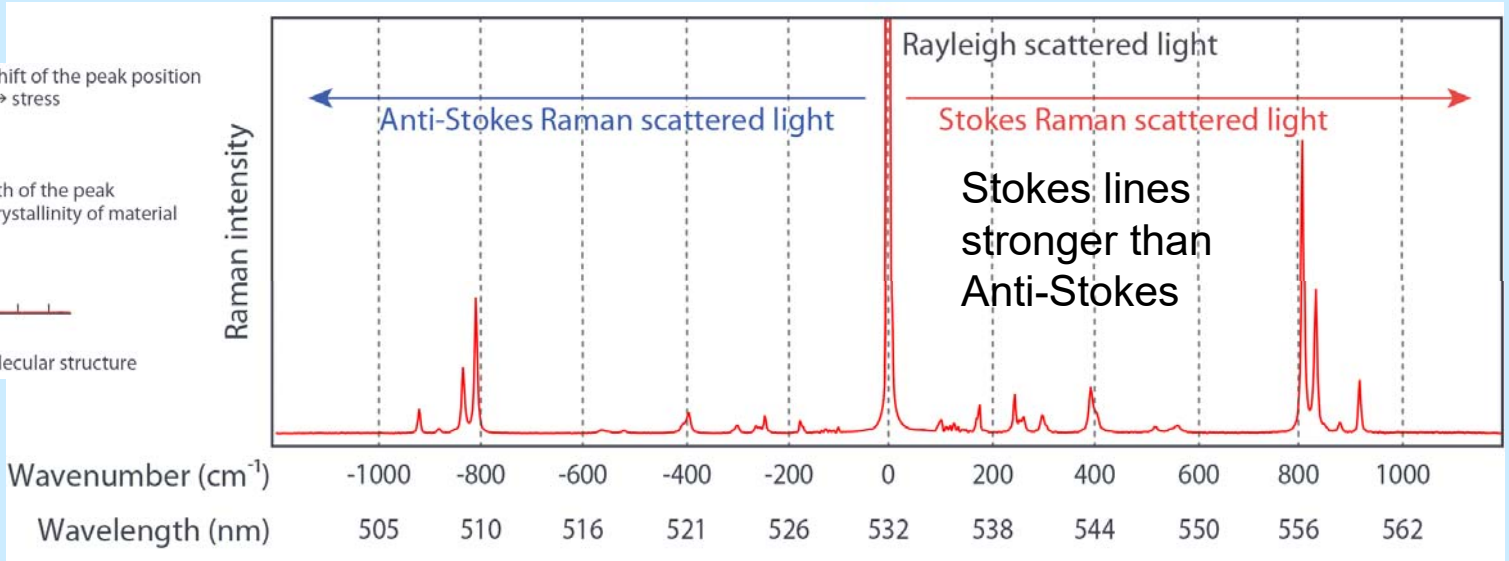

CNTs: Properties and Potential

Electronic: Bandgap $E_g \sim 1/d$
Ballistic conductivity in metallic CNTs,
the highest current density 10^9 A/cm^2 (Cu only 10^6 A/cm^2)
SWNT – metallic or semiconducting, MWCNT - metallic

Magnetic: Anisotropic magn. susceptibility $\chi\perp >> \chi||$

Mechanical: Young's Modulus
1.8 –4.5 TPa (SWNT, axial), 0.95 TPa (MWNT) (Steel: 230 GPa)
tensile strength above 100 GPa (steel: 1–2 GPa) the highest known

Thermal: Conductivity theor. 6600 W/m K axial, 1.5 perpendicular, 3500 experim. (Diamond 3000, Cu 400 W/m K) 300 W/m K bulk SWCNTs, 3000 W/m K individual MWCNTs

Thermal stability 650 °C (SW)–800 °C (MW) in air, 2800 °C in Ar (anealing to graphitize defects), 320 °C with metal oxides on the surface – O vacancies, Mars-van Krevelen catatlytic mechanism

Synthetic Routes to CNT

- **DC arc discharge**: growth on a cathode C electrode at 3000 °C, MWCNTs and SWCNTs (with catalyst), easy design, few structural defects, short tubes, low yield, low purity, random diameters

- **Laser ablation**: primarily SWCNTs, few defects, good control over diameter, most costly method, poor scalability, requires Class 4 lasers, Co and Ni catalyst

- **Molten salt**: primarily MWCNTs, simple process, used for filling CNTs, low yield and crystallinity, poor controllability

- **Chemical vapor deposition**: both types, high yields, easy scalability, long tubes, alignment and pattern growth, some defects, medium purity

Synthetic Routes to CNT

DC Arc discharge

NTs observed in carbon soot of graphite electrodes during arc discharge (during production of fullerenes)
The most used method of synthesis in early 1990´s

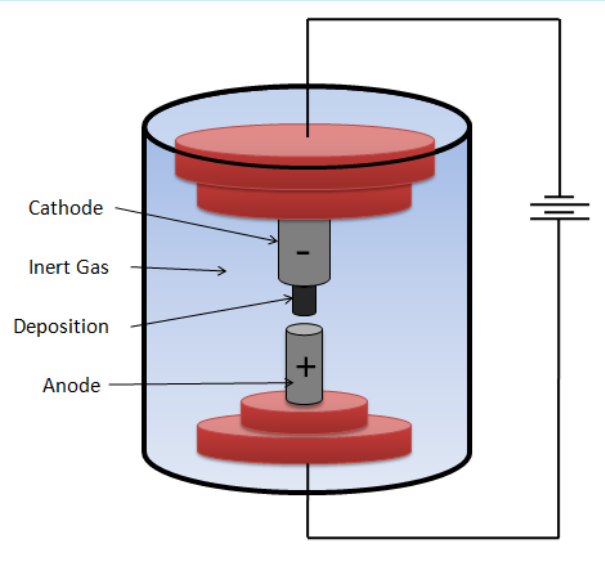

2 carbon electrodes touch, T rises, gap, electric arch, fast e^- from cathode ionize He gas
He^+ attracted to cathode (–)
Carbon (with catalyst) contained in negative electrode sublimes thanks to high temperatures of the electric discharge (3000 °C)

Yield up to 30 %wt, produces both SWNTs, MWNTs
Length up to 50 μm, few structural defects

Synthetic Routes to CNT

Laser ablation

Pulsed laser vaporizes graphite target in a high-temperature reactor filled with inert gas (650 mbar, Ar, N_2)

CNTs develop on the cooler surfaces of reactor as the carbon condenses

Pure graphite – MWNTs

Graphite + metal catalyst particles (Co + Ni) – SWNTs

Yield up to 70 %wt, few defects

Controllable diameter of SWNTs by changing p, T

More expensive than arc discharge, CVD

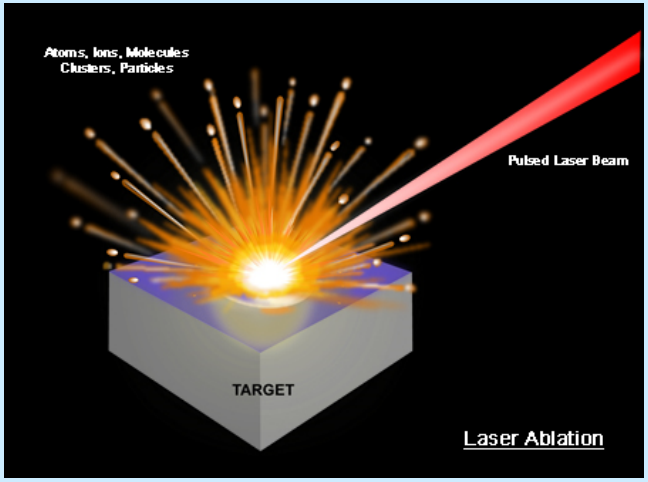

Synthetic Routes to CNT

Molten salt

LiCl, LiBr, 600 °C, graphite electrodes
Cathode exfoliates and graphite sheet wraps
MWCNTs
Yield up to 30 %wt, low purity
Large number of defects, amorphous carbon impurity, salt encapsulating

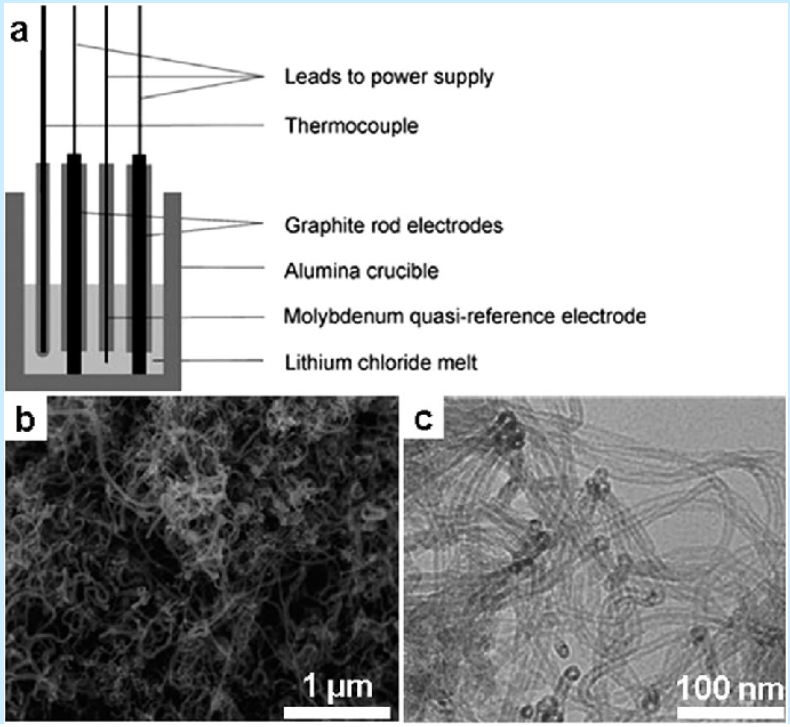

Synthetic Routes to CNT

CVD (Chemical Vapor Deposition)

Substrate + metal catalyst particles (cobalt, nickel, iron)
Distribution of metal catalyst and the size of the particles influence the diameter of NTs
Patterned (or masked) deposition of metal, annealing, plasma etching
Substrate is heated
Two gasses are bled into the reactor – process gas (ammonia, nitrogen, hydrogen) and carbon-containing gas (acetylene, methane, ethylene)
Carbon-containing gas is broken apart at the surface of the metal catalyst particle, carbon is transported to the edges of the particle, where it forms the NT
Catalyst is removed by acid treatment
Resulting NTs are randomly oriented

Synthetic Routes to CNT

CVD (Chemical Vapor Deposition)

CH_4 + metal catalyst particles (cobalt, nickel, iron) $\rightarrow$ $Fe_3C/C + H_2$

Tip growth
Base growth

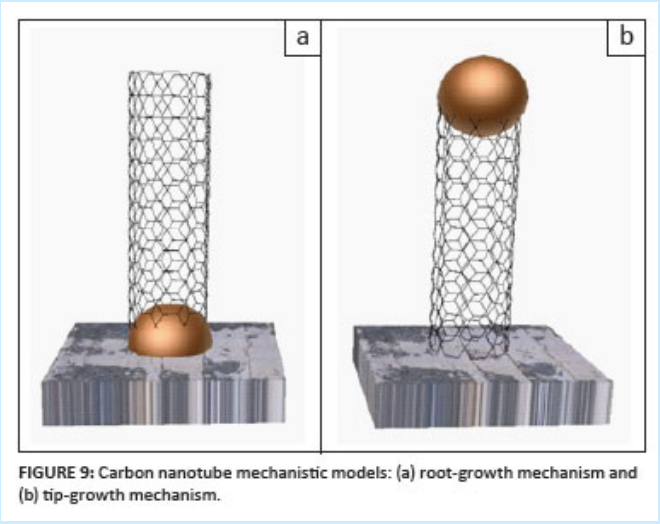

FIGURE 9: Carbon nanotube mechanistic models: (a) root-growth mechanism and (b) tip-growth mechanism.

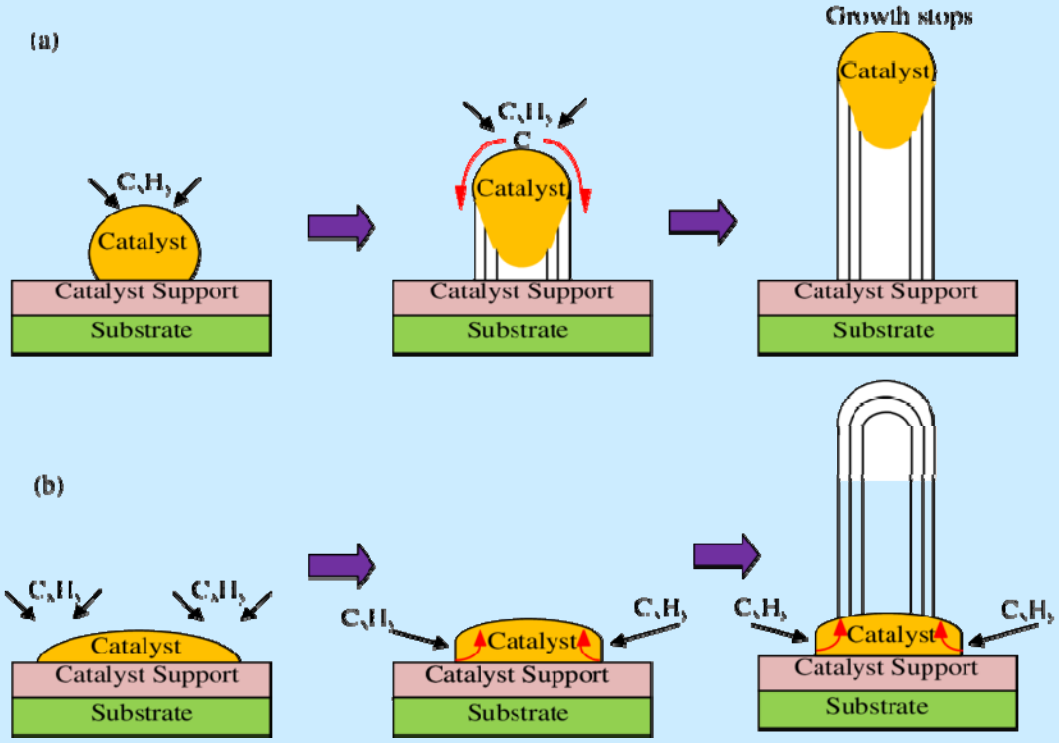

Synthetic Routes to CNT

CVD (Chemical Vapor Deposition)

Plasma Enhanced CVD
Plasma is generated by the application of strong electric field during growth
Growing NTs follow the direction of the electric field
With the correct use of reactor geometry, vertically aligned (perpendicular to substrate) NTs can be grown

Substrate patterned (lithography) with Fe NPs

CDV shows the best promise for industrial manufacturing of CNTs
Better price/unit ratio
NTs grown on desired substrates

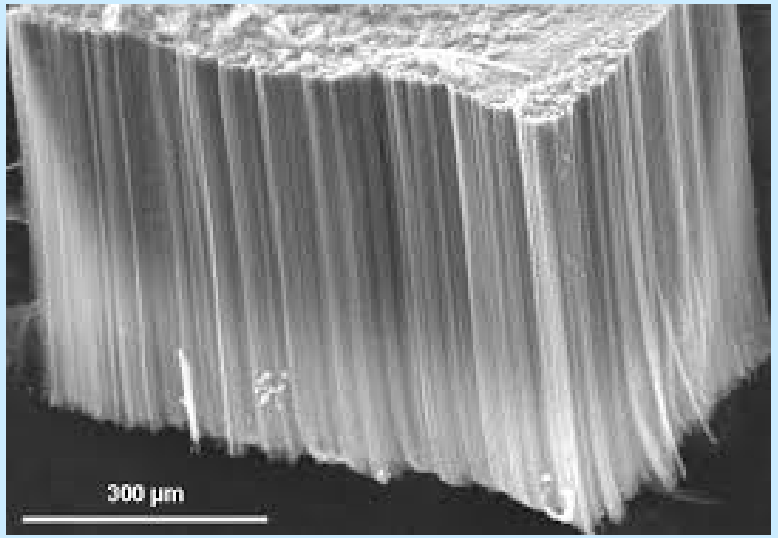

Synthetic Routes to CNT

Super-growth CVD

New methods of CVD using different substrates, catalysts

Activity and lifetime of catalyst can be enhanced by adding water into the reactor

Growing CNTs then form „forests“ up to several mm high, aligned normaly

Improved efficiency, reaction time and purity of CNTs (more than 99,9%)

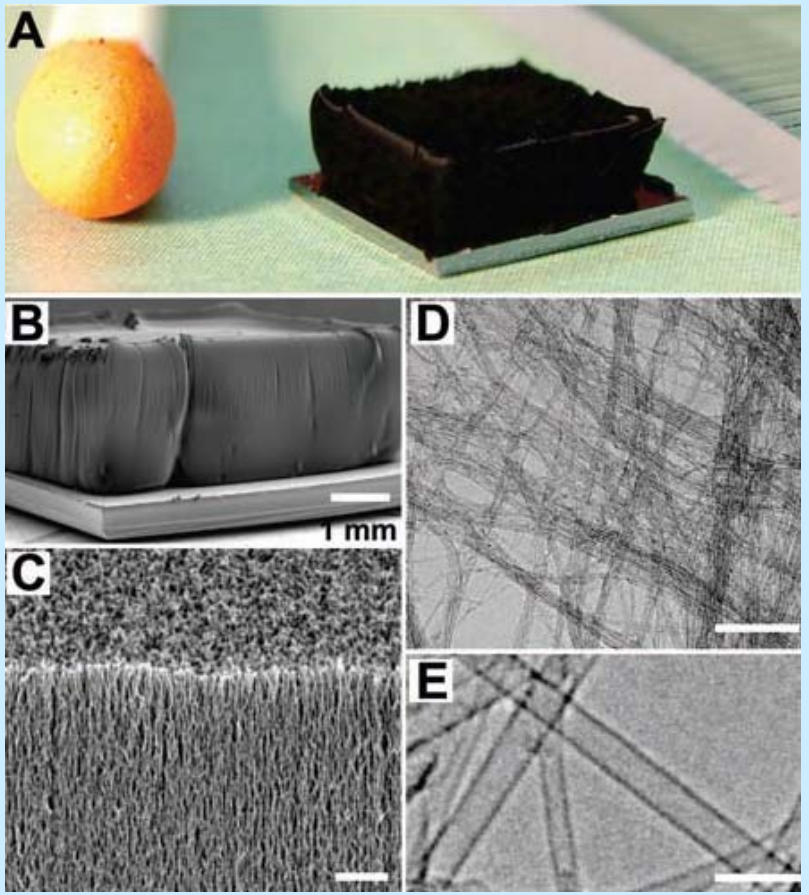

Hata, K.; Futaba, DN; Mizuno, K; Namai, T; Yumura, M; Iijima, S (2004). "Water-Assisted Highly Efficient Synthesis of Impurity-Free Single-Walled Carbon Nanotubes". *Science* **306** (5700): 1362–1365. doi:10.1126/science.1104962. PMID 15550668

Synthetic Routes to CNT

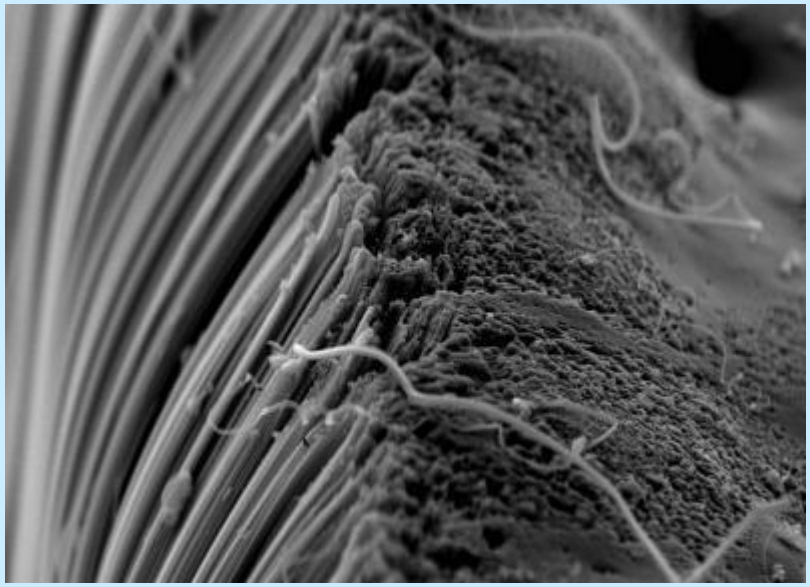

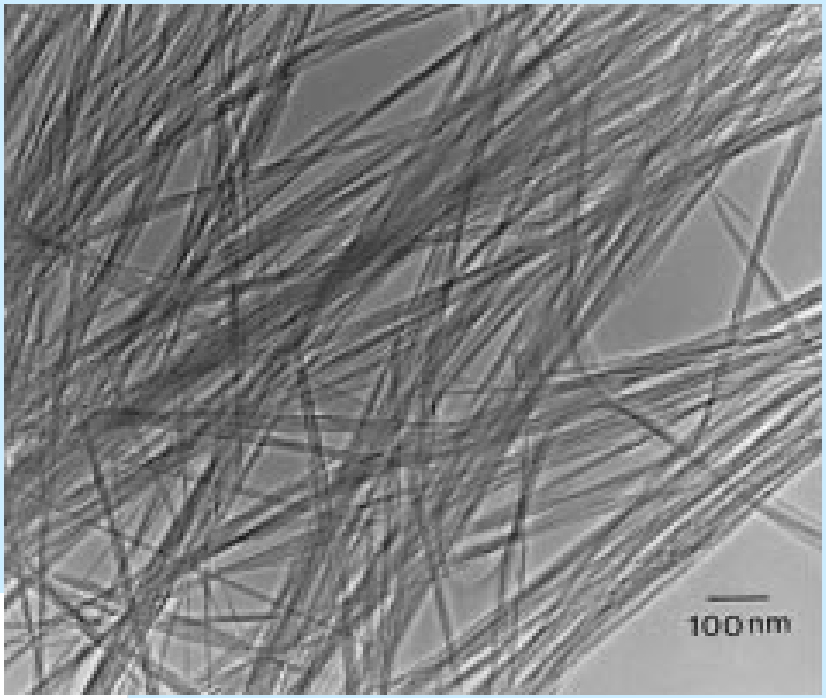

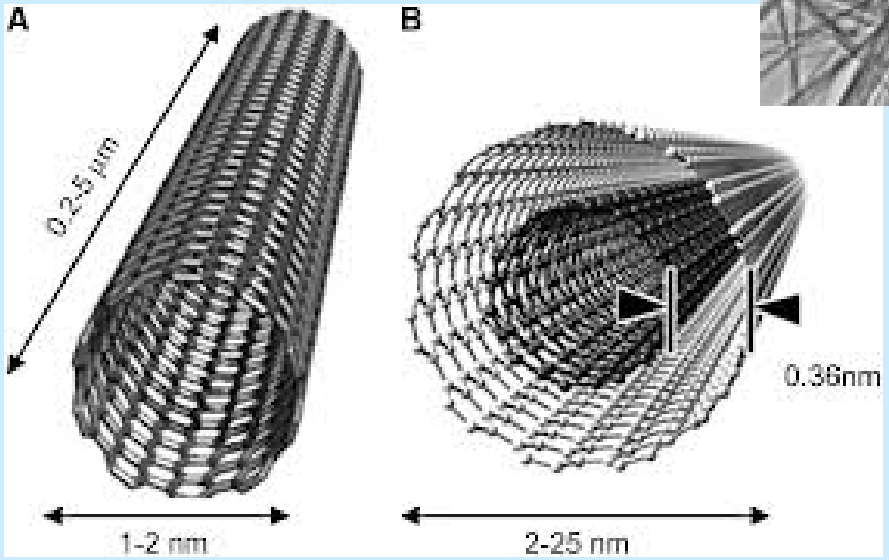

Defect-free (n,m) SWNTs with Open Ends

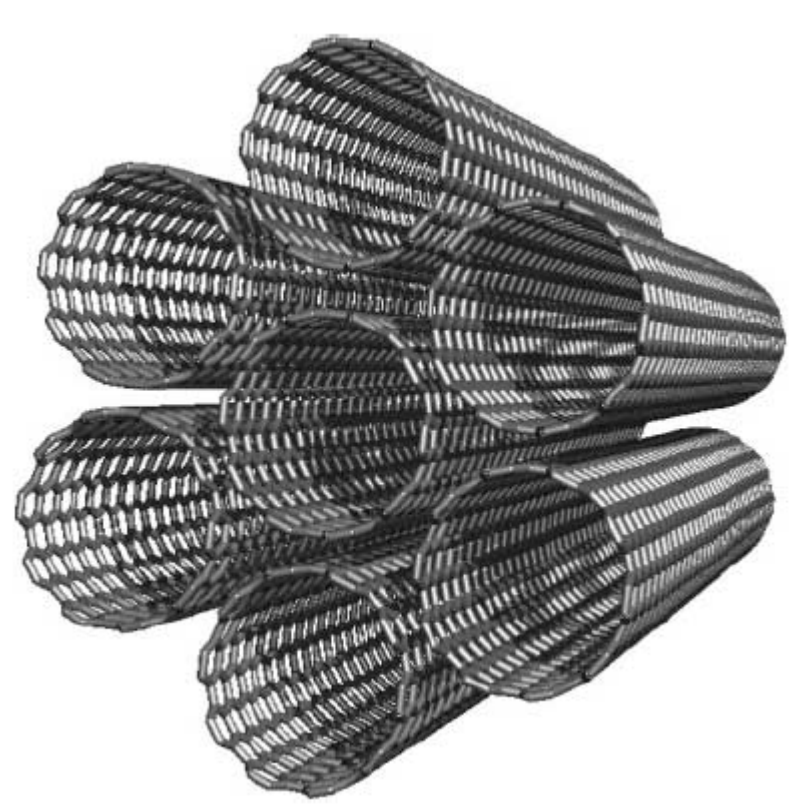

A bundle of (10,10) nanotubes held together with strong π-π-stacking interactions

Roll-up of (n,m) SWNTs

Chiral vector (n,m)

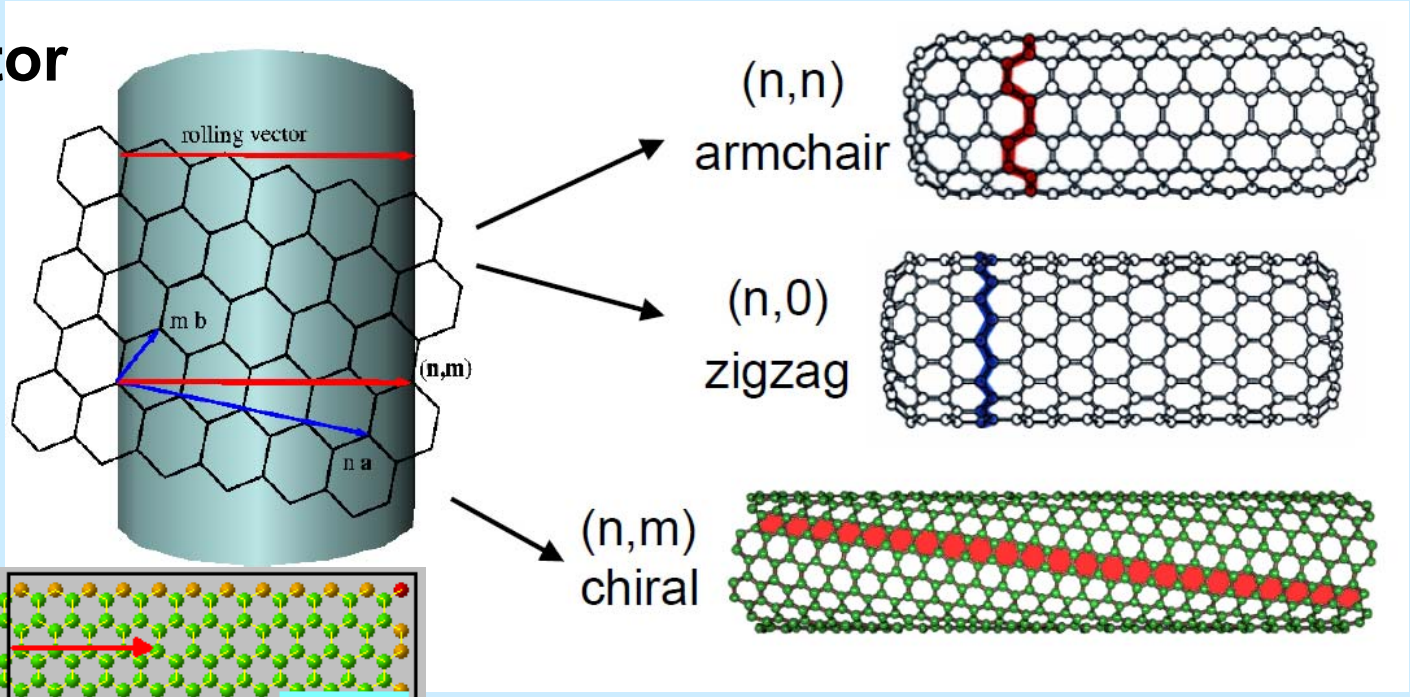

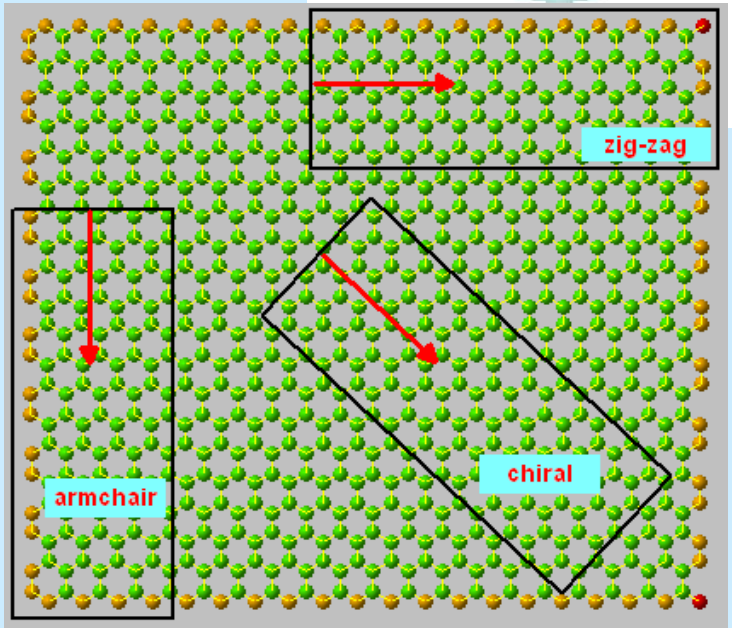

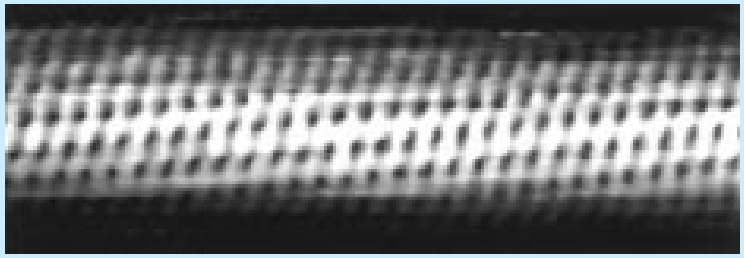

TEM of a chiral CNT

Roll-up of (n,m) SWNTs

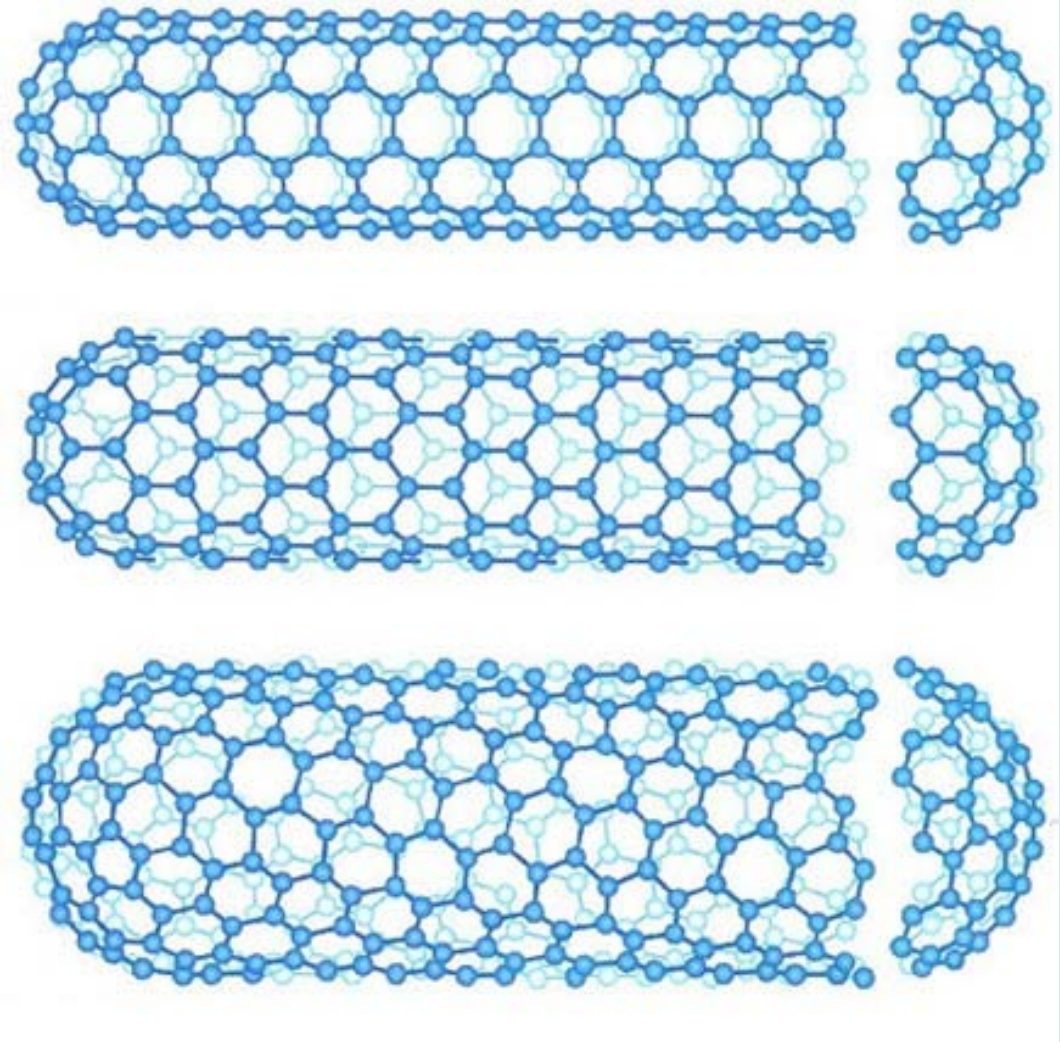

Roll-up of (n,m) SWNTs

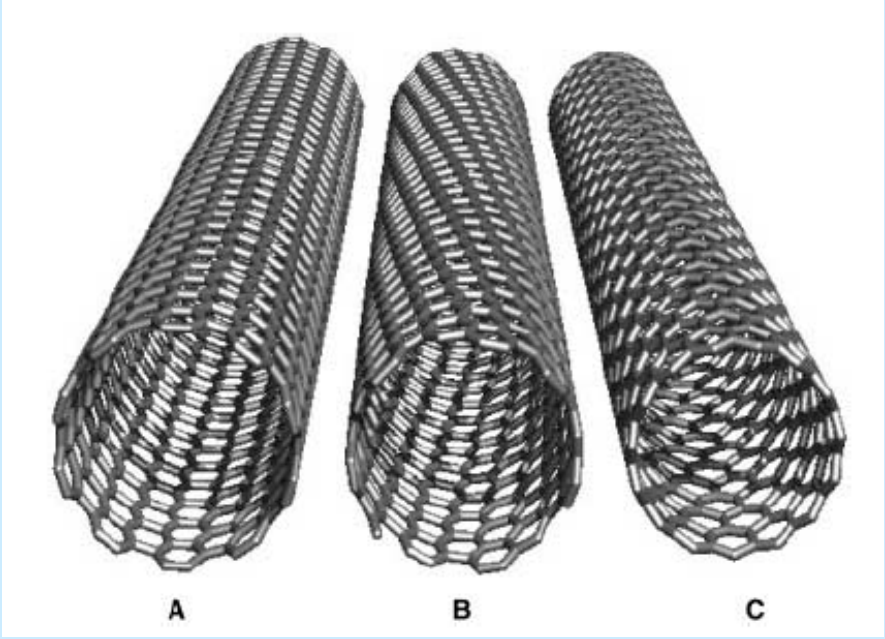

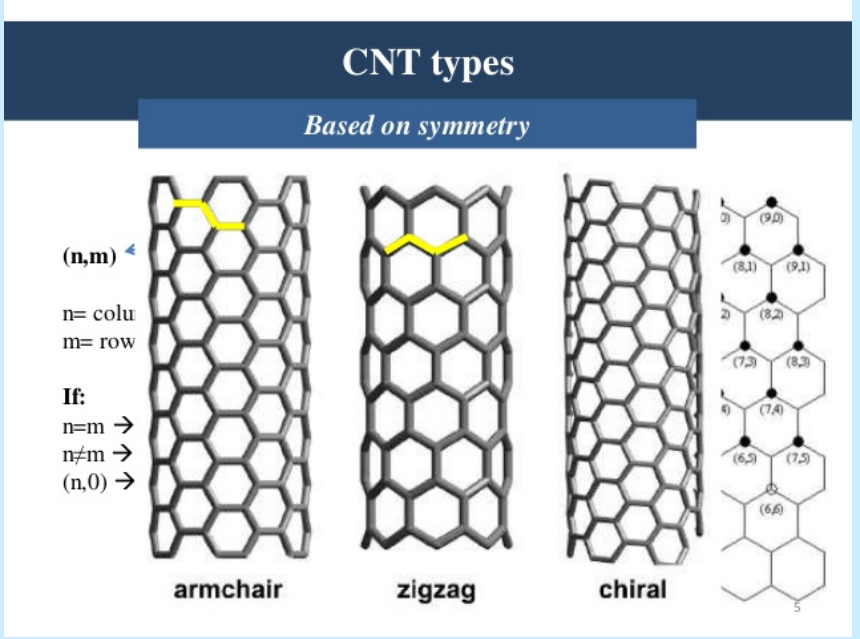

A) Armchair - an achiral metallic conducting (10,10) tube
B) Chiral - semiconducting (12,7) tube
C) Zigzag - an achiral conducting (15,0) tube

All the (n,n) armchair tubes are metallic
Chiral or zigzag tubes are metallic only if (n – m)/3 is a whole number, otherwise, they are semiconductors

Roll-up of (n,m) SWNTs

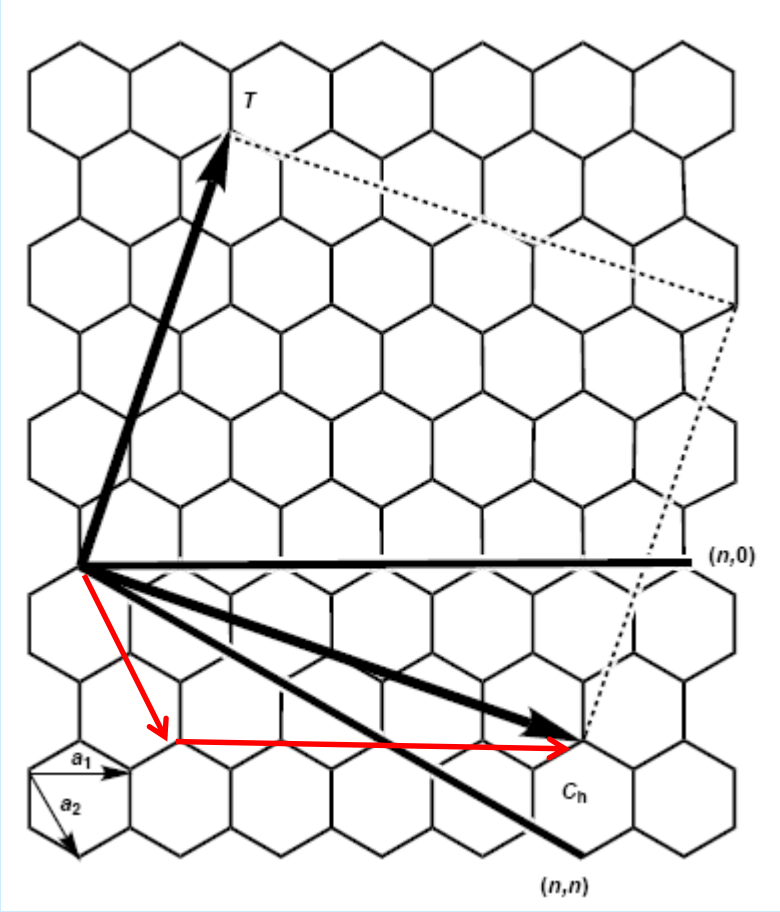

(n,m) = (4,2)

A 2D graphite layer
the lattice vectors a_1 and a_2

The roll-up vector $C_h = na_1 + ma_2$
Achiral tubes exhibit roll-up vectors derived from (n,0) (zigzag) or (n,n) (armchair).

The **translation vector T** is parallel to the tube **axis** and defines the 1D unit cell.

The rectangle represents an unrolled **unit cell,** defined by T and C_h

Roll-up of (n,m) SWNTs

Chiral vector:

$C_h = na_1 + ma_2$

(n,m) = (3,3)

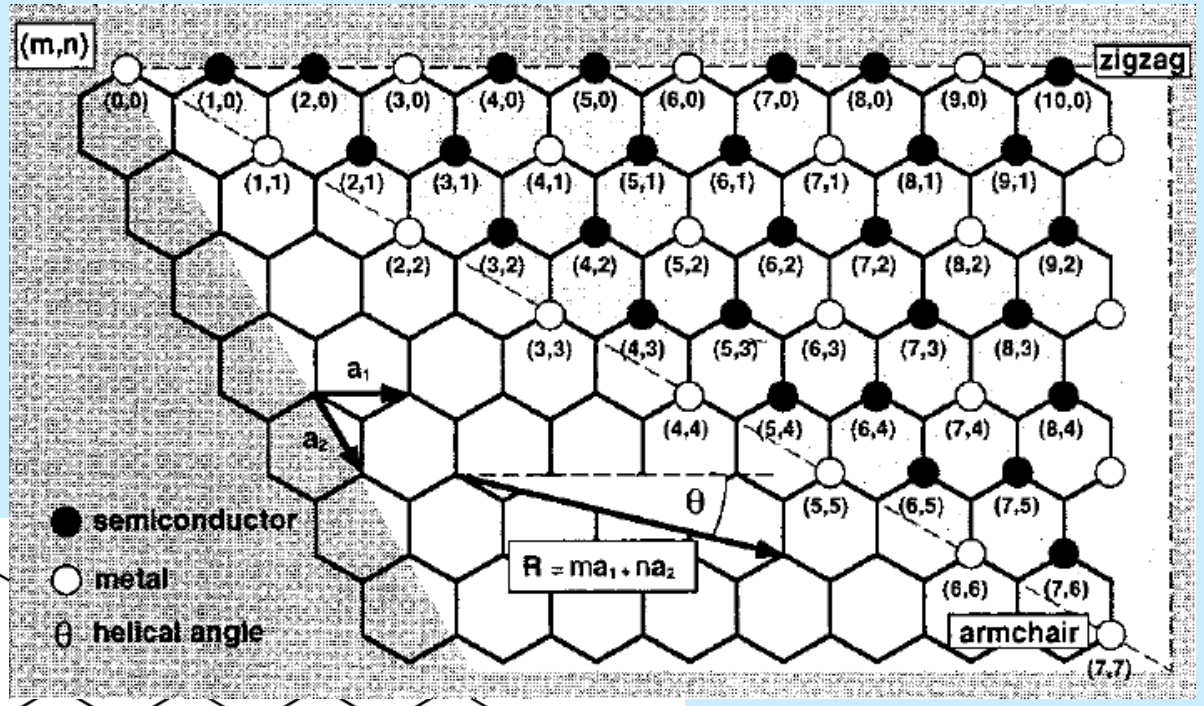

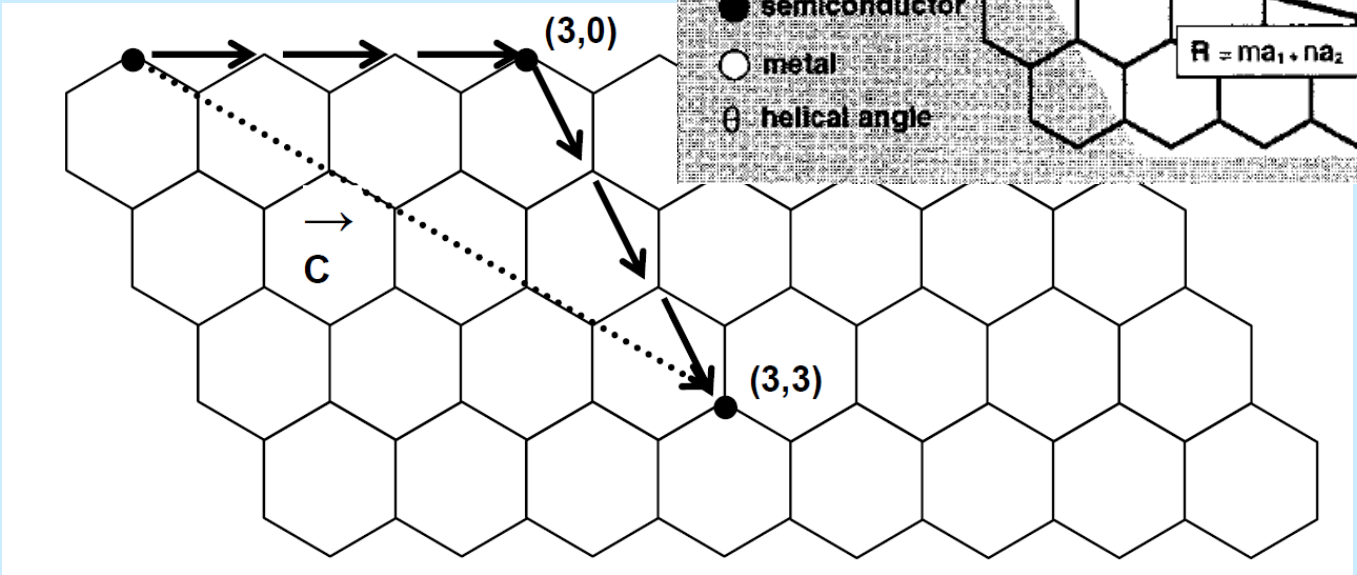

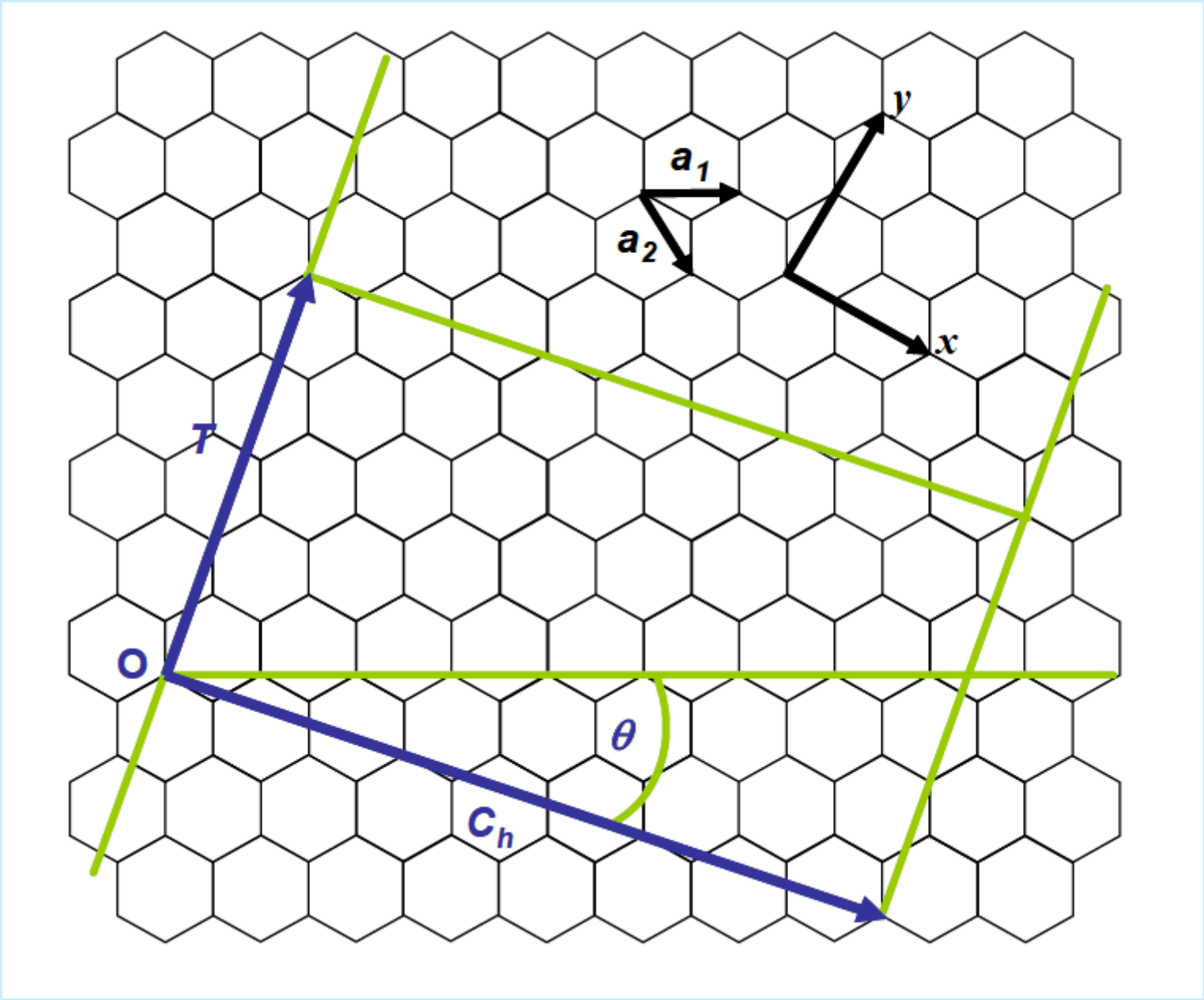
y
a_1
a_2
x
T
O
θ
C_h

Roll-up of (n,m) SWNTs

$$\vec{C_h} = n\vec{a_1} + m\vec{a_2} \equiv (n,m) \qquad (\text{ and } \; 0 \le |m| \le n \;)$$

Tube diameter

$$d_t = \frac{|C_h|}{\pi} = \frac{a_0\sqrt{\left(n^2 + nm + m^2\right)}}{\pi}$$

$$|a_1| = |a_2| = a_0 = 0.249 \text{ nm}$$

$$\theta = \tan^{-1}\left[\sqrt{3}m/\left(m + 2n\right)\right]$$

$\theta = 0$–$30°$

a = 1.42 √3 = 2.49 Å

d(Csp^2-Csp^2) = 1.42 Å

Defects in SWNTs

Atomic vacancies – reduction of tensile strength, electrical and thermal conductivity

Topological (Stone Wales) defect – rearrangement of bonds into pentagonic and heptagonic pair (connected, no other types of rings known)

Defects lead to phonon scattering – increased phonon relaxation rate – reduction of mean free path (reduction of ballistic conductivity) leads to reduced thermal conductivity

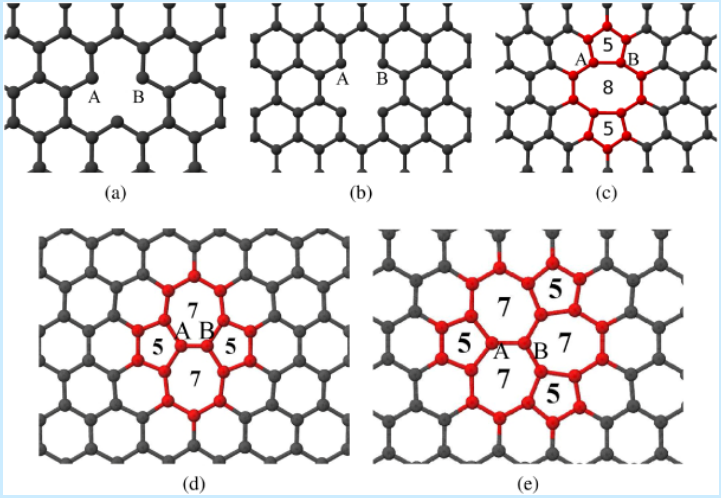

Defects in SWNTs

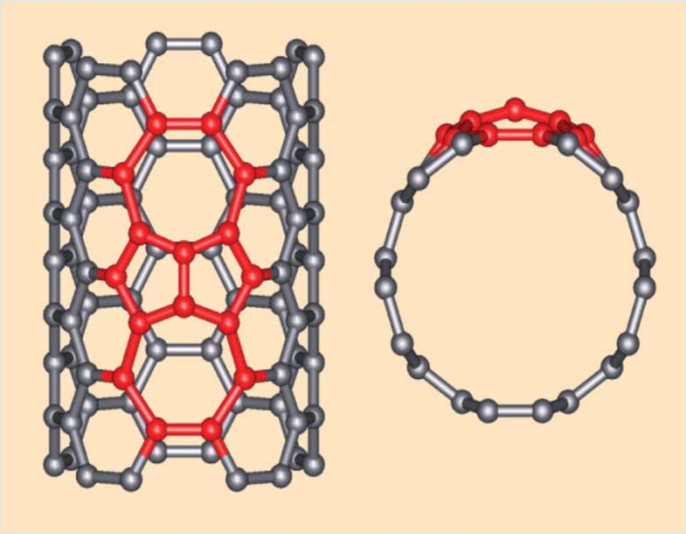

Stone-Wales defect (7-5-5-7 defect) ⇒ Larger curvature, esp. where the 5-membered rings are condensed ⇒ addition reactions at this C=C favored

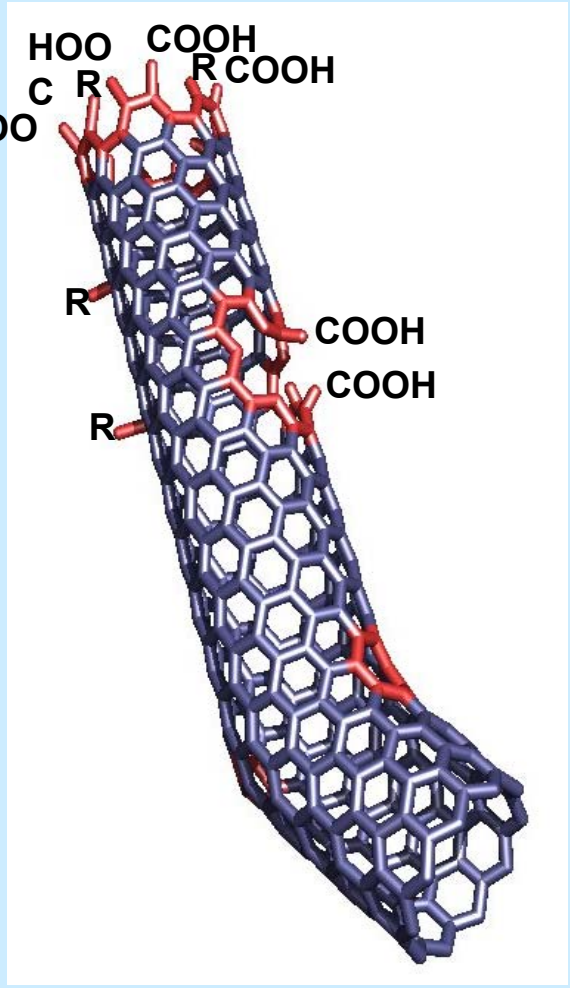

Separation of CNTs

Semiconducting CNTs
- Separation by surfactants, (octadecylamine), a strong affinity

Metallic CNTs
- Separation by diazonium reagents, biomolecules, DNA
- AC dielectrophoresis – 10 MHz, induced dipole, causes the two types of CNTs to migrate along the electric field gradient in opposite directions

Doping of CNTs

Intercalation CNTs

- Between walls of MWCNT – during synthesis or posttreatment

On-wall substitution CNTs

- N or B substitute for C
- In-situ – element-containing precursor
- Ex-situ – removal of C atom – graphite (n) or pyridine (n or p) type of group

Functionalization Possibilities for SWNTs

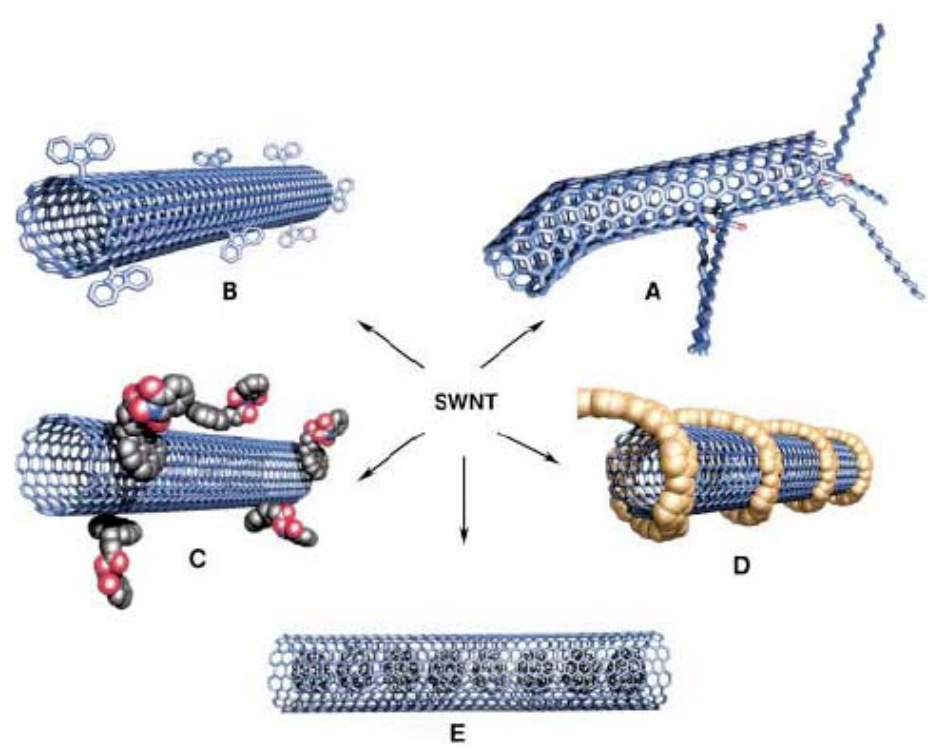

A) defect-group functionalization

B) covalent sidewall functionalization

C) noncovalent exohedral functionalization with surfactants – wrapping

D) noncovalent exohedral functionalization with polymers

E) Endohedral functionalization with C_{60} (C_{60}@CNT, “peapods)

Functionalization Possibilities for SWNTs

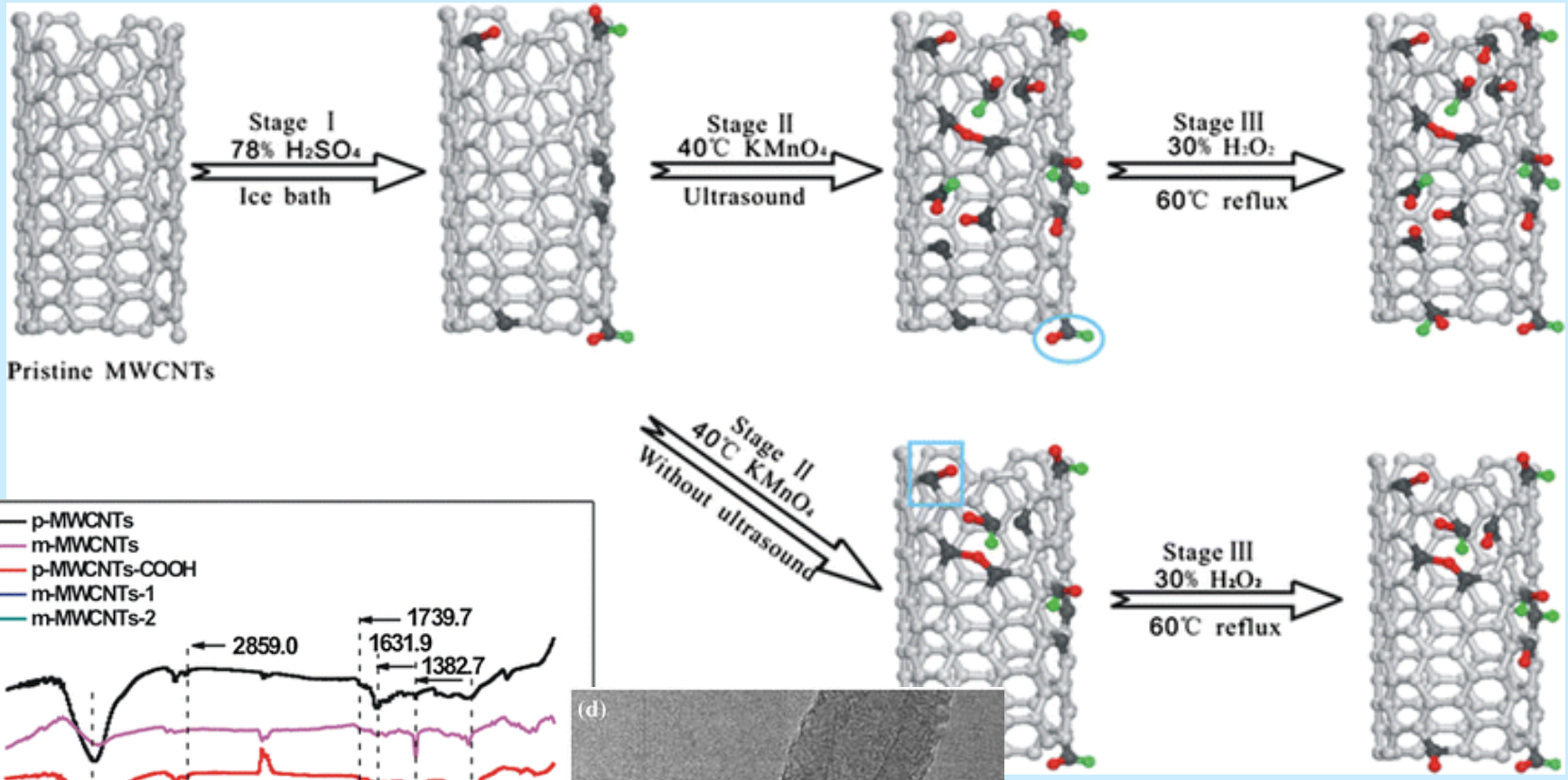

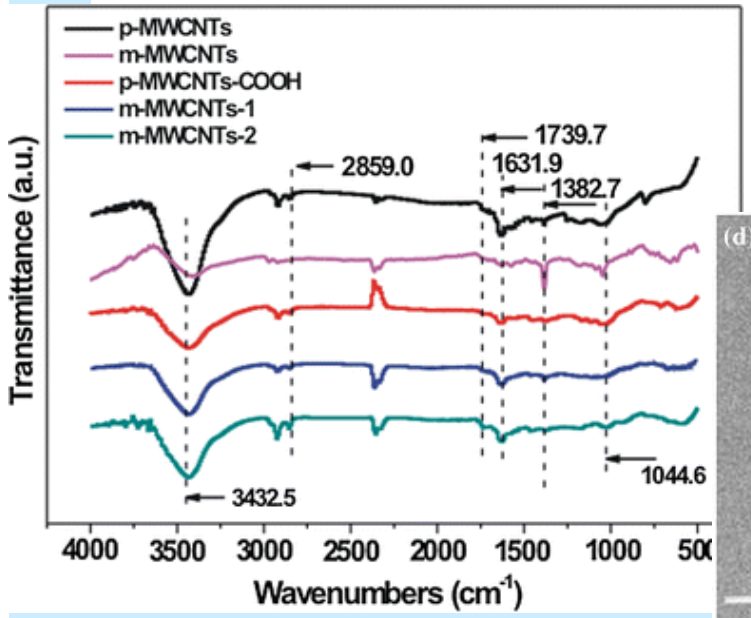

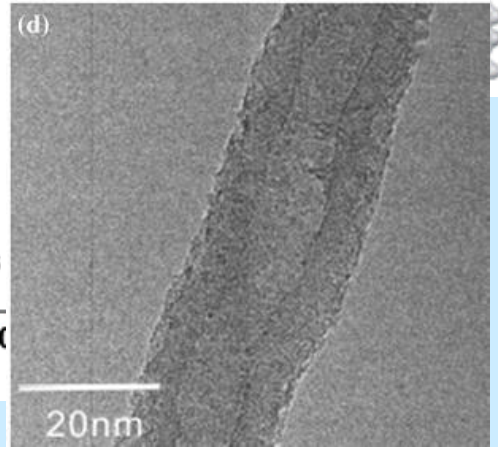

Functionalization Possibilities for CNTs

Reactions will occur **first at the end caps**, then on the surface, at structural defects

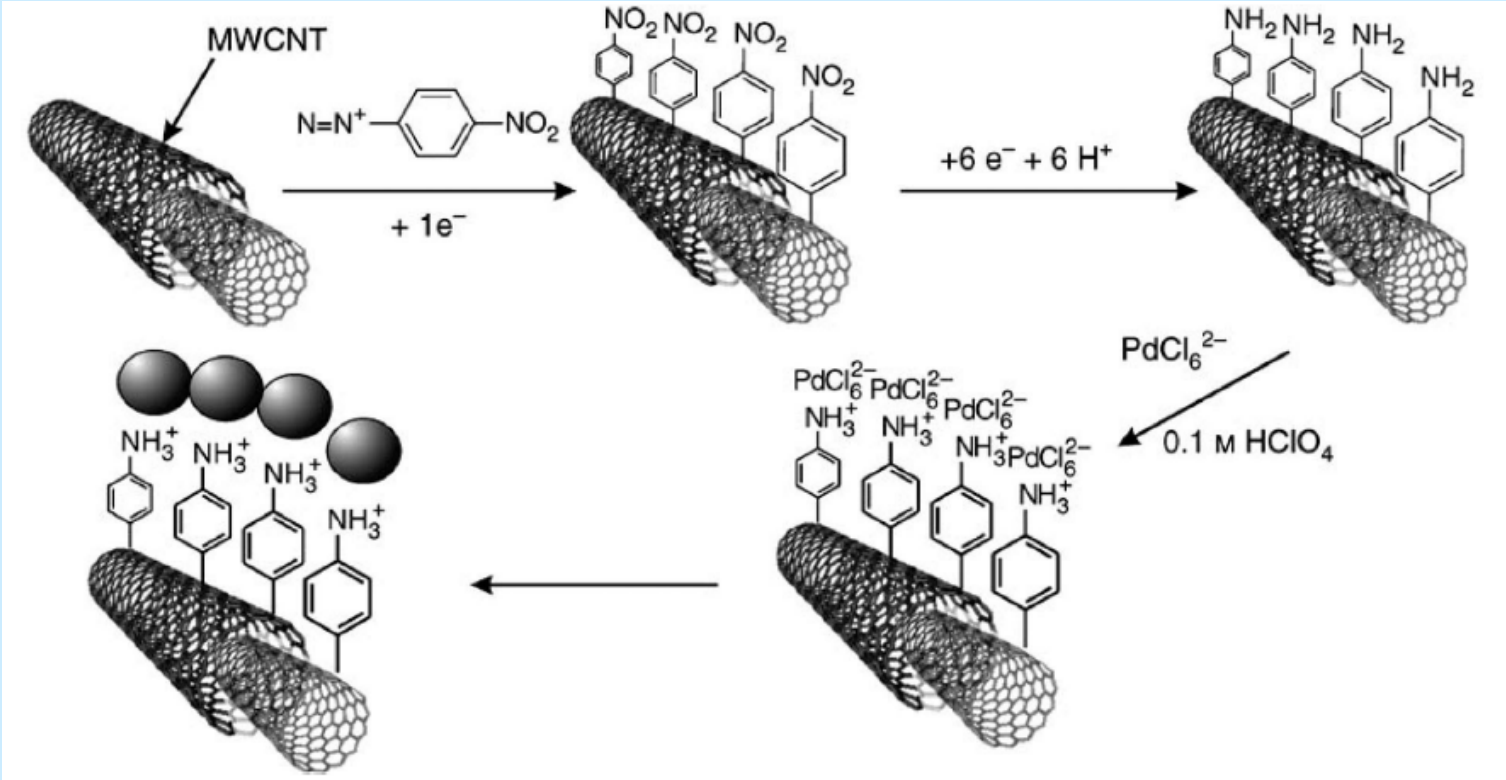

Functionalization Possibilities for CNTs

TiO_2 and SiO_2 on acid-treated CNTs via ALD
SEM image for the case of SiO_2
TEM image of vertically grown CNT coated with RuO_2 both outside and inside

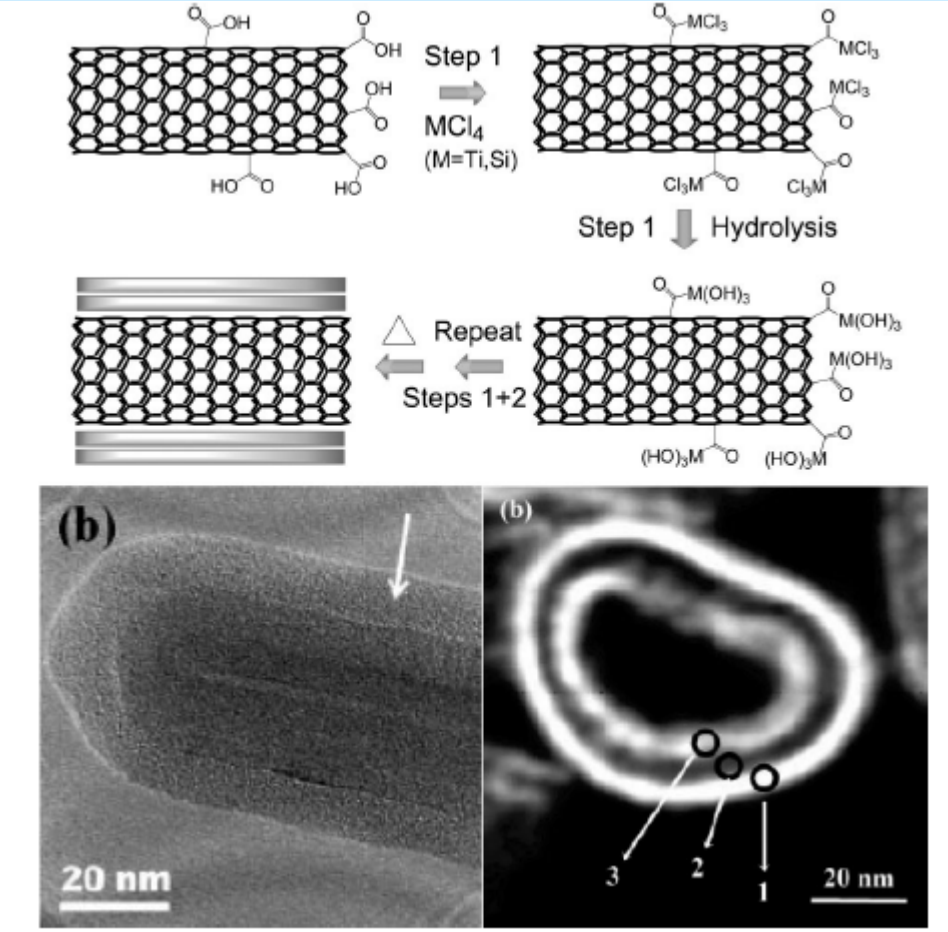

Assembly of CNTs

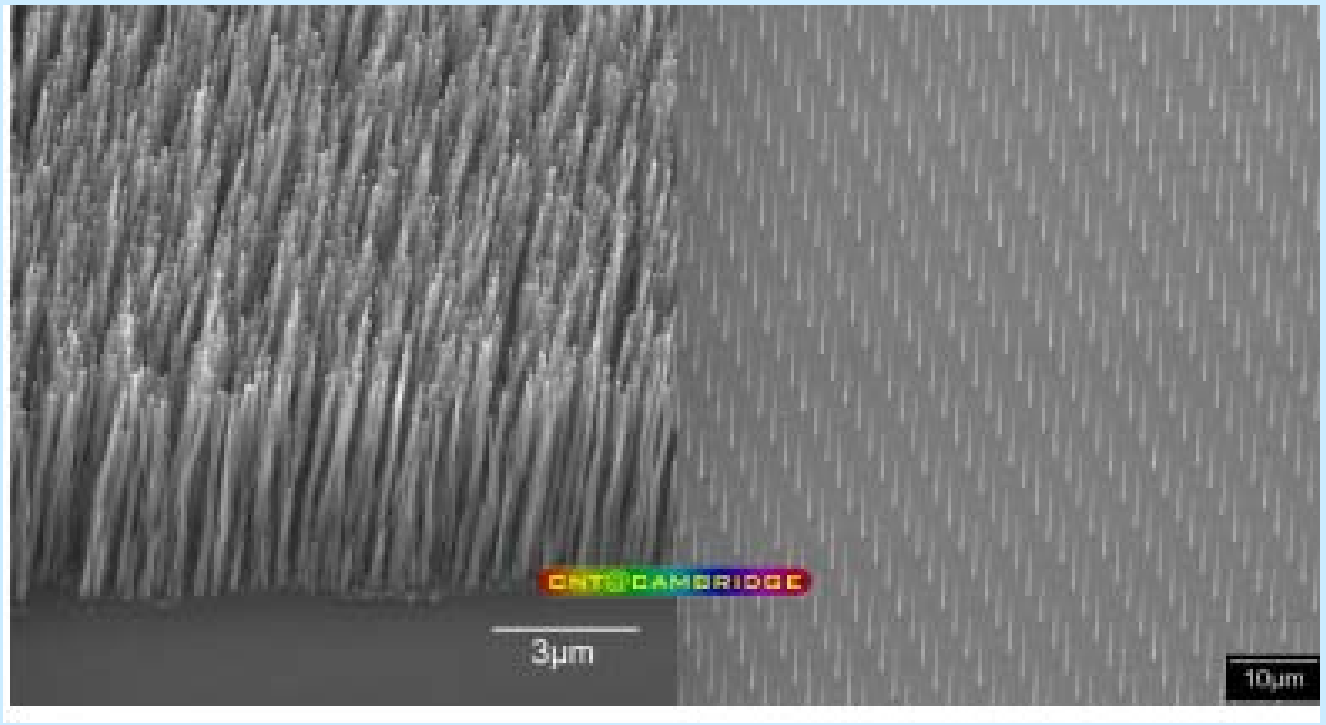

CNT applications:
Ultra-hard Composites
Nanopipettes
Field Emission Transistor
Nanomanipulator

CNT Applications

Interconnect

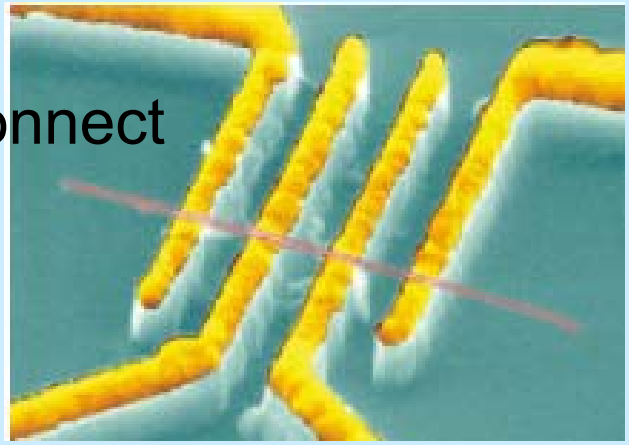

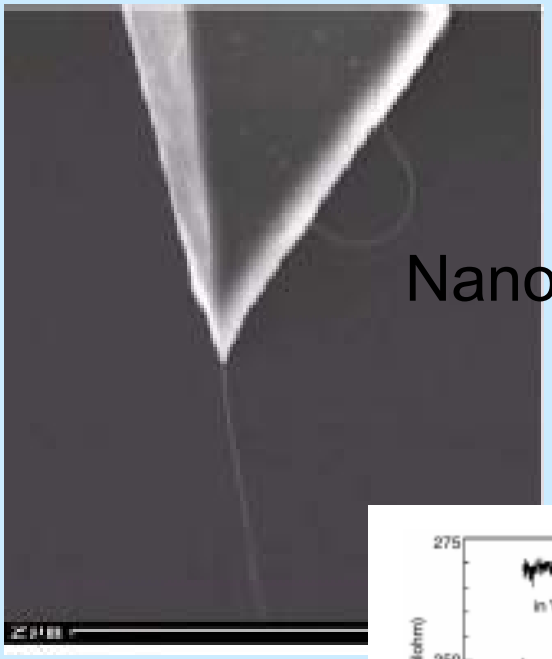

Nanomanipulator

IBM

Transistor

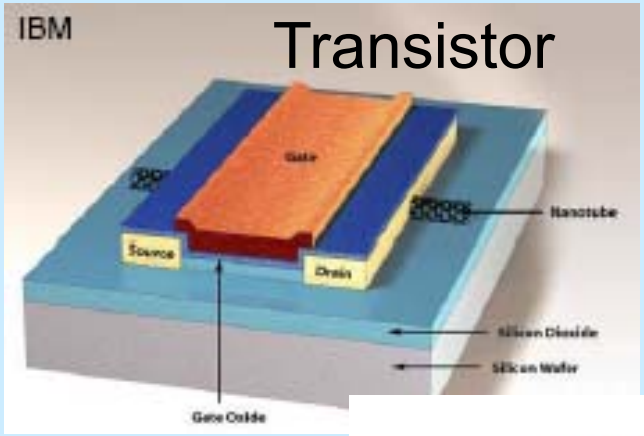

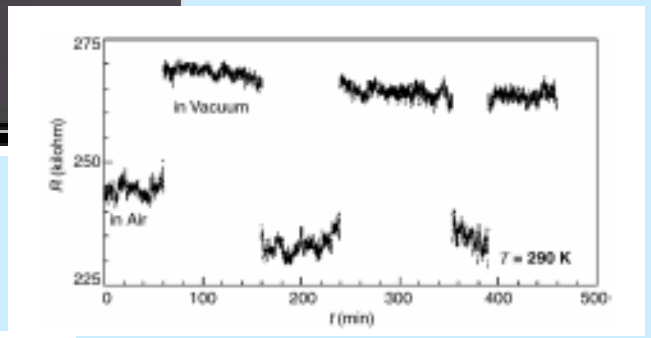

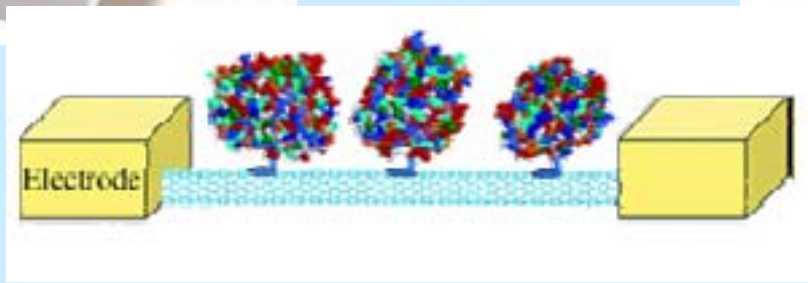

Chemical Sensor

Bio-Sensor

CNT Applications

CNTs as photosensitizers:

(a) electron injection into the conduction band of TiO_2

(b) electron back-transfer to CNTs with the formation of a hole in the valence band of TiO_2 and reduction of the hole by oxidation of adsorbed OH^- species

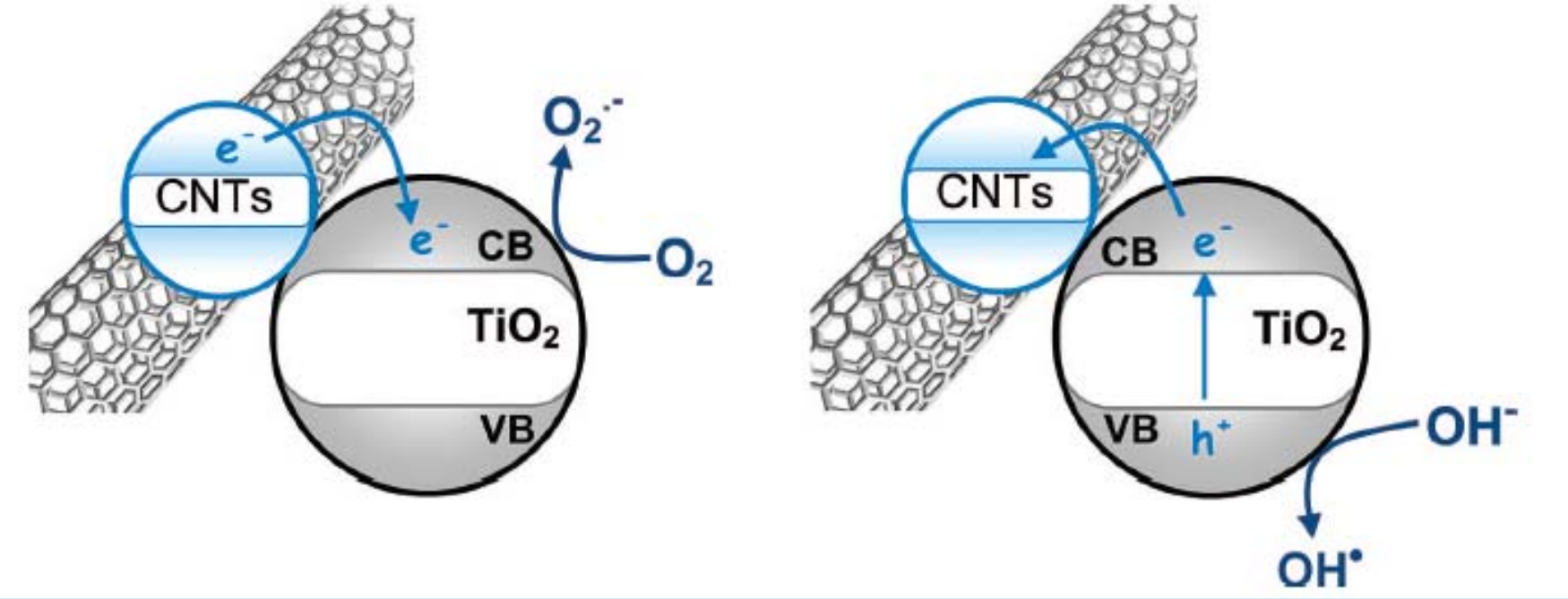

Nanowires

Good transport properties – Single crystalline nature

Mechanically robust – Defect free

Flexibility in composition

Doping possible to create p- and n-type nanowires

Nanowires-based FETs and basic logic circuits demonstrated in the laboratory

Techniques for mass manufacture

Synthetic Routes to Nanowires

Epitaxial growth

Catalytic VLS growth

Catalytic base growth

Colloidal synthesis

Defect nucleation

Templated growth

Arrested growth

Assembly of nanoparticles

Epitaxial Growth

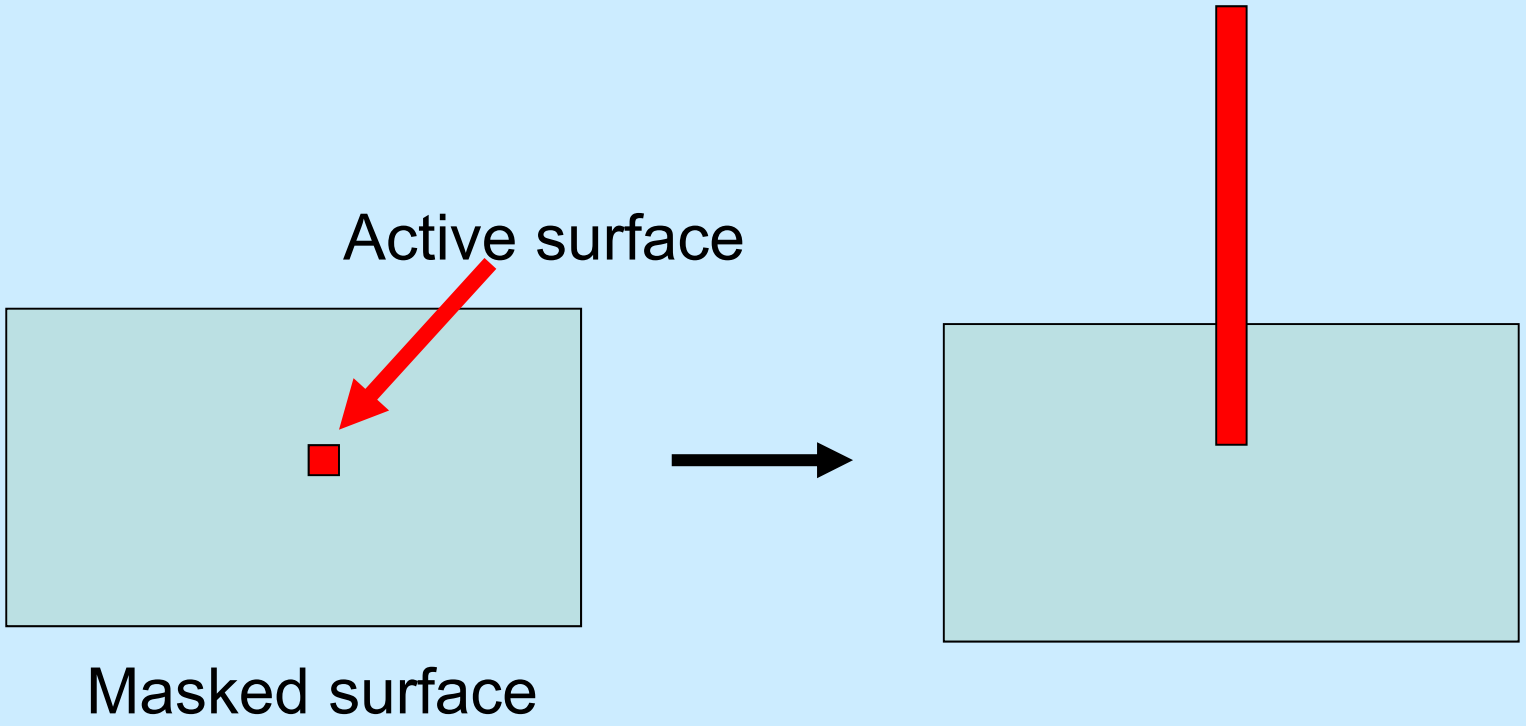

Vapor-Liquid-Solid (VLS) Growth

(1) Metal catalyst nanoparticles - Au(s)

Feed another element (Ge vapor, GeH_4 or SiH_4) at an elevated temperature (440-800 °C/ultra-high-vacuum)

Gaseous precursor feedstock is absorbed/dissolved in Au(s) till the solid solubility limit is reached (2)

A liquid phase appears, melts to a droplet (3)
The droplet becomes supersaturated with Ge

When the solubility limit is reached (4), an excess material is precipitated out to form solid NWs beneath the droplet

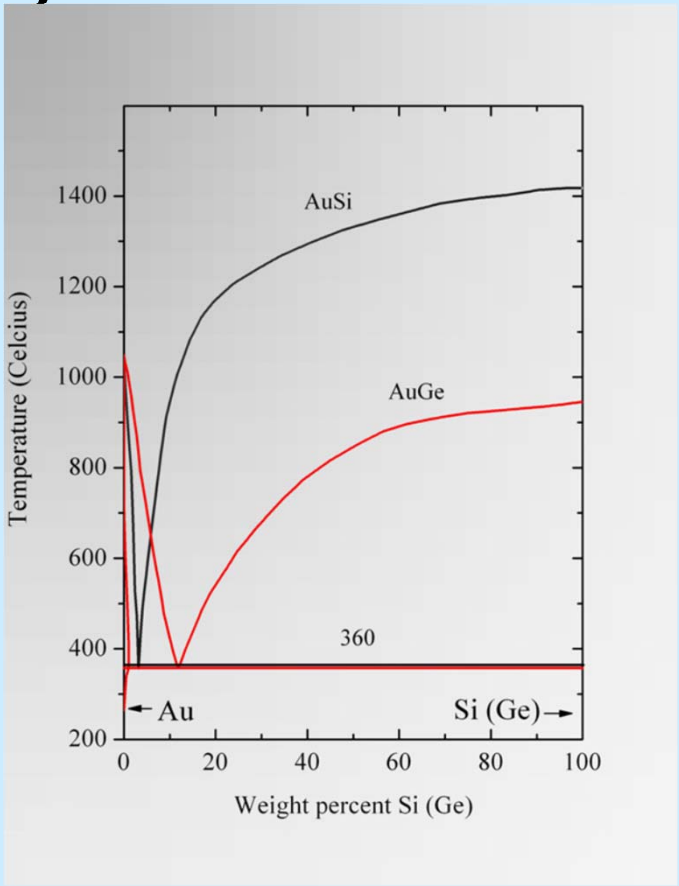

Eutectic 360 °C
Au (mp 1064 °C)
Si (mp 1410 °C)
Ge (mp 938 °C)

Vapor-Liquid-Solid (VLS) Growth

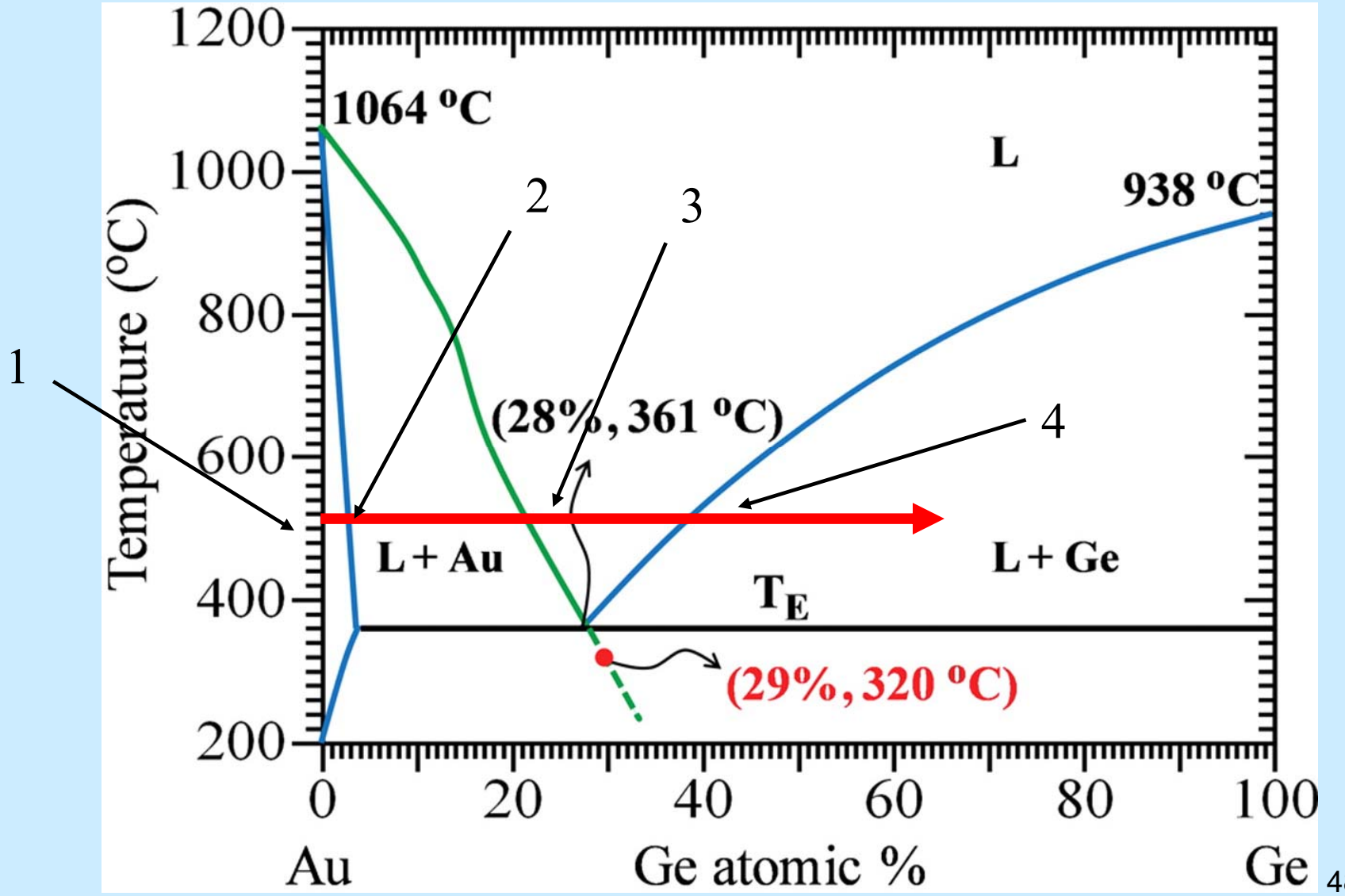

Vapor-Liquid-Solid (VLS) Growth

Au/Ge Eutectic Liquid Alloy

Au Particles

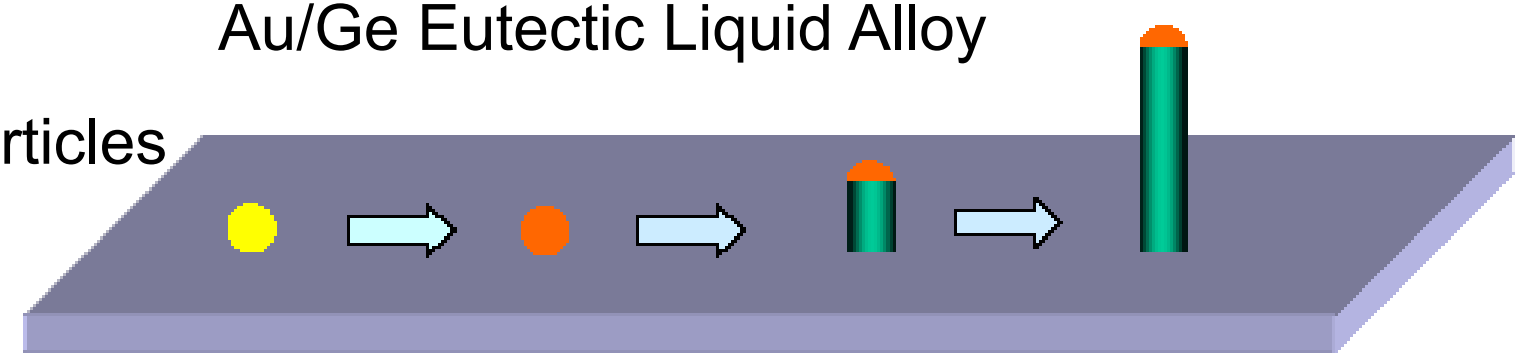

Nucleation of NWs

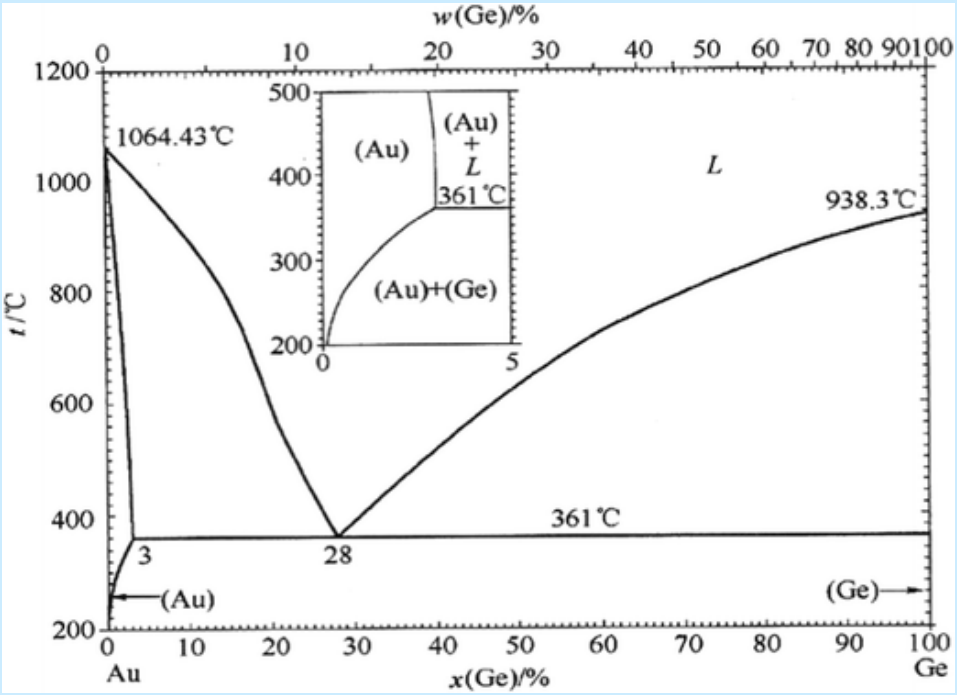

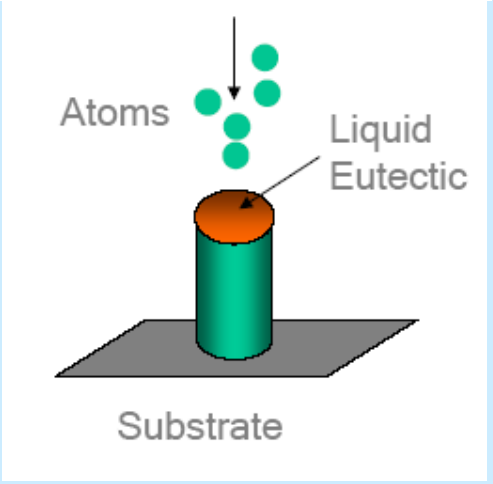

NW Growth

In-situ TEM images of the VLS process

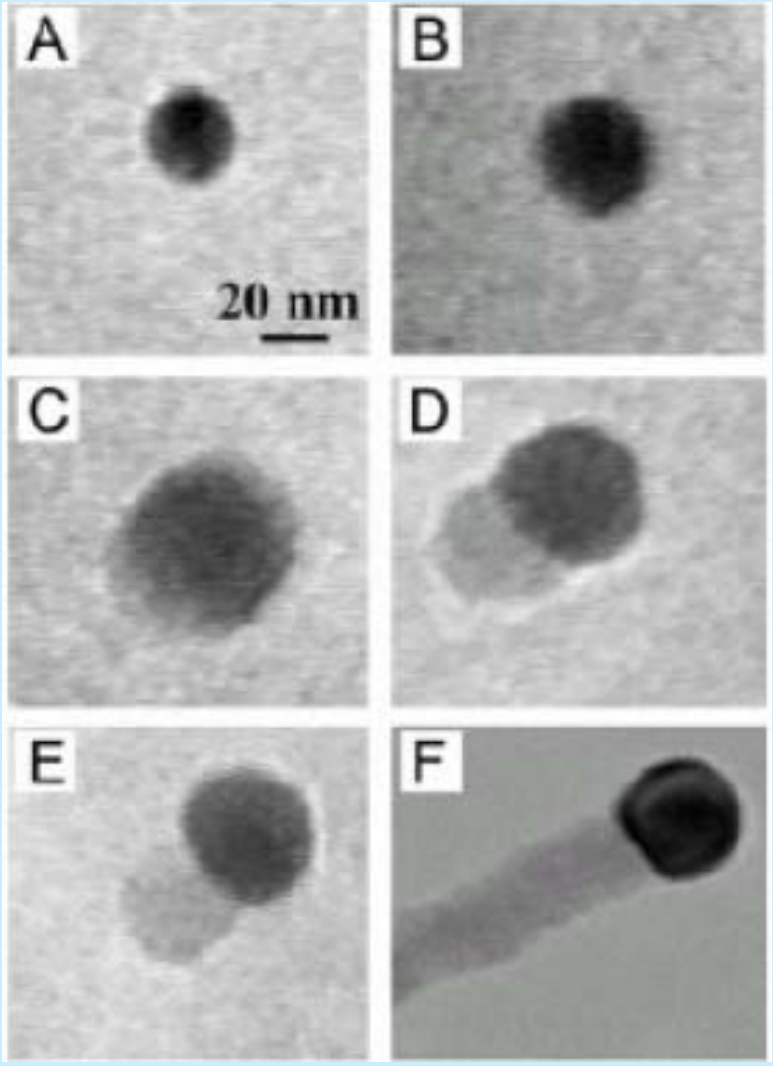

In-situ TEM images recorded during the process of nanowire growth:
(a) Au nanoclusters in solid state at 500 °C
(b) alloying initiated at 800 °C, at this stage Au exists mostly in solid state
(c) liquid Au/Ge alloy
(d) the nucleation of Ge nanocrystal on the alloy surface
(e) Ge nanocrystal elongates with further Ge condensation
(f) Ge forms a wire

Ge NWs on the Bare Ge(110) Substrate

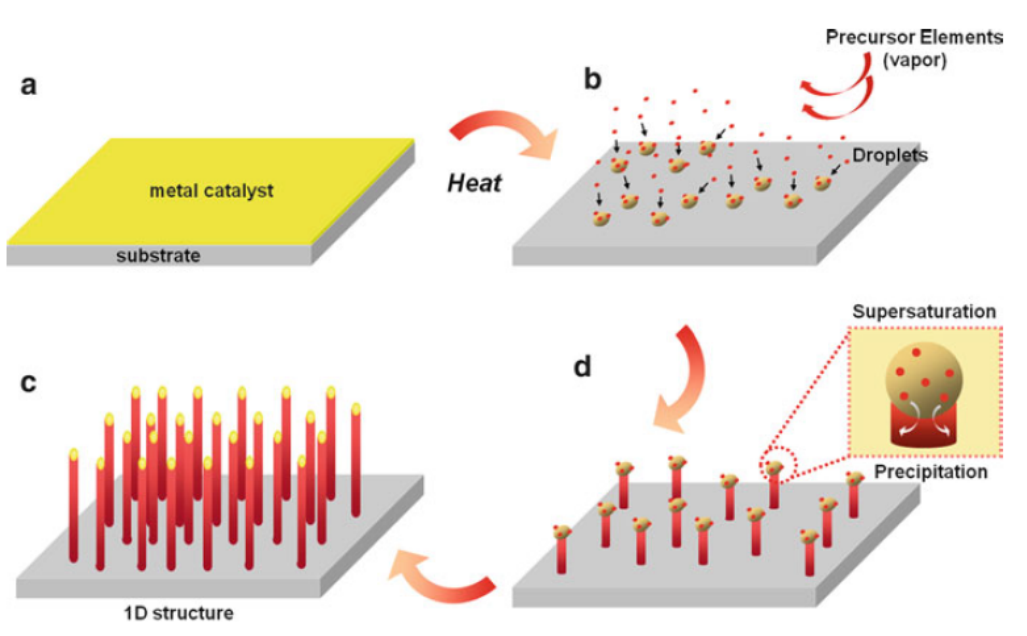

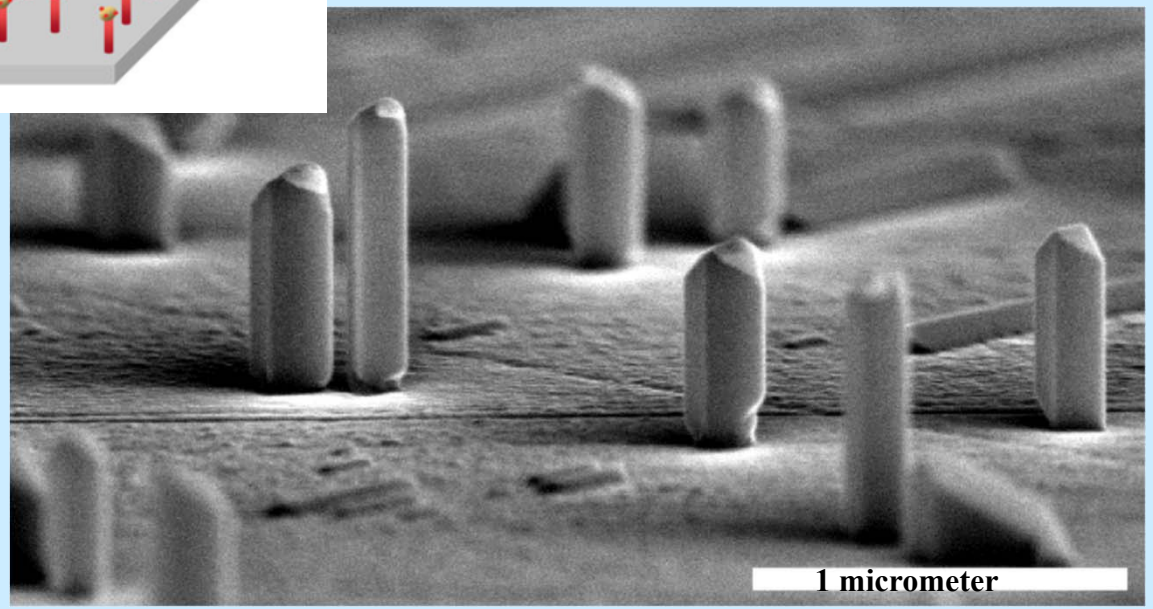

Si Nanowire Growth

$$SiH_4 \rightarrow Si + 2H_2$$

Mass transport in the gas phase

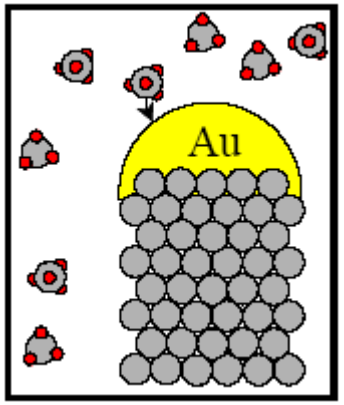

Diffusion in molten catalyst

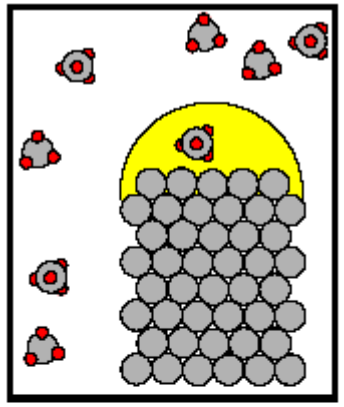

Chemical reaction at the V-L interface

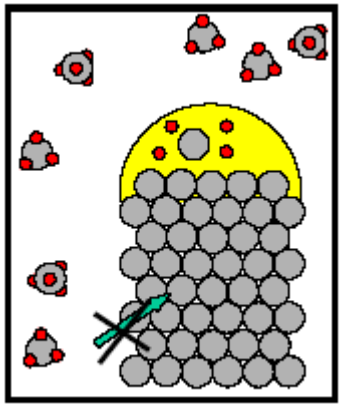

Incorporation of material in the crystal lattice

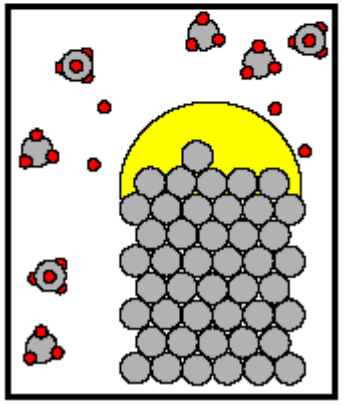

Si Nanowires

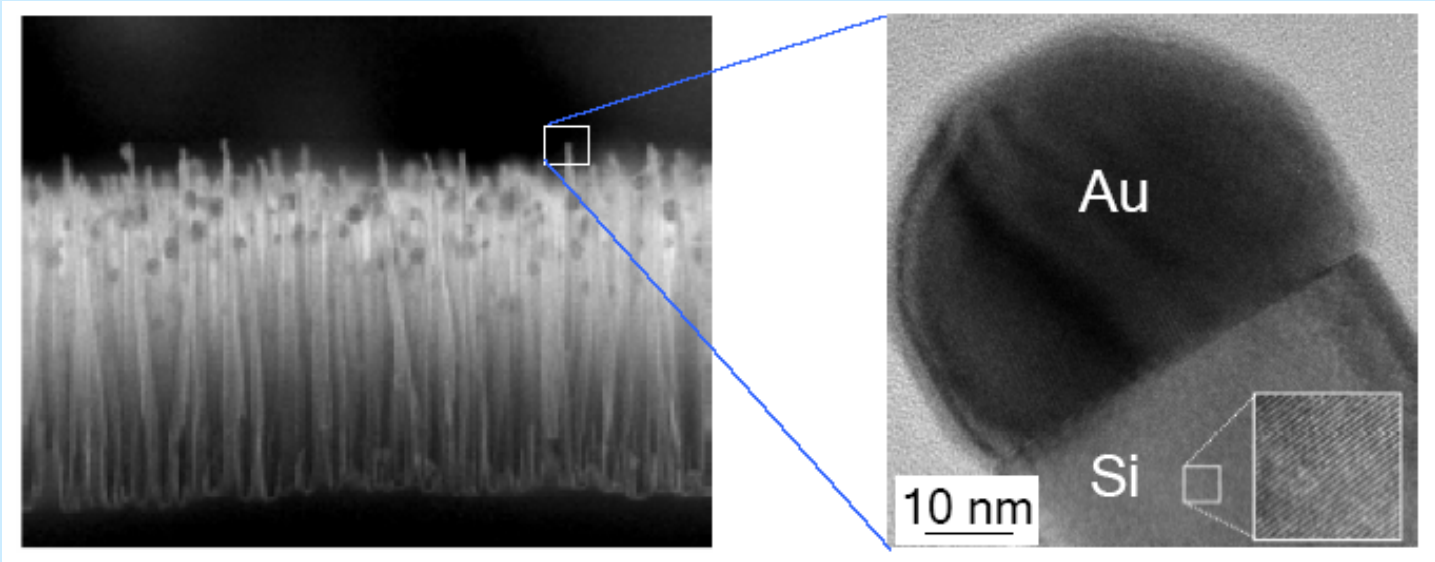

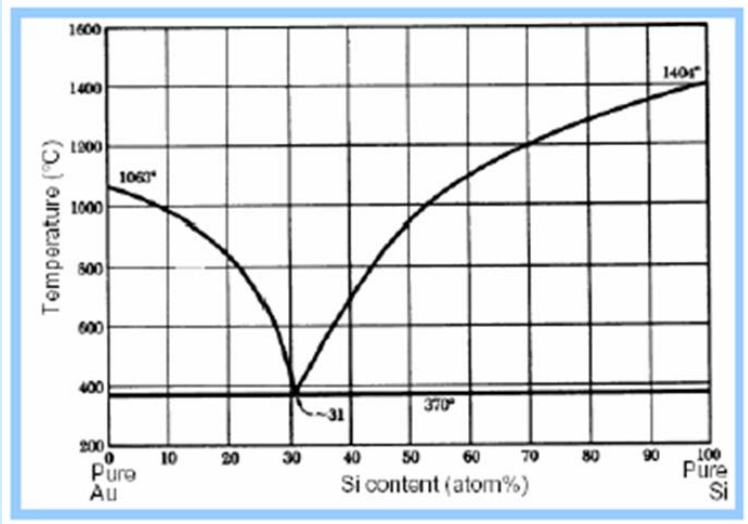

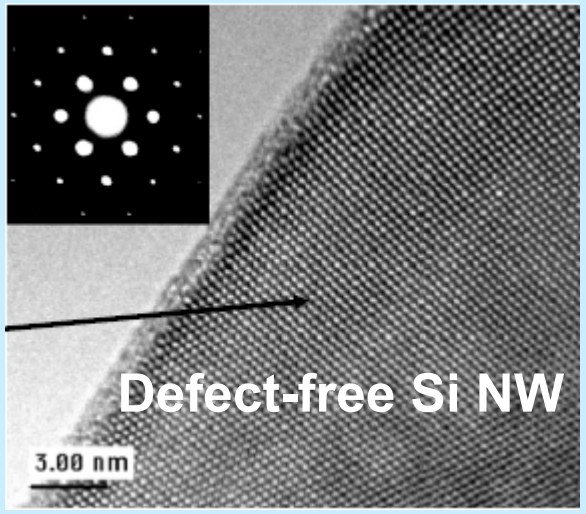

Size Control

Metal particle acts as a soft template to control the diameter of the nanowire

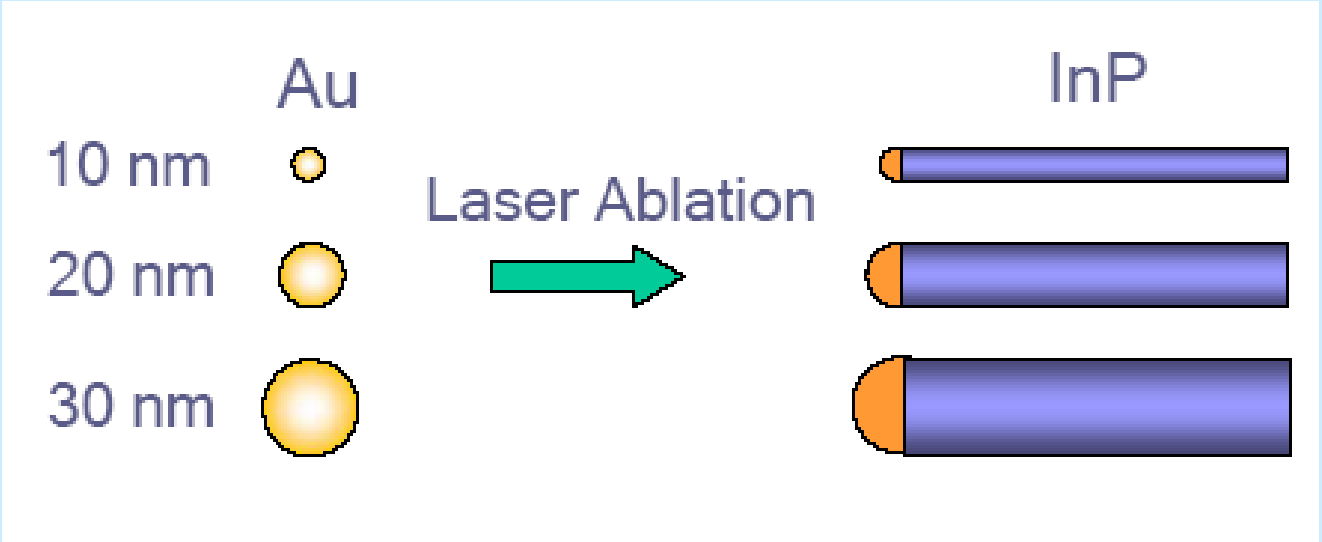

Catalytic Base Growth

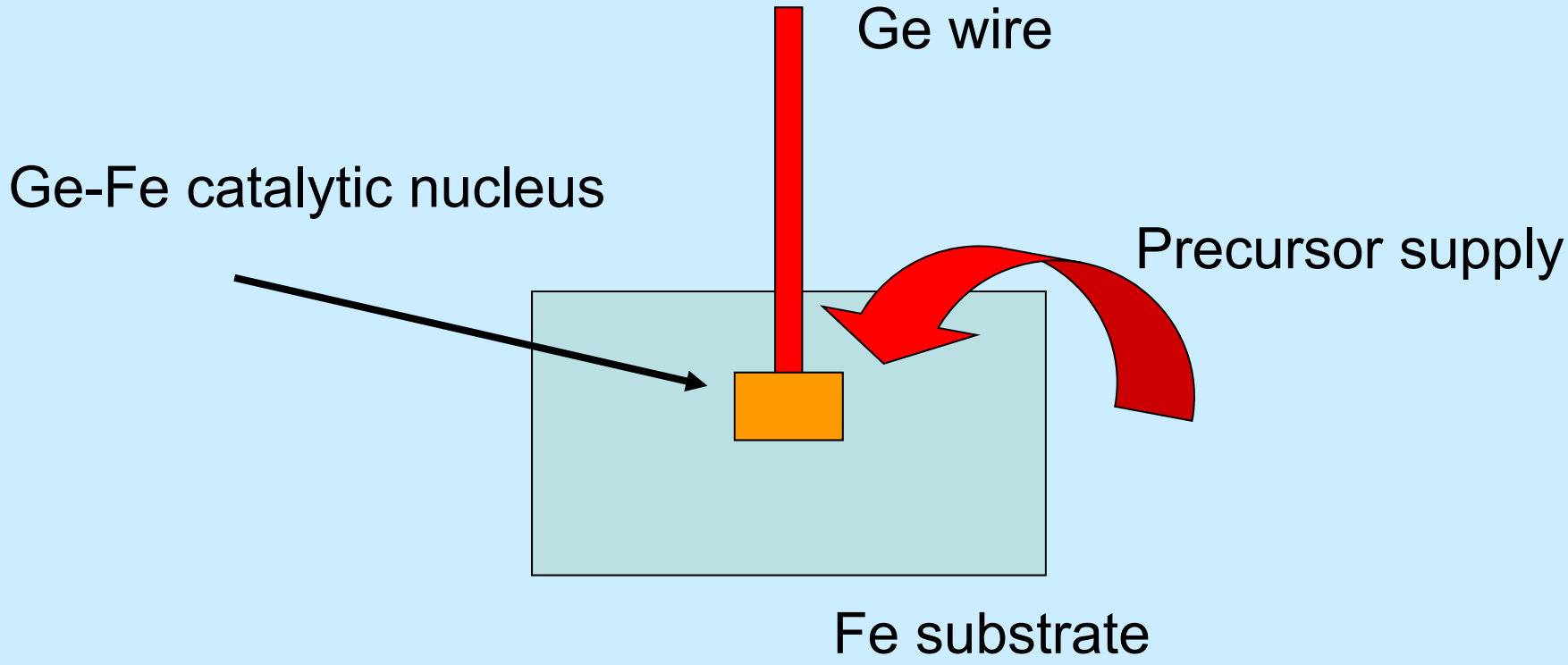

Colloidal Synthesis

Anisotropic shape
1D instability
LaMer mechanism

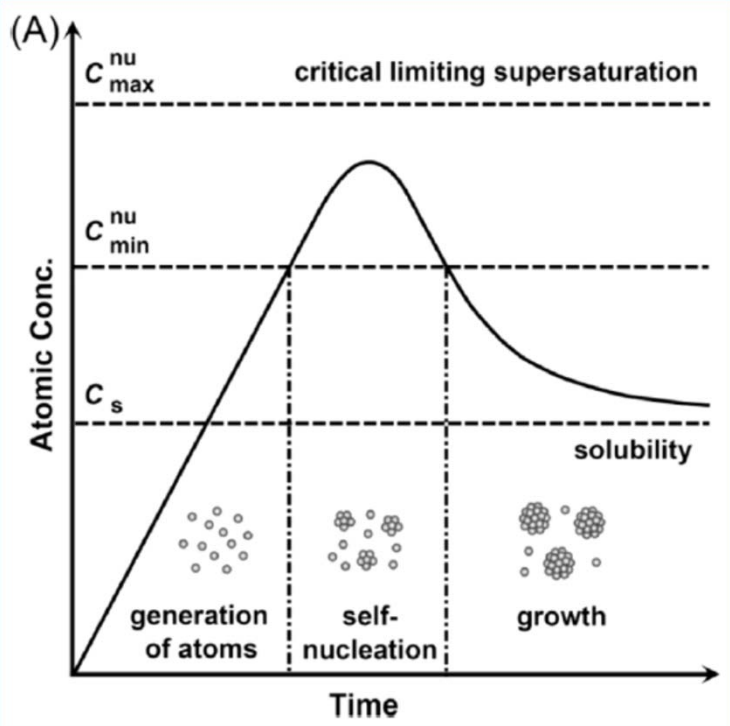

The concentration of atoms increases with time as the precursor is decomposed

The concentration reaches the minimum level of supersaturation, C_{min}, the atoms start to aggregate to generate nuclei and then seeds - homogeneous nucleation

The seeds grow in an accelerated manner because of autocatalysis, the concentration of metal atoms in the solution drops quickly

The concentration drops below the minimum level of supersaturation, no more nucleation

A continuous supply of atoms - decomposition of the remaining precursor, the seeds will grow into nanostructures with increasing sizes until the synthesis is terminated or an equilibrium state is reached between the atoms on the surface of the nanostructures and free atoms in the reaction solution

Colloidal Synthesis

Seeding - heterogeneous nucleation - a much smaller driving force a lower concentration of atoms or a lower reaction temperature) is needed

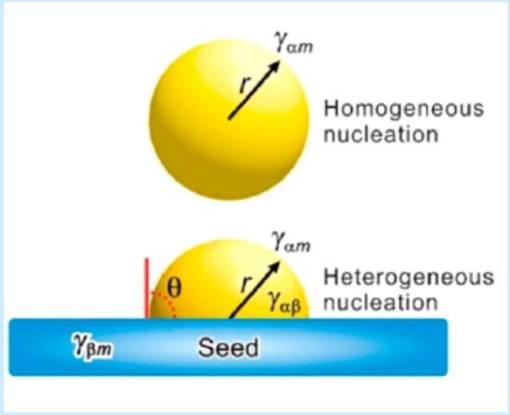

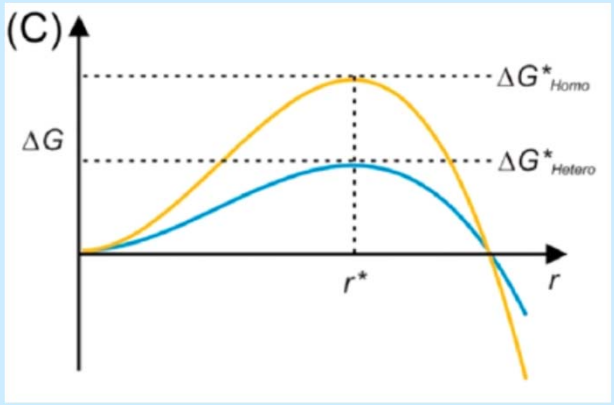

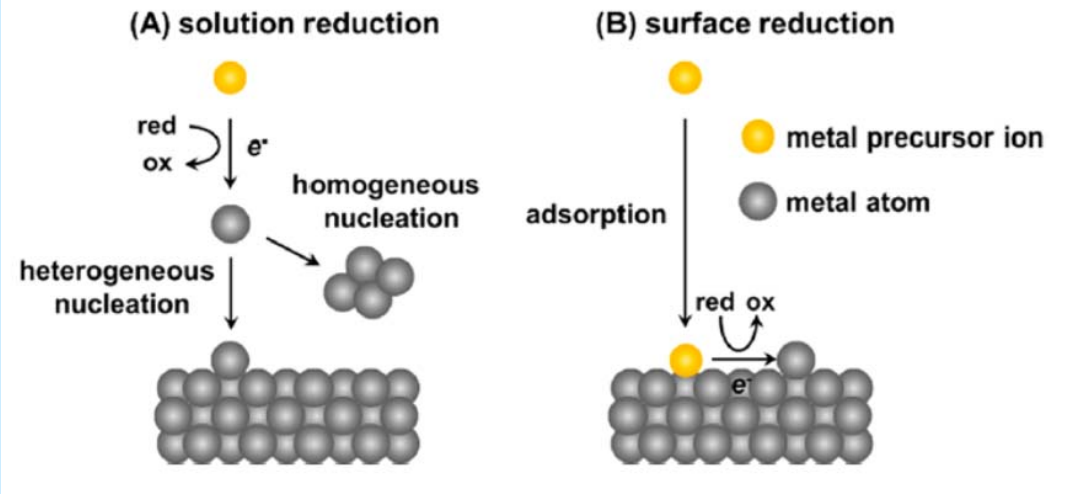

Assembly of Nanoparticles

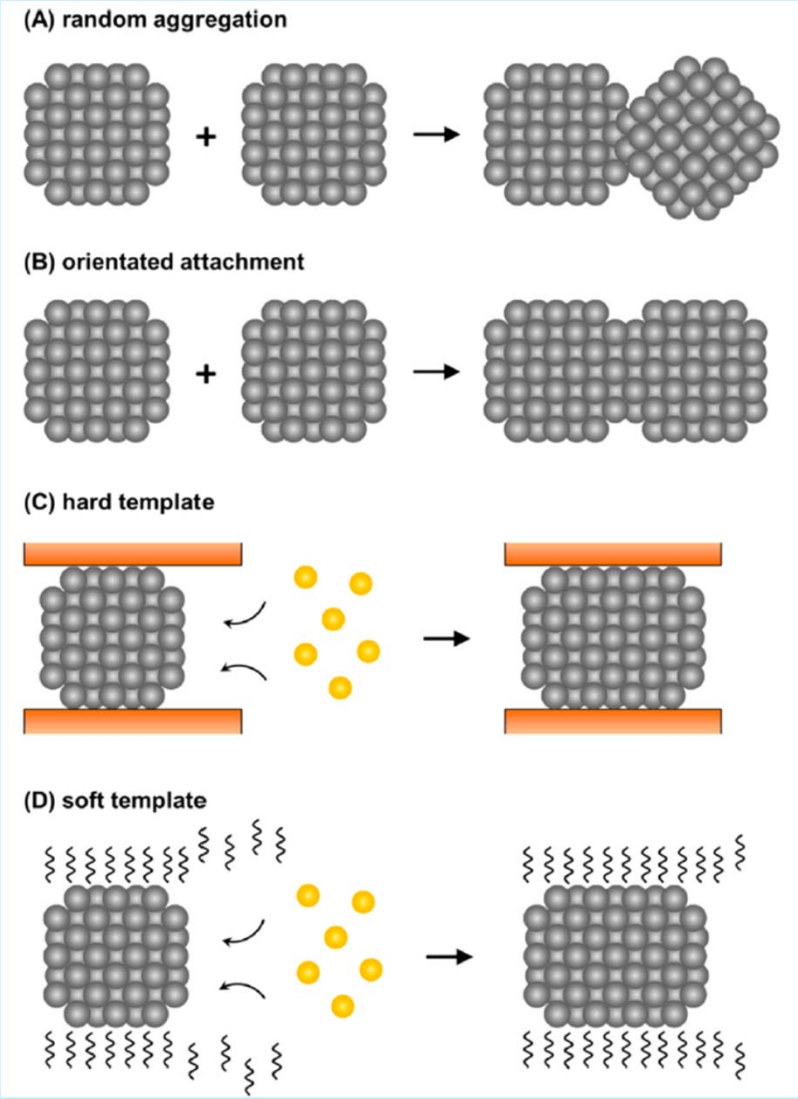

Templated Growth

1. Pores filled with material by CVD

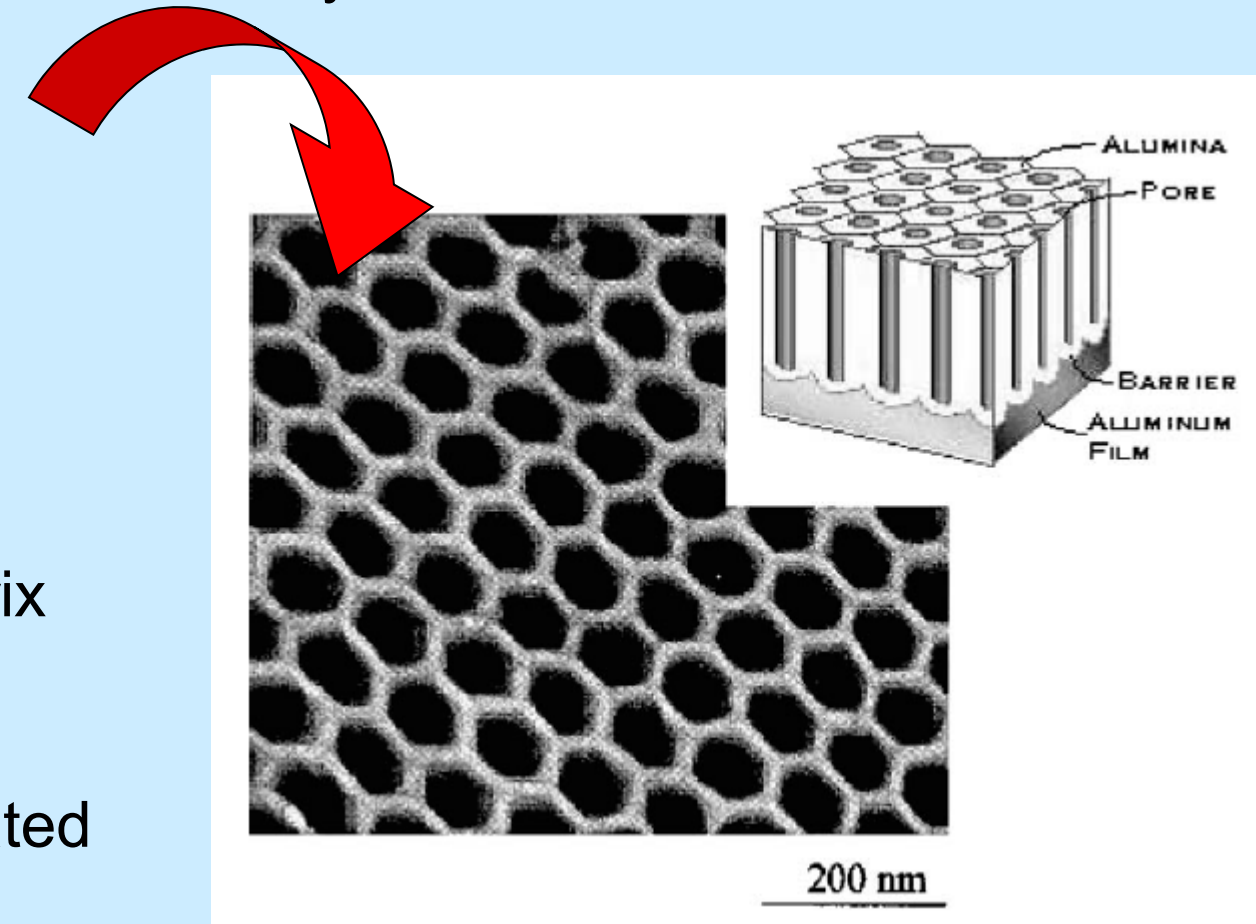

2. Alumina matrix dissolved

3. Wires separated

Arrested Growth

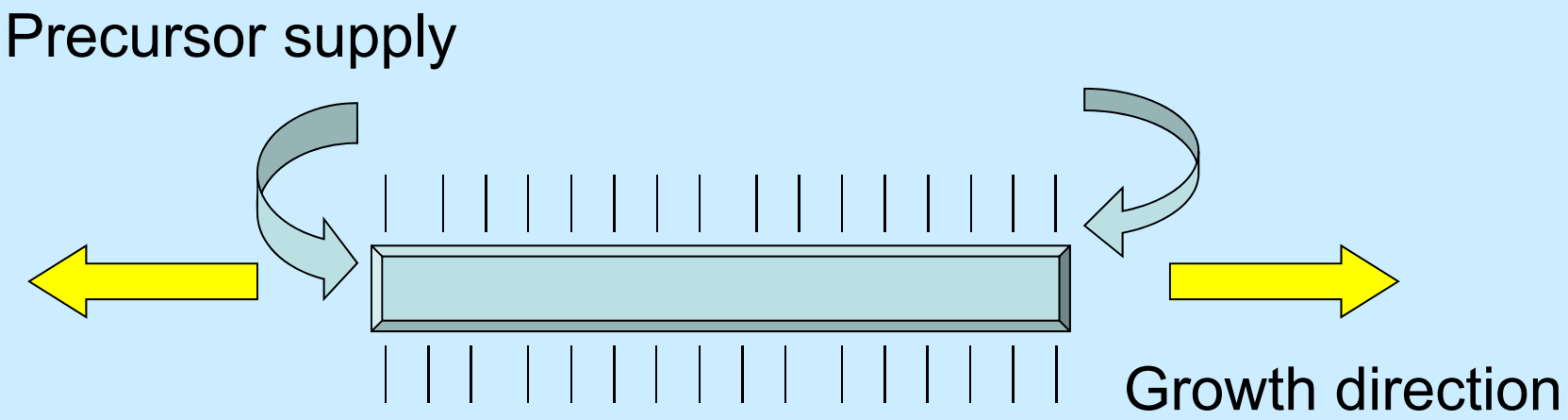

Selective binding of a compound to certain crystal faces

CdTe, TOPO blocks (111)

Alivistos

SLS-growth Mechanism

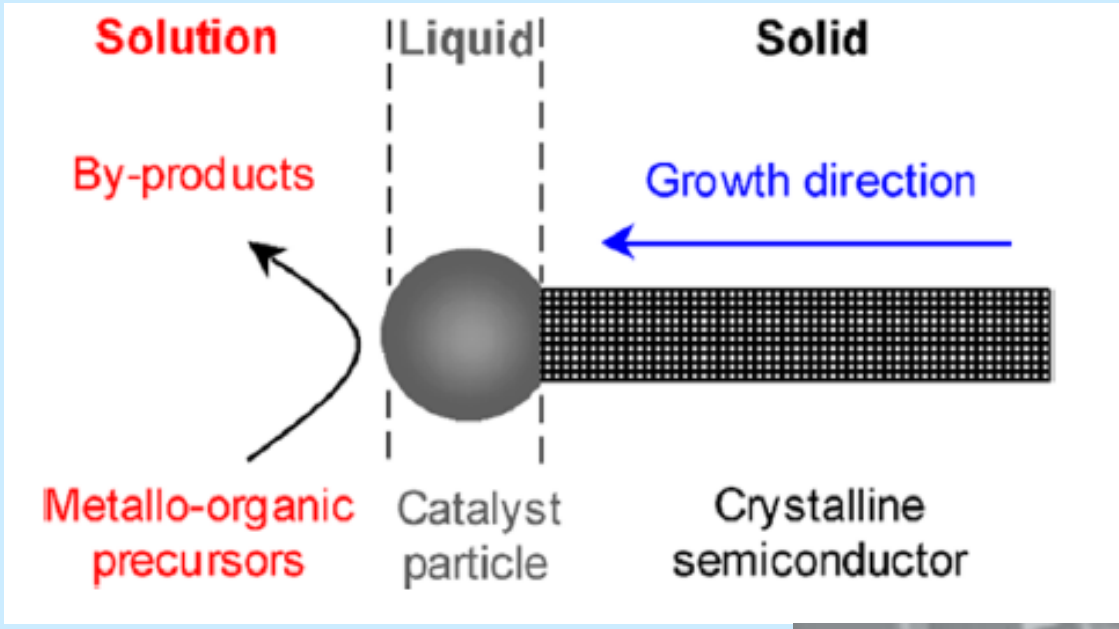

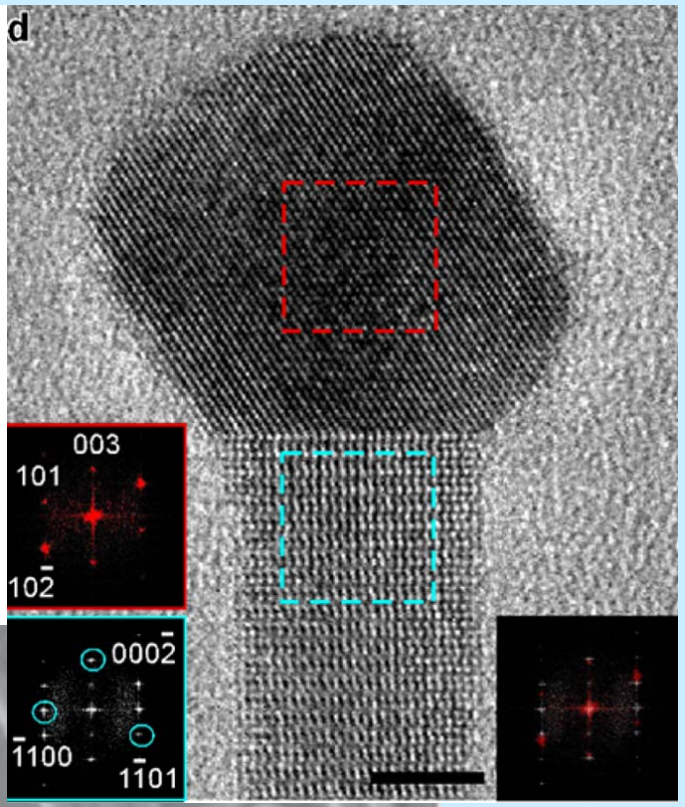

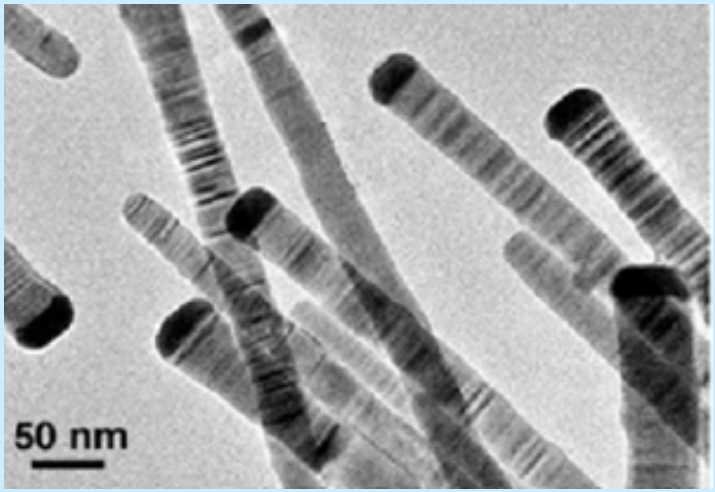

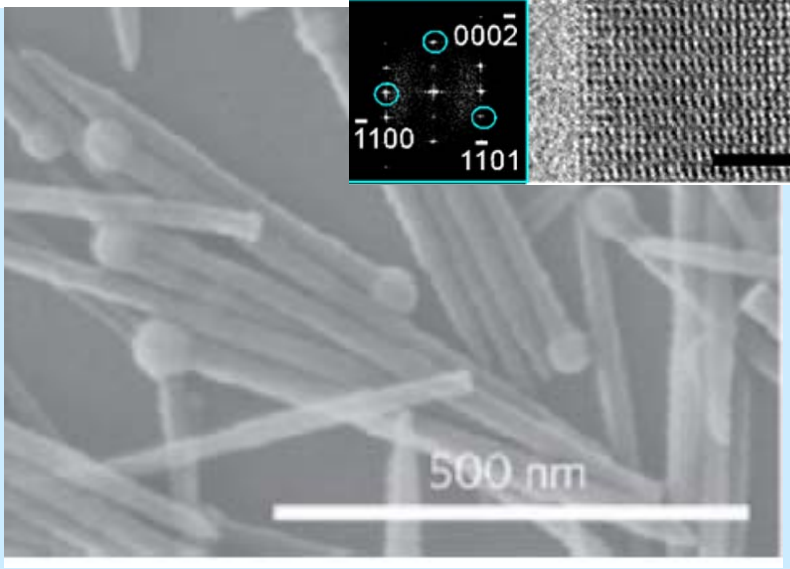

Nanoengine

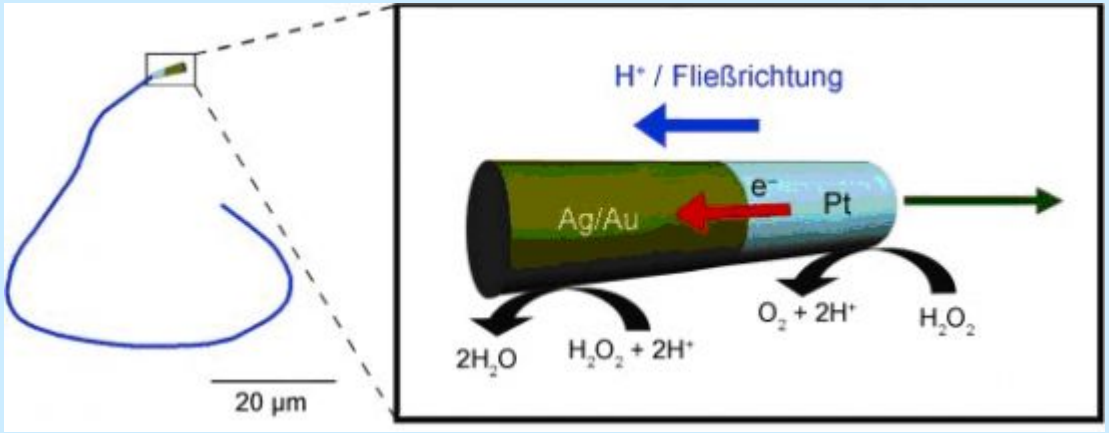

Nanoengine runs on catalytic reactions:

Pt part splits H_2O_2 to O_2 and protons H^+.

Excess electrons move to Ag/Au, reduce H_2O_2 and protons to water.

Release of O_2 causes streaming that propels the engine through the liquid

150 micrometers per second

Joseph Wang UC San Diego and Arizona State

Inorganic NanoTubes INT - MoS_2, WS_2

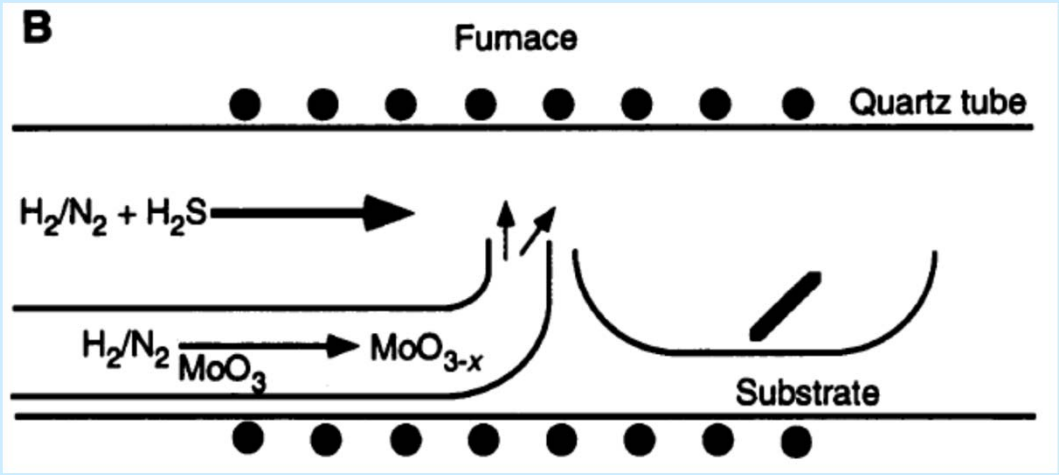

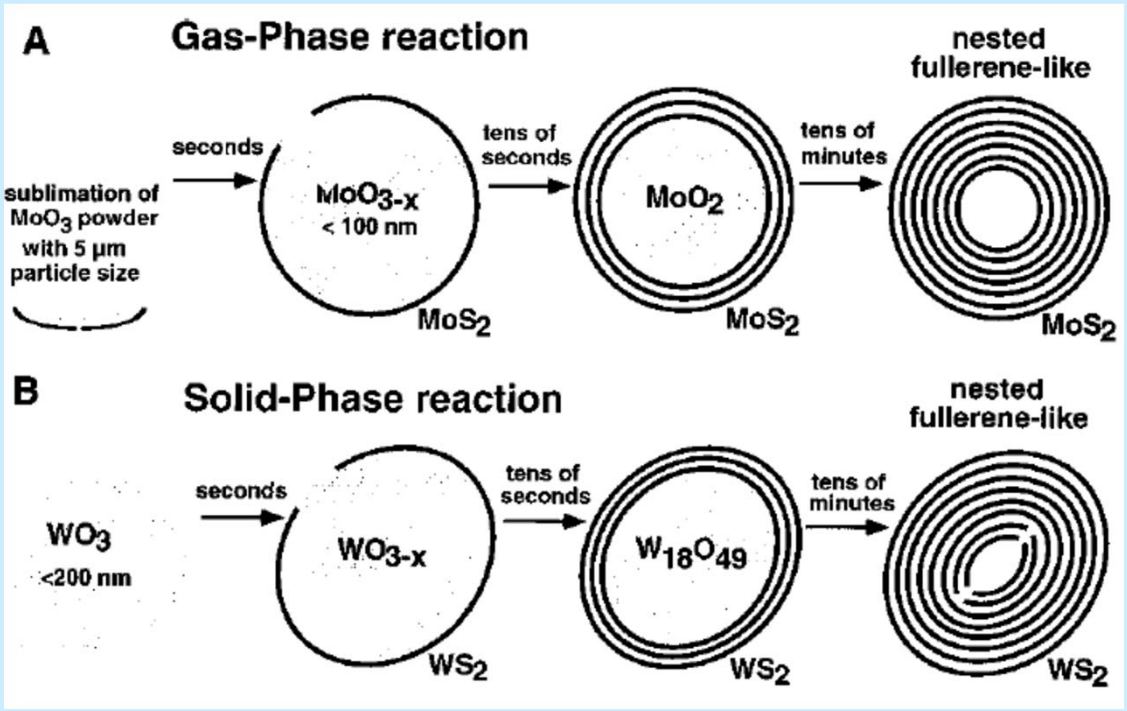

Inorganic NanoTubes INT

$$WO_3 + 2\,H_2S + H_2 \rightarrow 3\,H_2O + WS_2$$

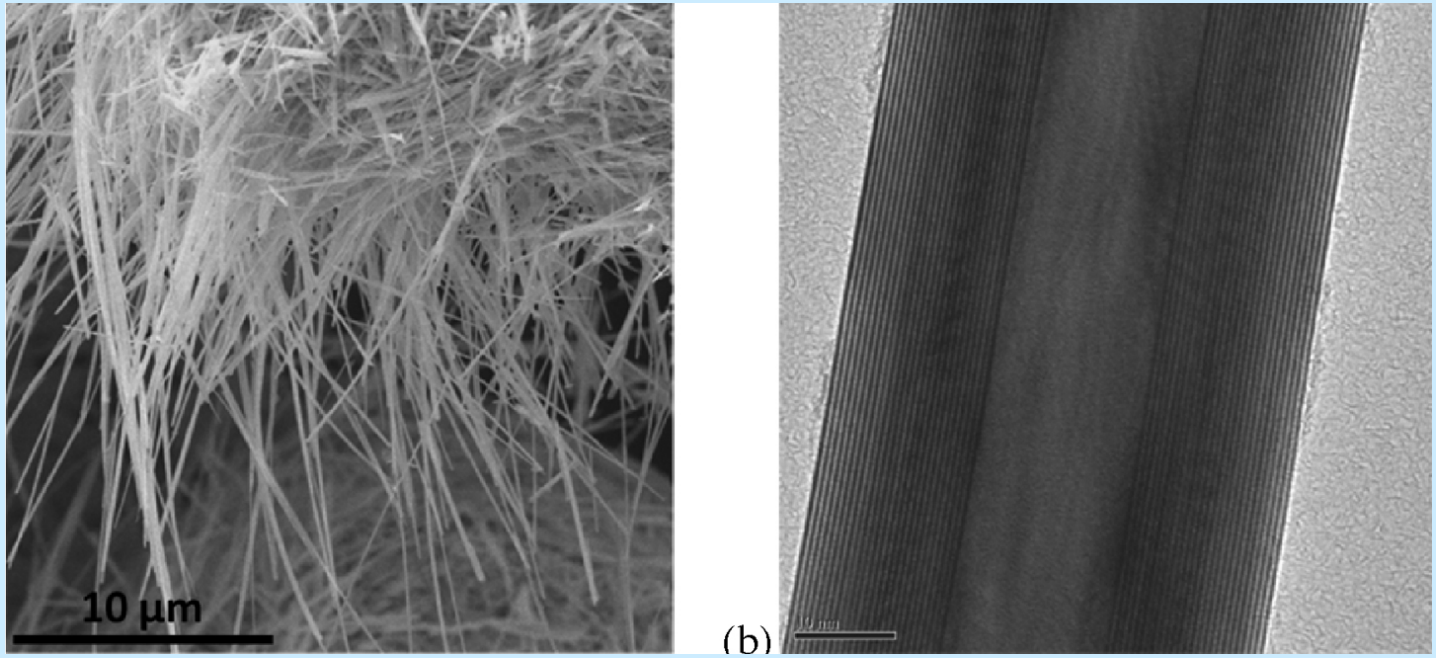

Defect free INT-WS_2; (a) SEM image (b) TEM image (scale bar 10 nm)

ZnO Nanorods

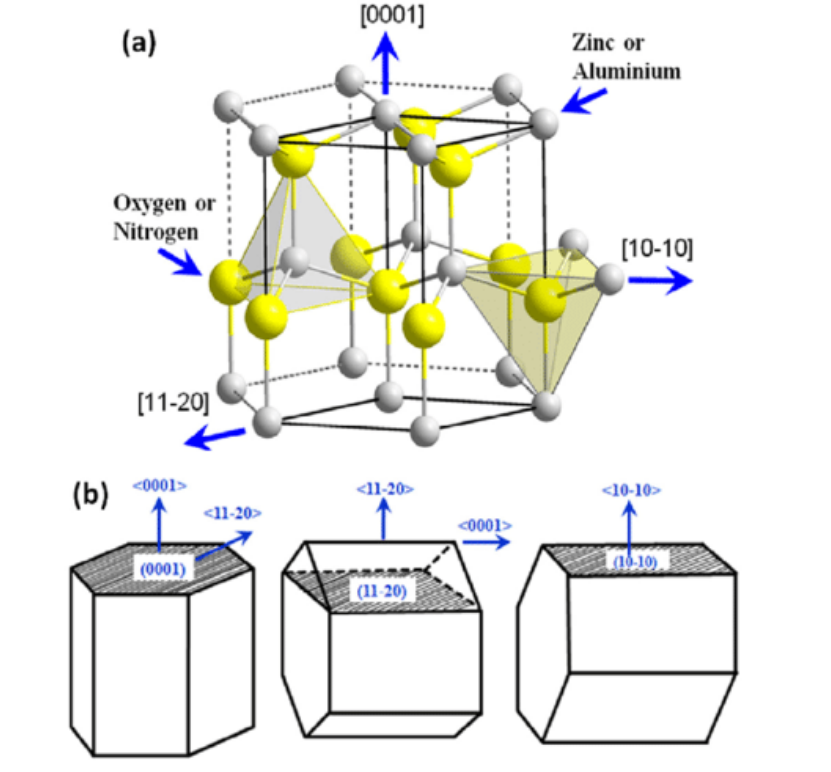

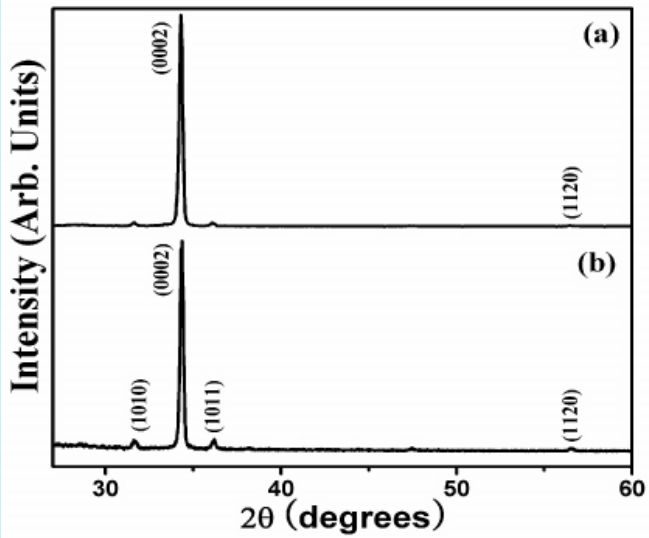

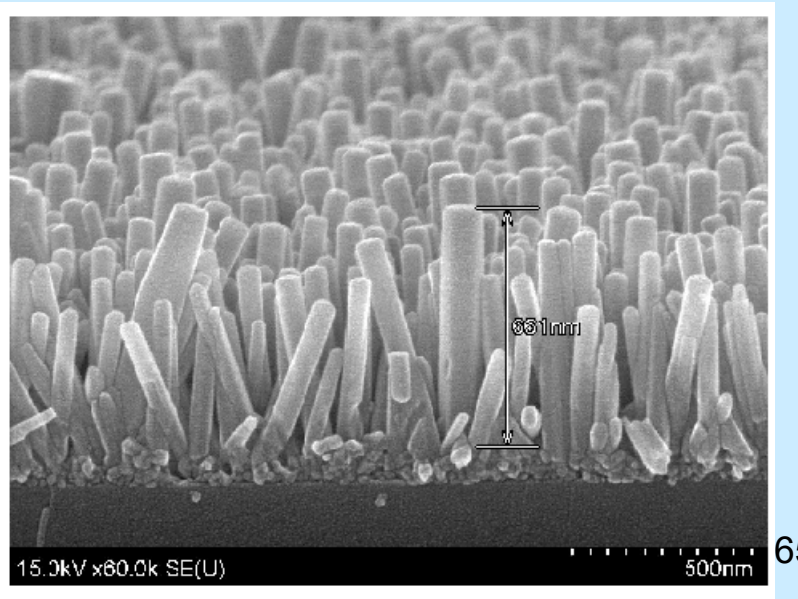

Molecular Rods

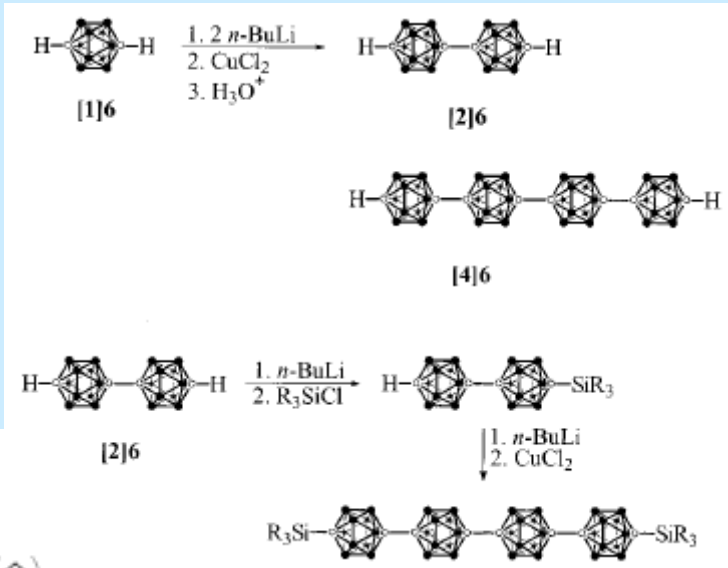

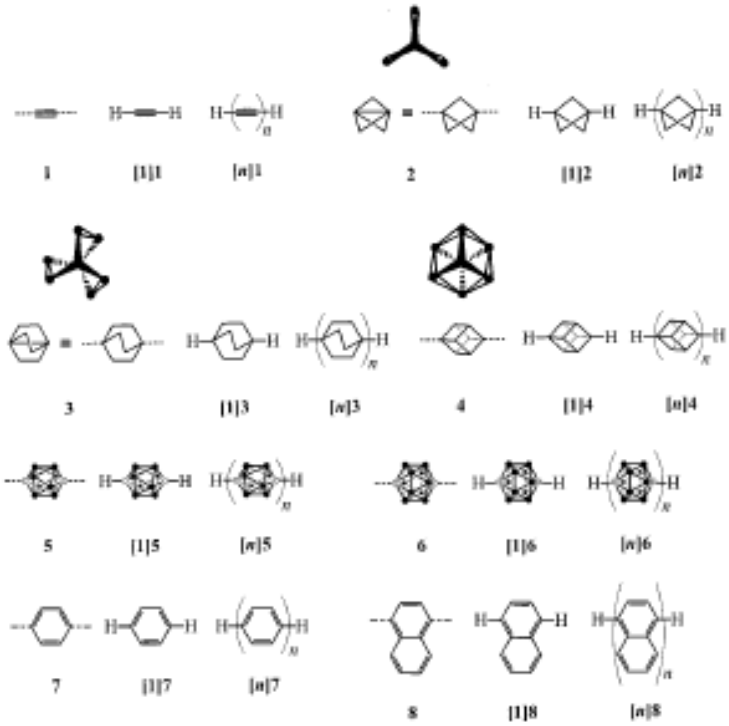

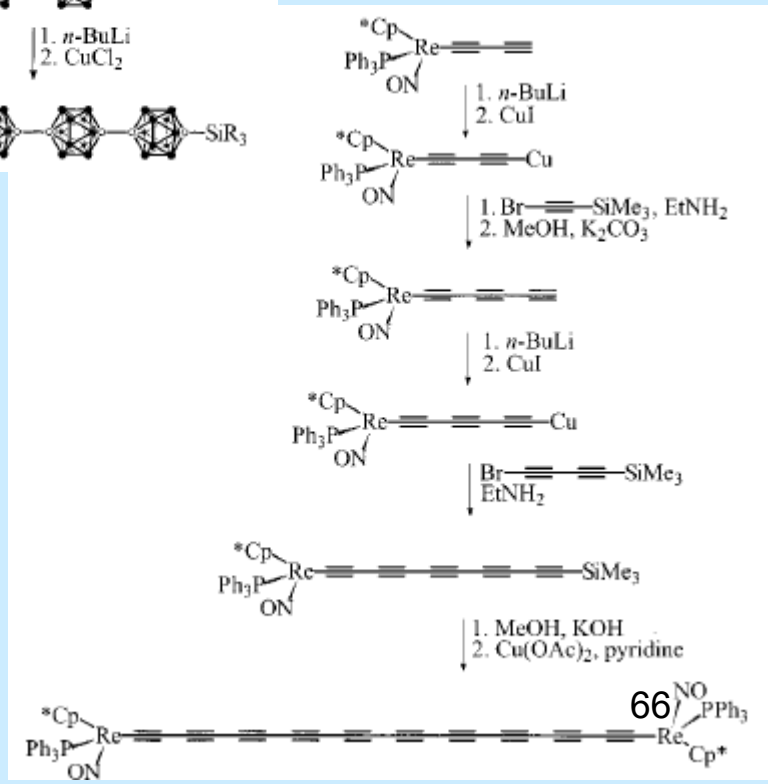

Fibers

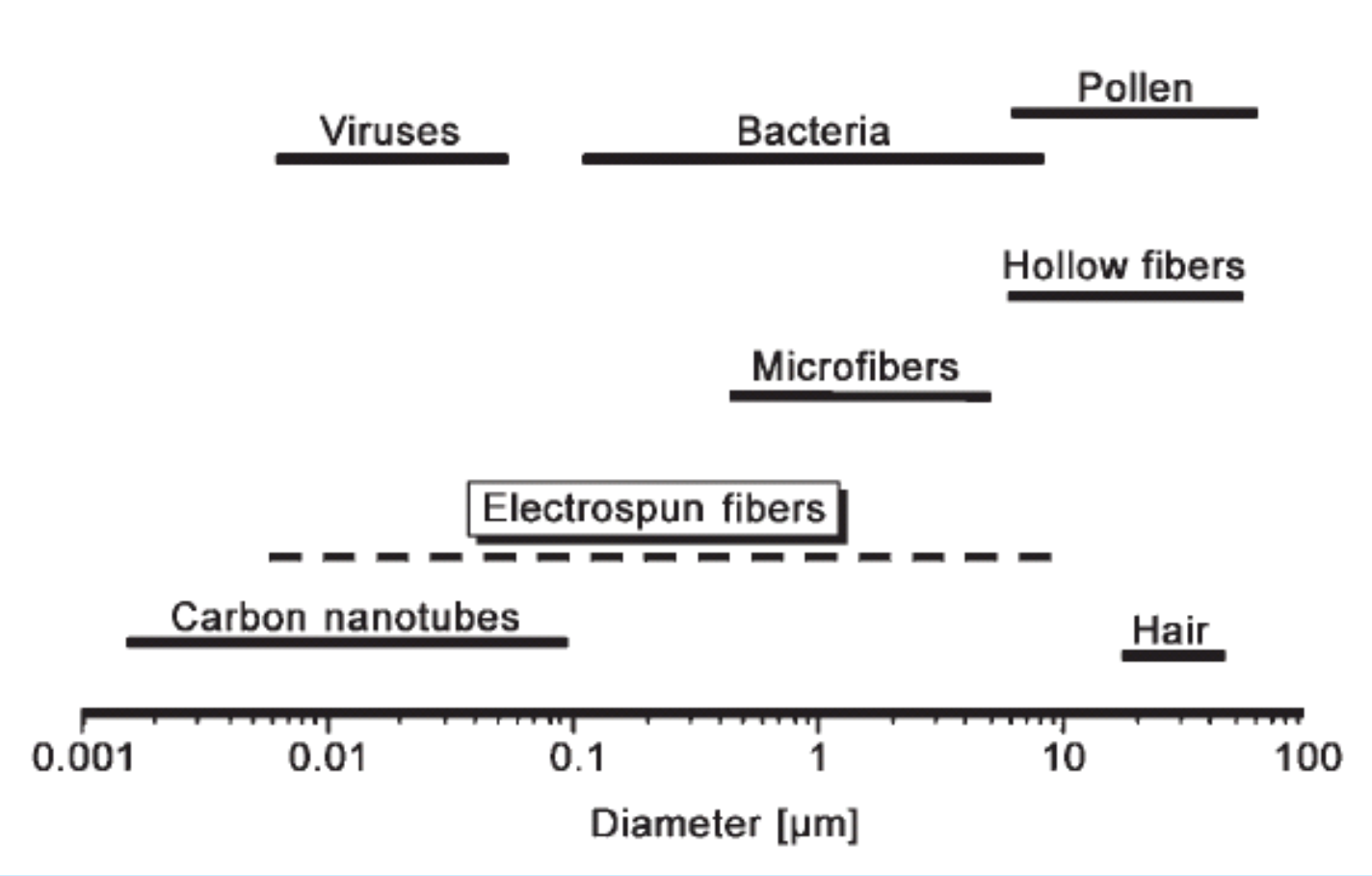
Pollen
Viruses
Bacteria
Hollow fibers
Microfibers
Electrospun fibers
Carbon nanotubes
Hair
0.001
0.01
0.1
1
10
100
Diameter [μm]

Electrospinning

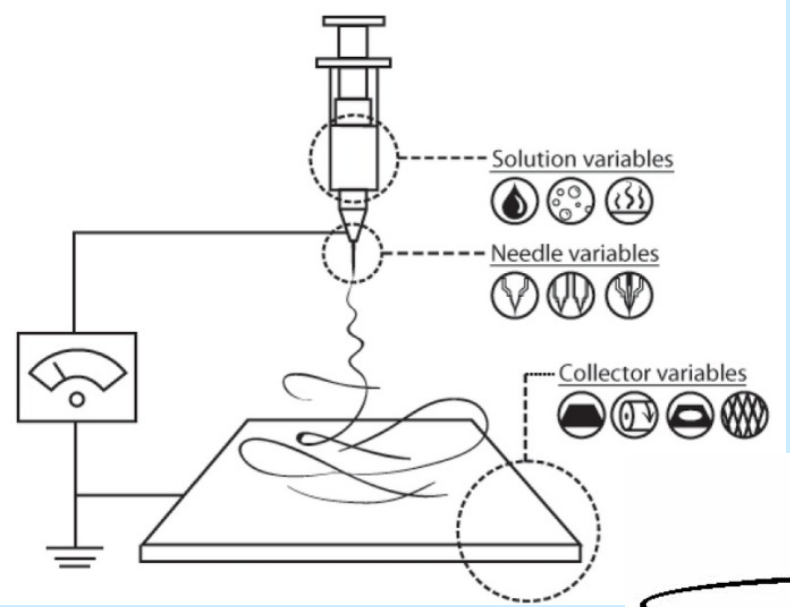

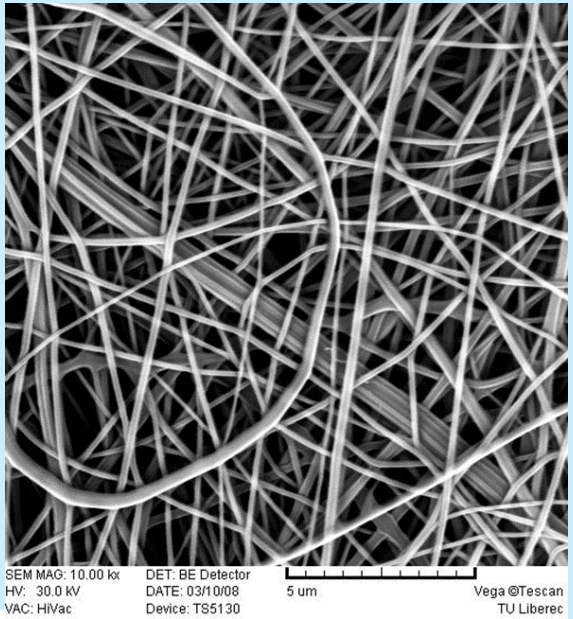

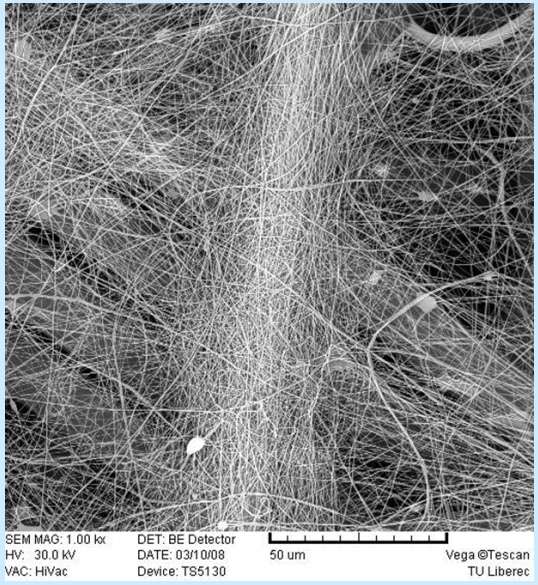

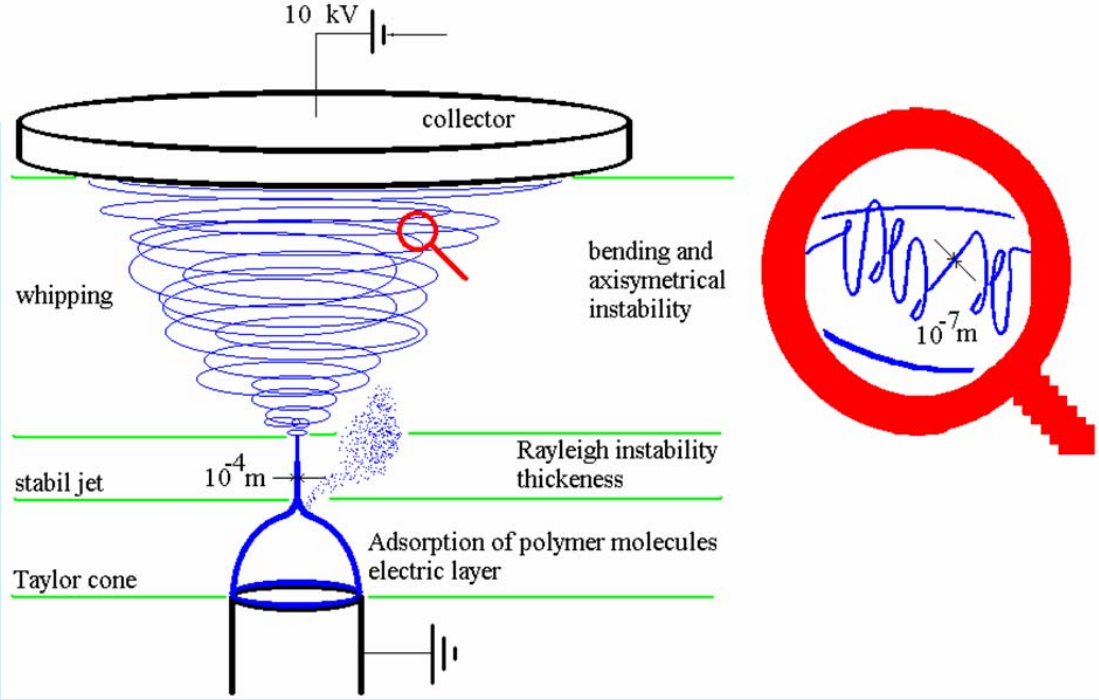

Electrospinning

Electrospraying

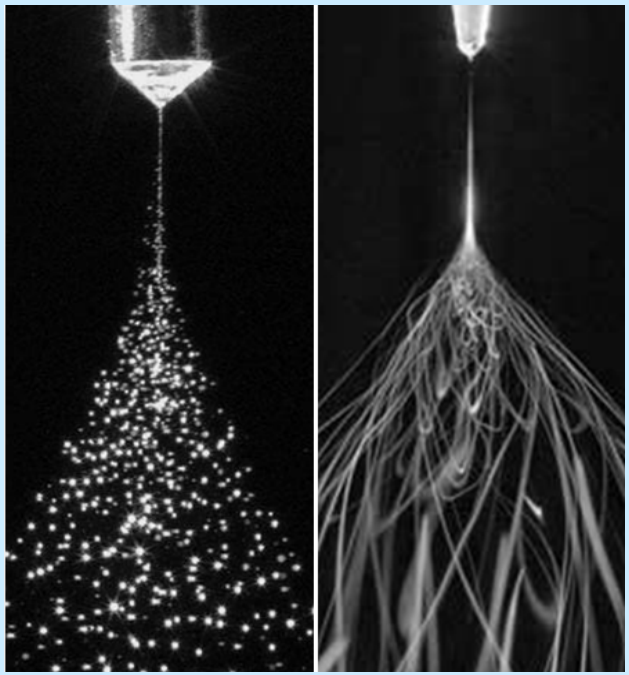

Electrospinning

Parameters:

- Solution (viscosity, conductivity, surface tension)
- Instruments (voltage, distance b/w electrodes, collector shape)
- Ambient (temperature, humidity, atmosphere)

Electrospinning

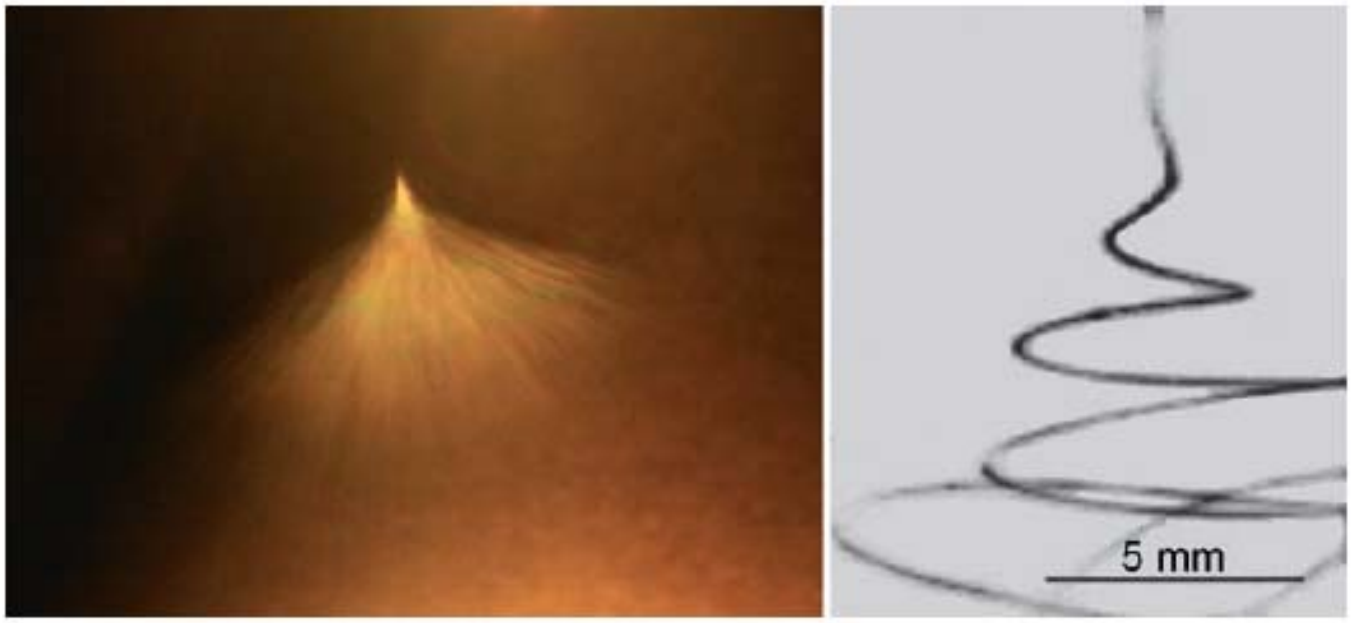

Left: Photograph of a jet of PEO solution during electrospinning
Right: High-speed photograph of jet instabilities

Taylor Cone

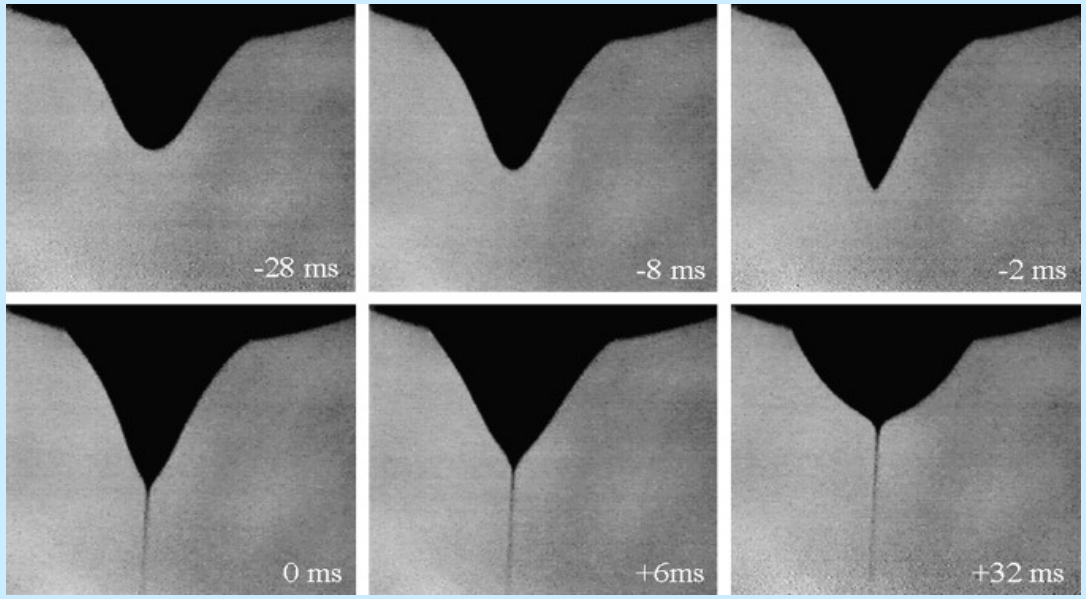

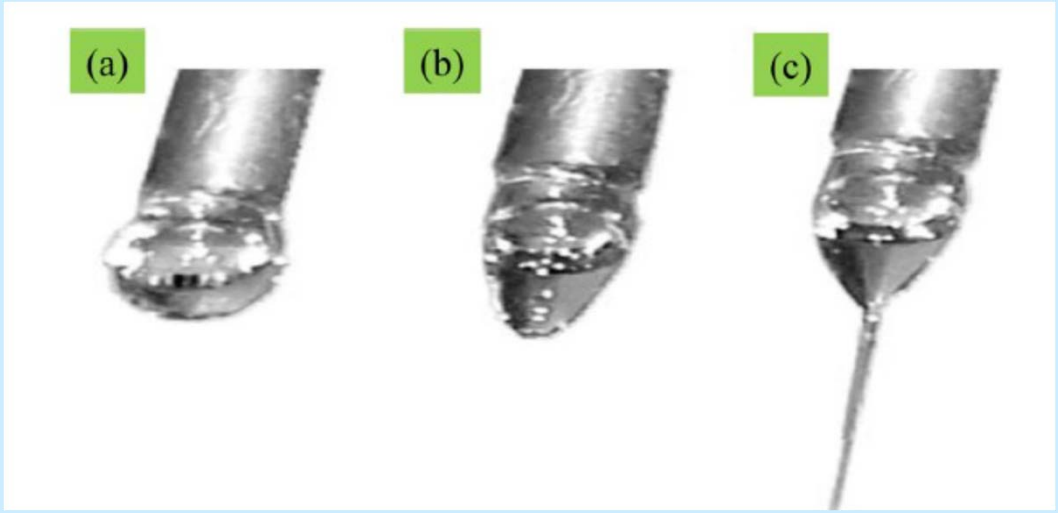






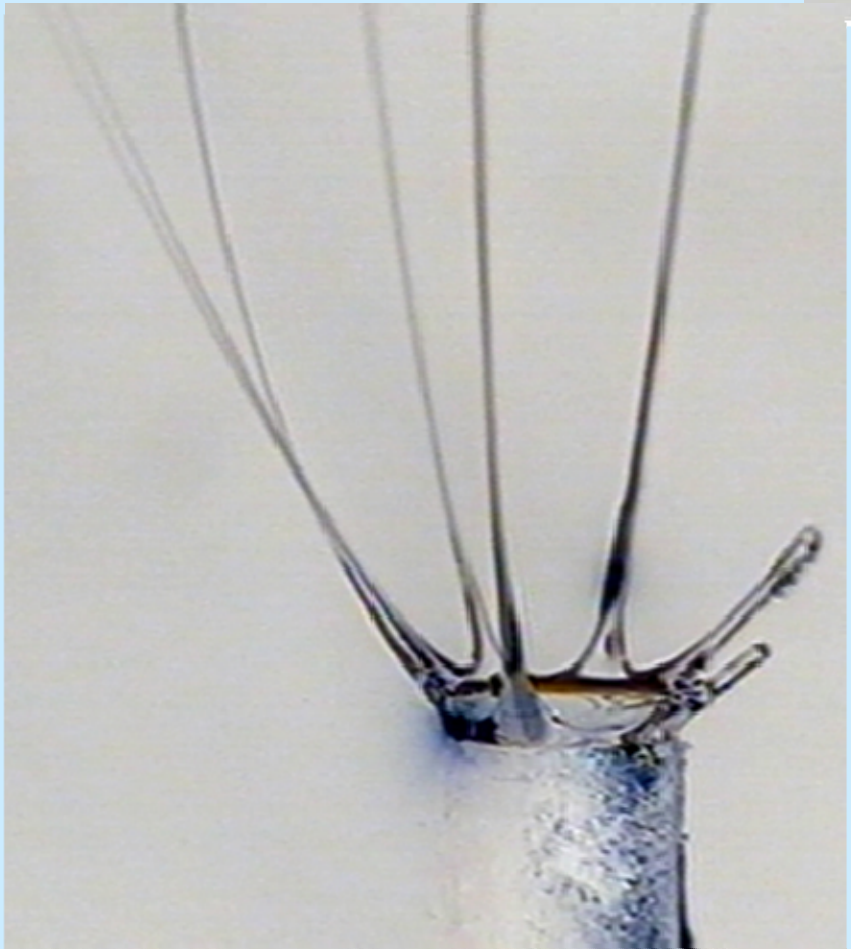

Viscosity

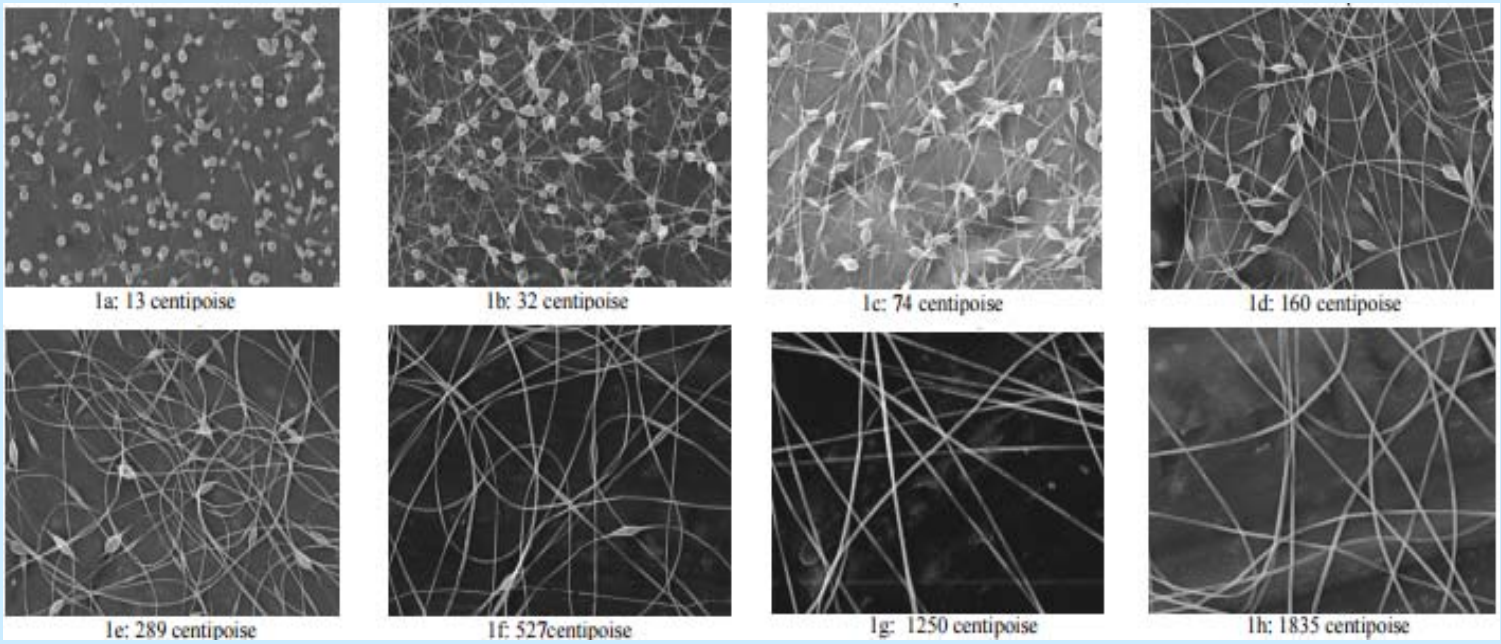
1a: 13 centipoise
1b: 32 centipoise
1c: 74 centipoise
1d: 160 centipoise
1e: 289 centipoise
1f: 527centipoise
1g: 1250 centipoise
1h: 1835 centipoise

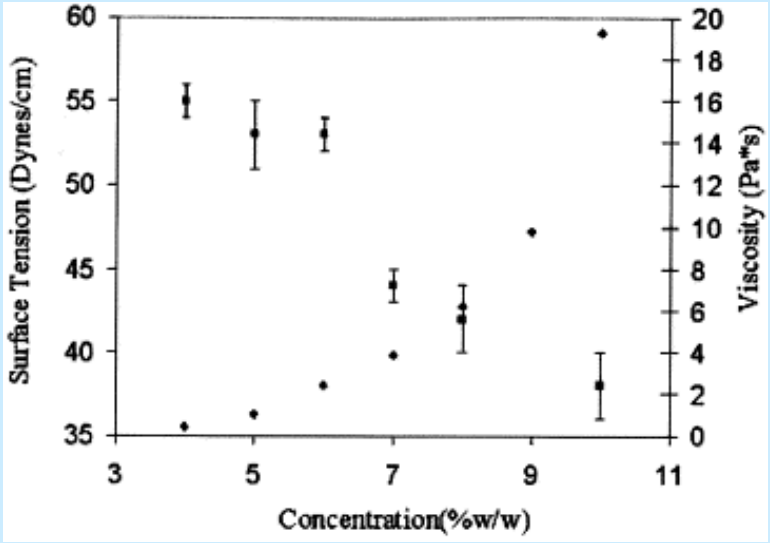
Surface Tension (Dynes/cm)
Viscosity (Pa*s)
Concentration(%w/w)
60
55
50
45
40
35
20
18
16
14
12
10
8
6
4
2
0
3
5
7
9
11

Volume Charge Density

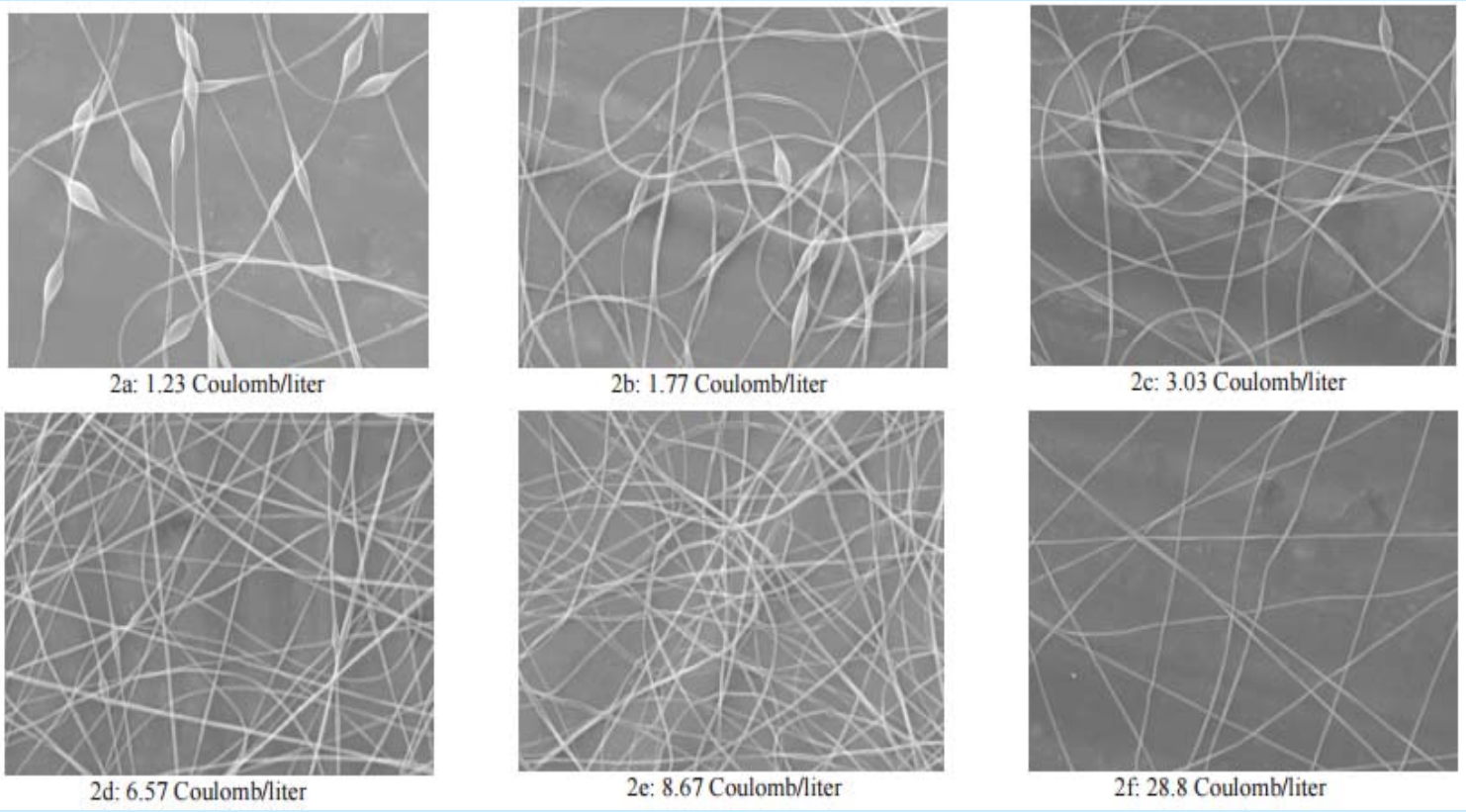

2a: 1.23 Coulomb/liter

2b: 1.77 Coulomb/liter

2c: 3.03 Coulomb/liter

2d: 6.57 Coulomb/liter

2e: 8.67 Coulomb/liter

2f: 28.8 Coulomb/liter

Needle-Collector Distance

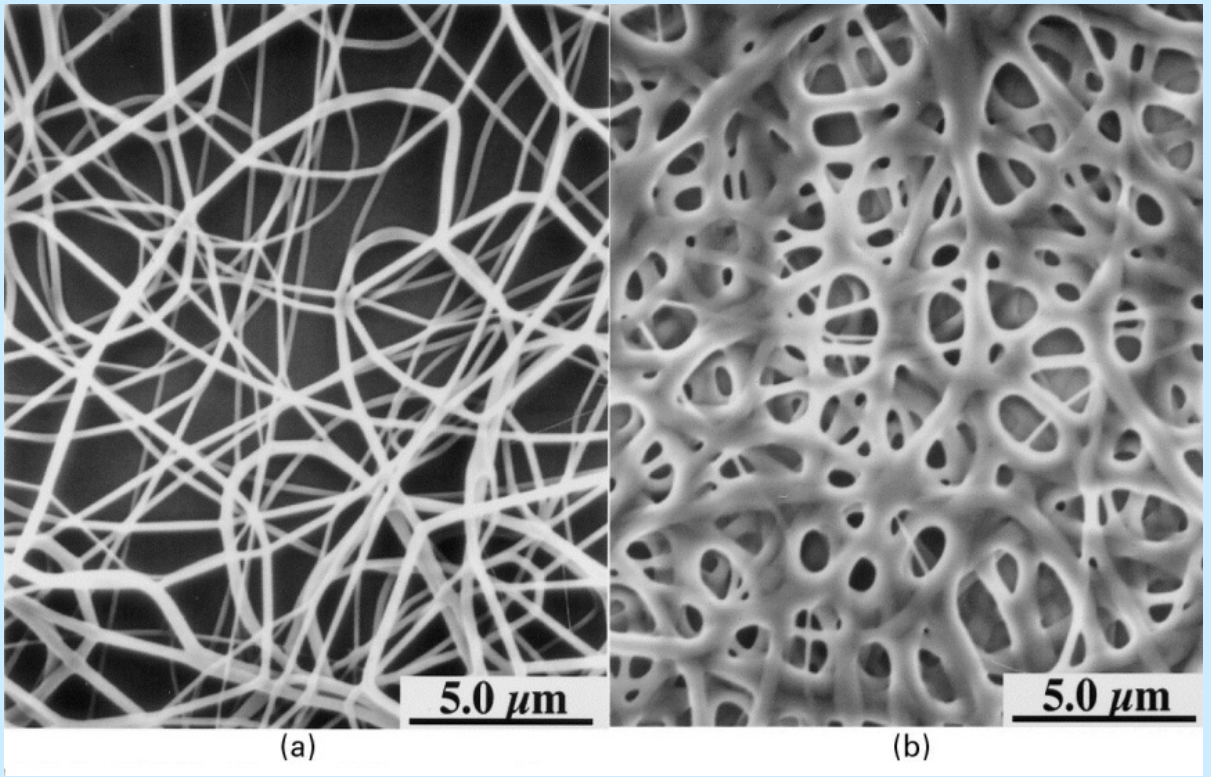

PA fibers, electrode distance 2 cm (a) and 0.5 cm (b)

Conductivity

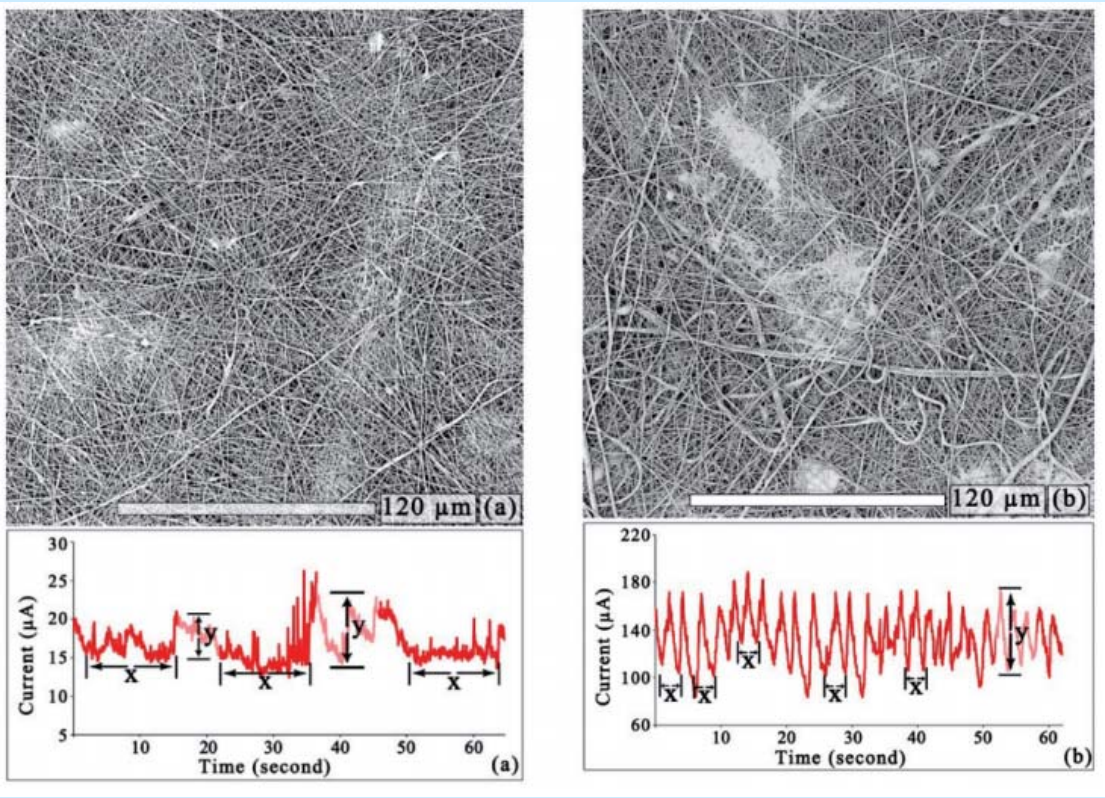

Morphology of fibers as a function of electric current
(a) 20 hm.% PU (b) 20 hm.% PU with addition of 1.27% TEAB

Relative Humidity

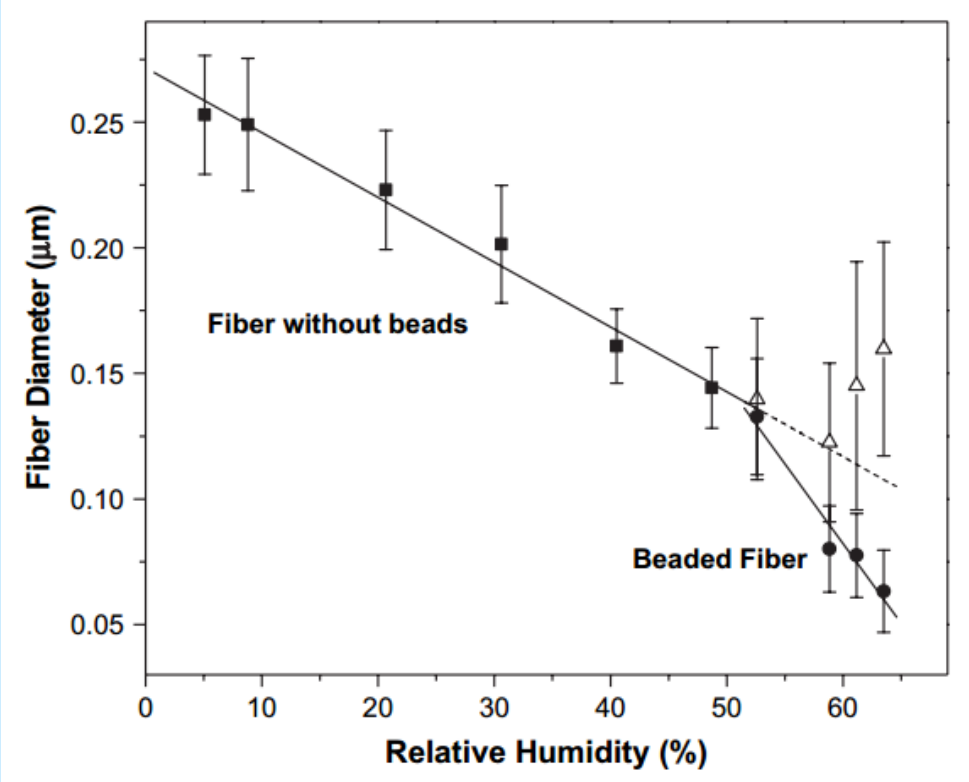

PEO fiber diameter as a function of relative humidity

Coaxial Electrospinning

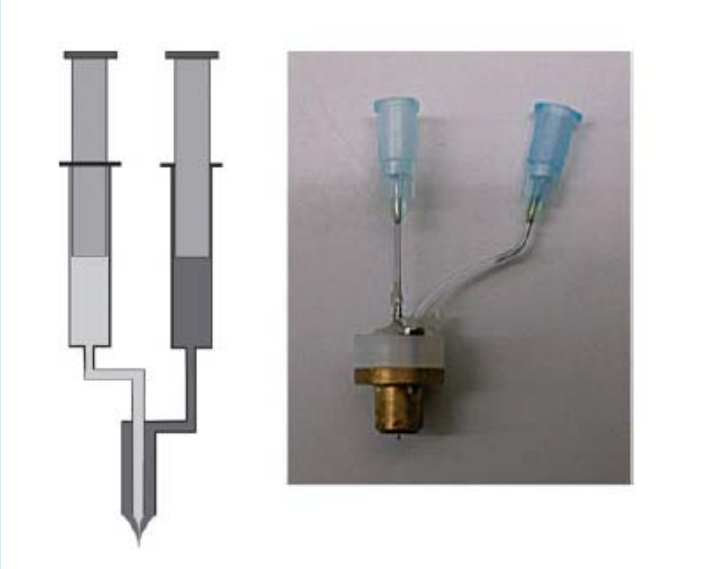

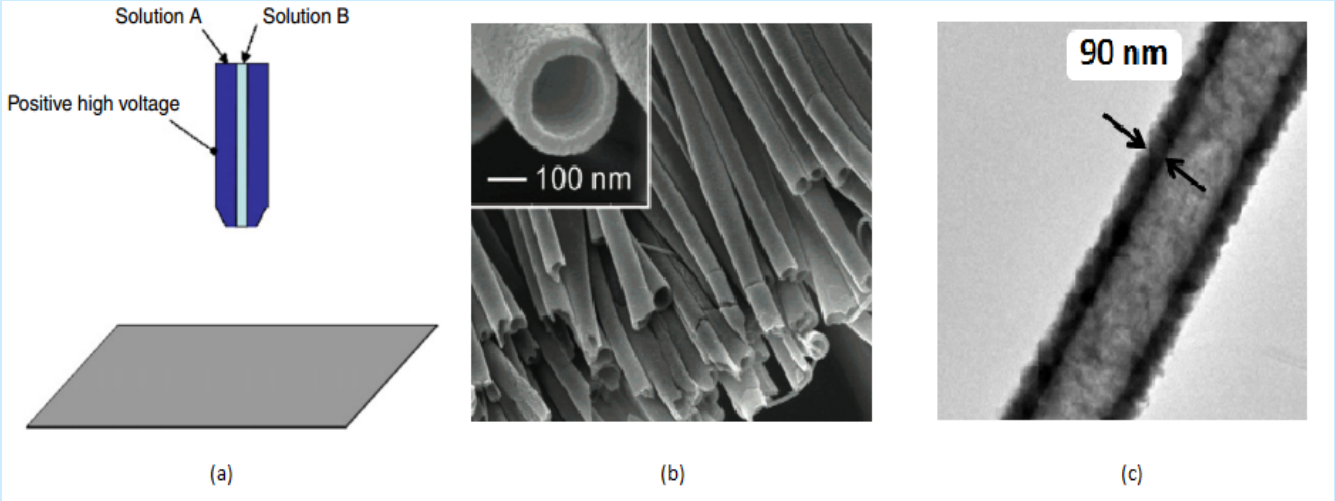

Side-by-Side Electrospinning

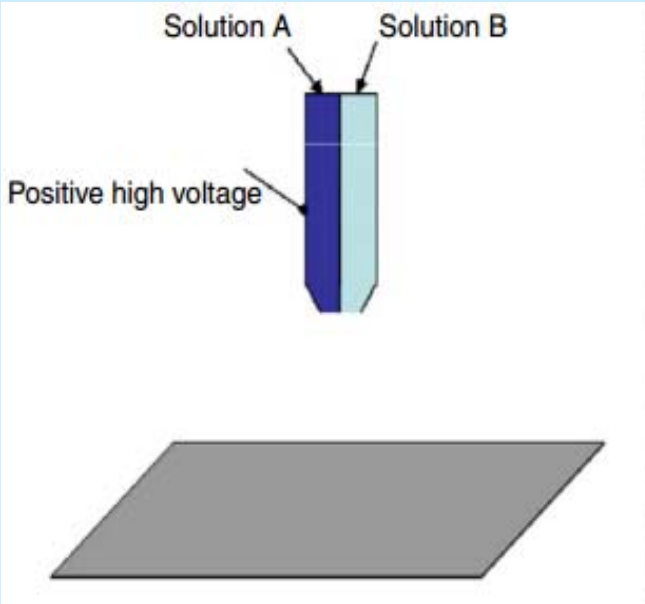

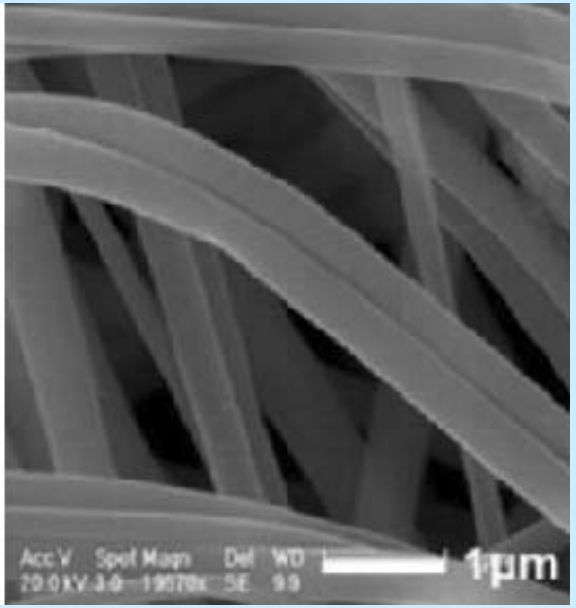

Multijet Electrospinning

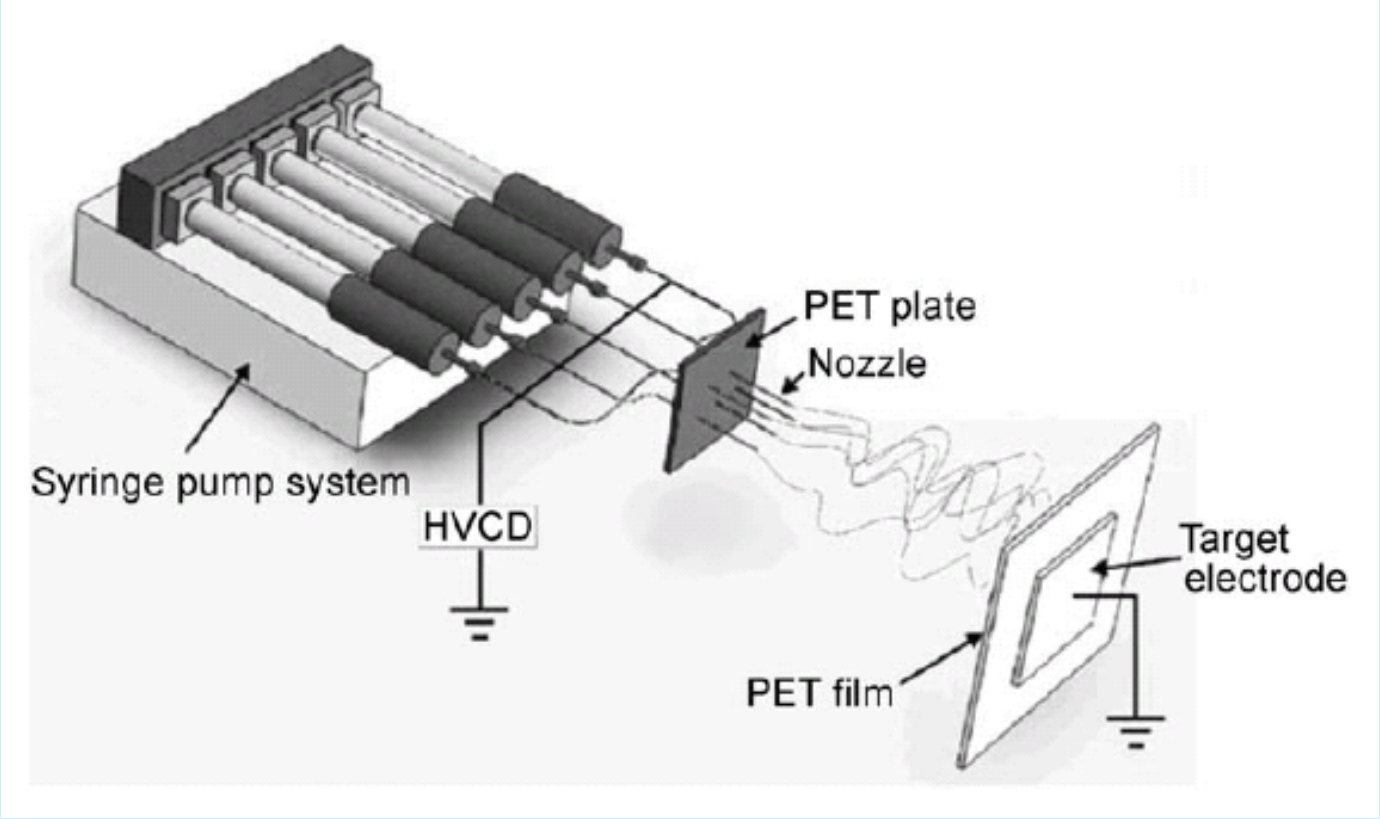

Needle-less Spinning

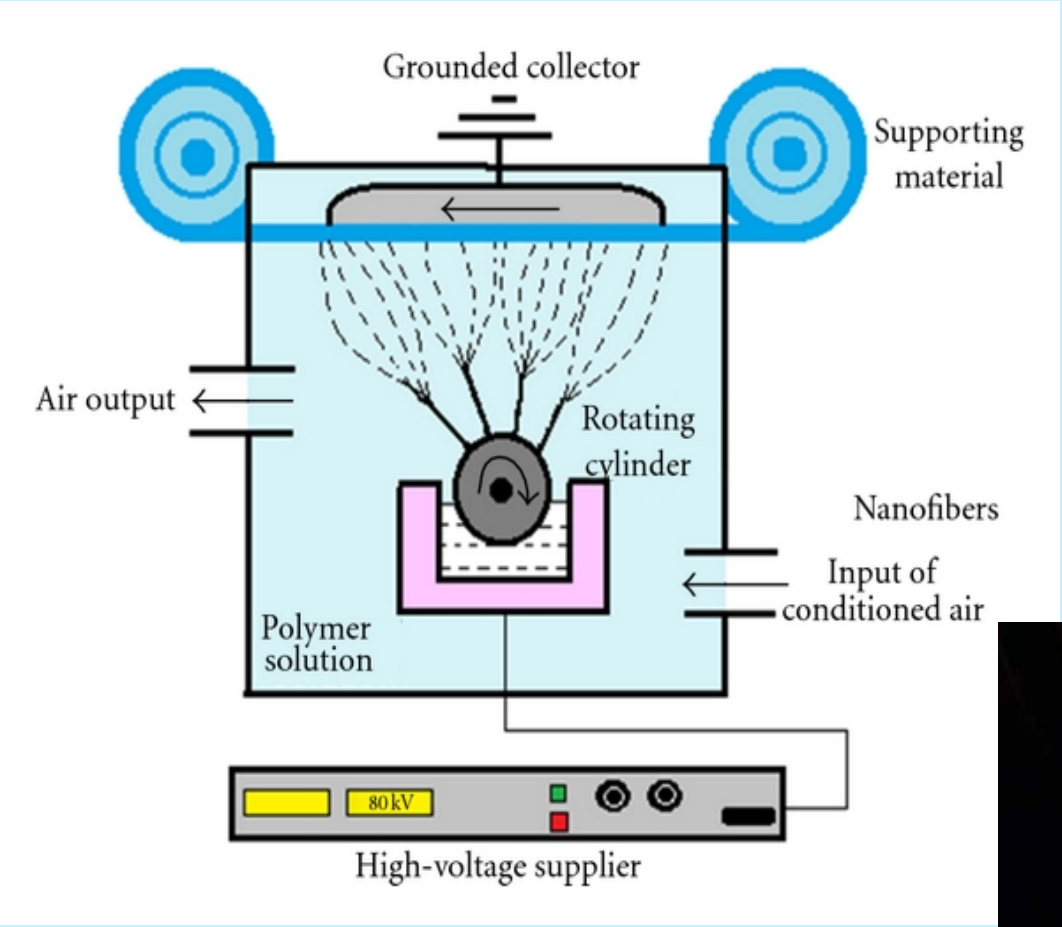

Inorganic Fibers

$Th(acac)_4$; PVP; EtOH; acetone

Electrospinning

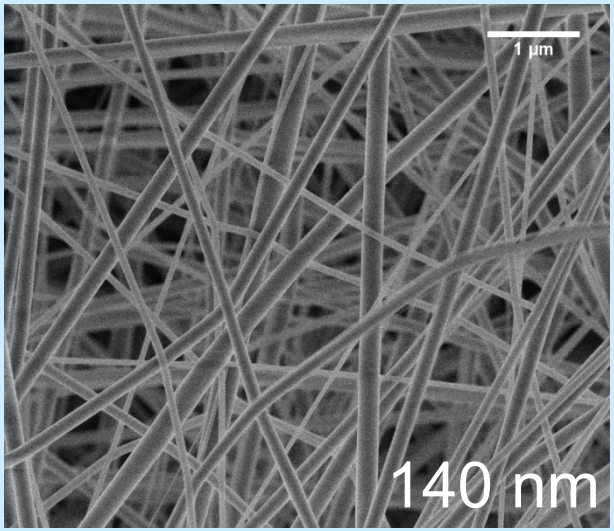

Calcination at 400 °C

ThO_2

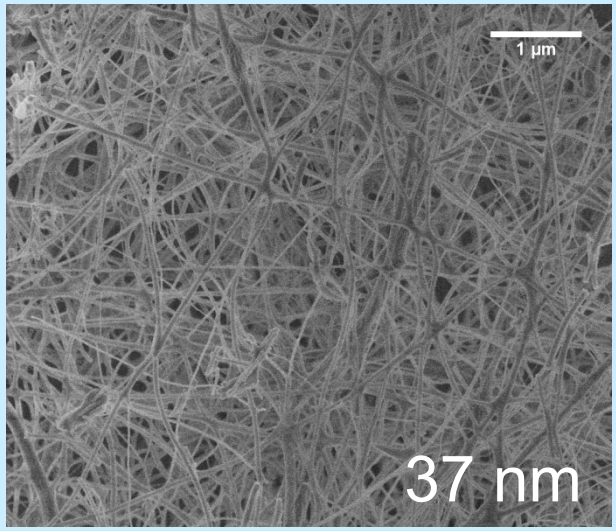

Soft-Templating

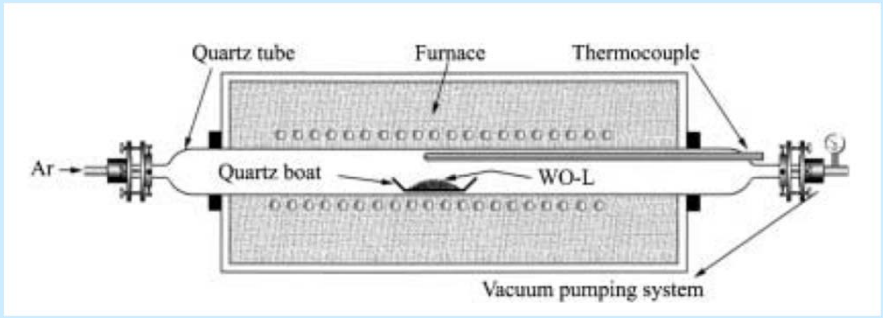

Na_2WO_4 + CTAB – hydrothermal = lamellar mesostructured composite $[CetylMe_3N]^+ WO_4^{2-}$

Pyrolysis and carbothermal reduction in vacuo at 500 - 850 °C

W nanowires - single crystallites grew along the [110] direction

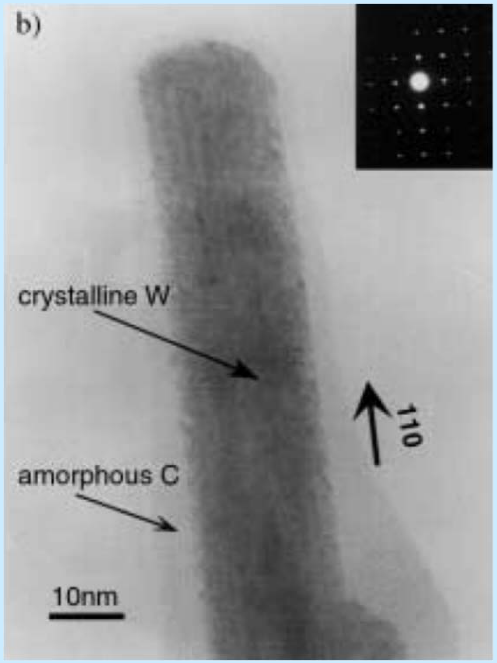

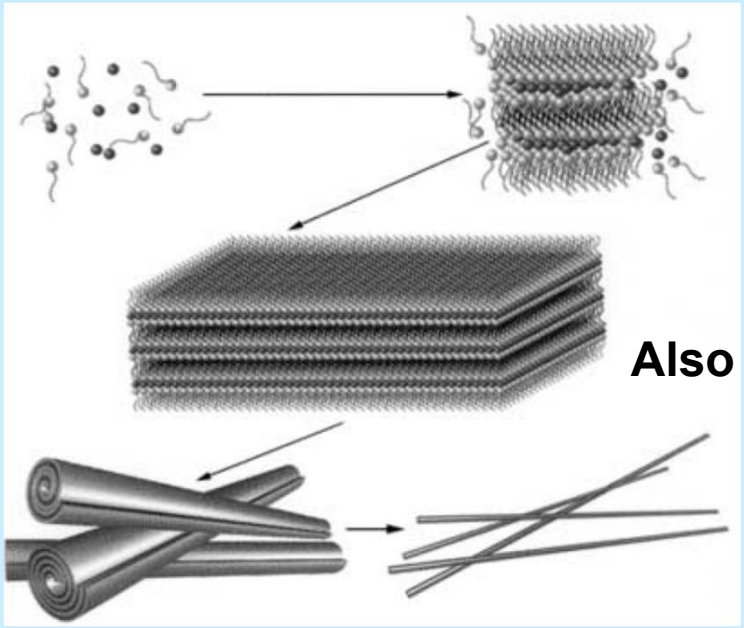

Also Cd, Cu and Co

Hard-Templating

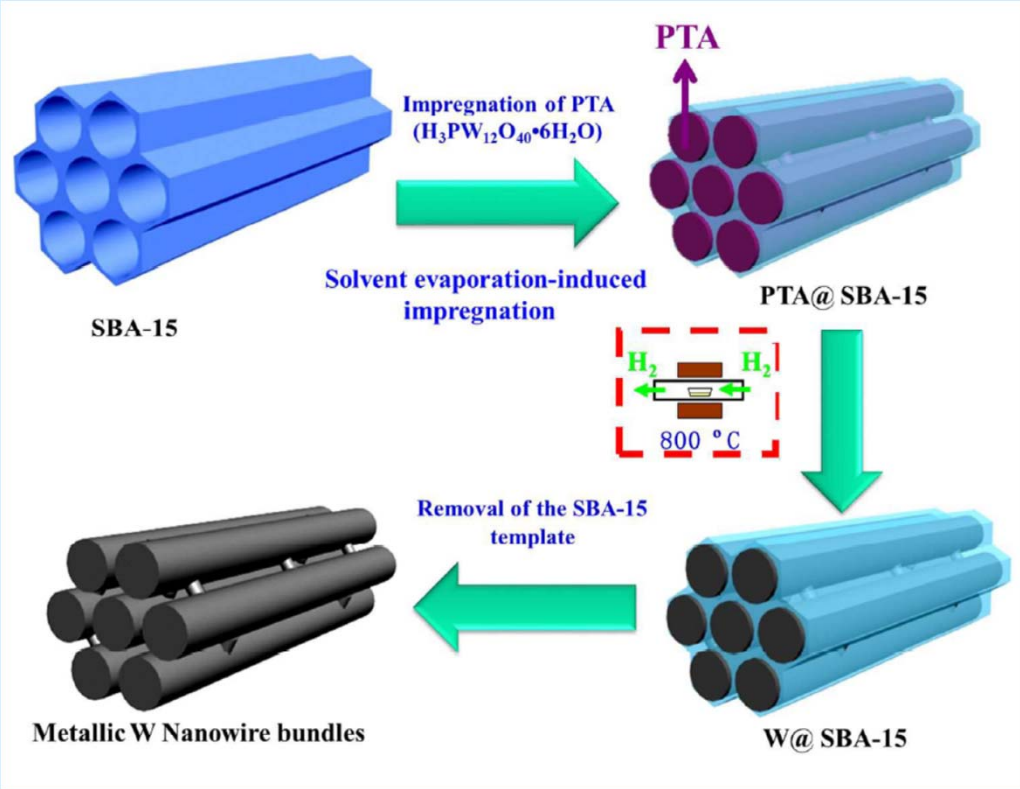

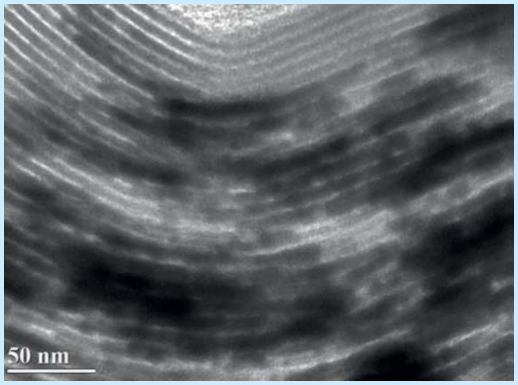

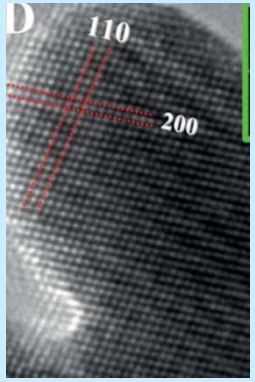

Phosphotungstic acid ($H_3PW_{12}O_{40}.6H_2O$, PTA) precursor is completely filled into the mesochannels of SBA-15 via a solvent evaporation-induced impregnation

H_2 as a reducing agent at a temperature of 800 °C for 3 h

Etching the SBA-15 template with HF 5% aqueous

Hard-Templating

Tobacco mosaic virus (TMV)
the first virus discovered

Inner diameter 4 nm
Length 300 nm

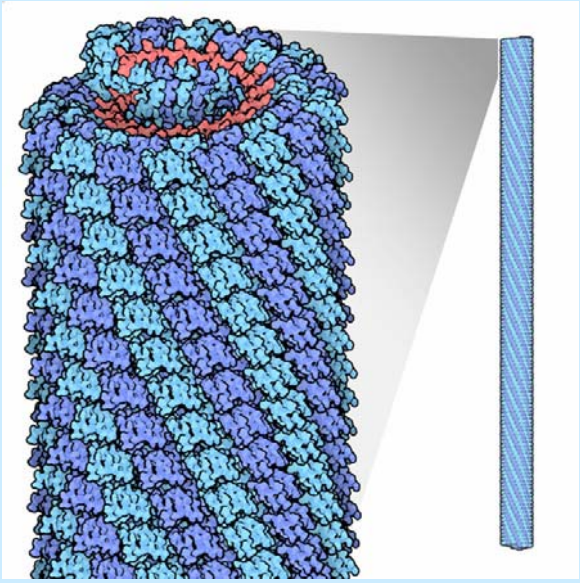

Amine groups in the channel complex with Pd(II) or Pt(II)

The outer surface no amine groups

The selectivity for binding of metal ions to the interior of the TMV

After activation of the channel with Pt(II) or Pt(II), Ni deposited within the TMV channel in an electroless plating bath:
Ni(II) + (CH3)2NHBH3

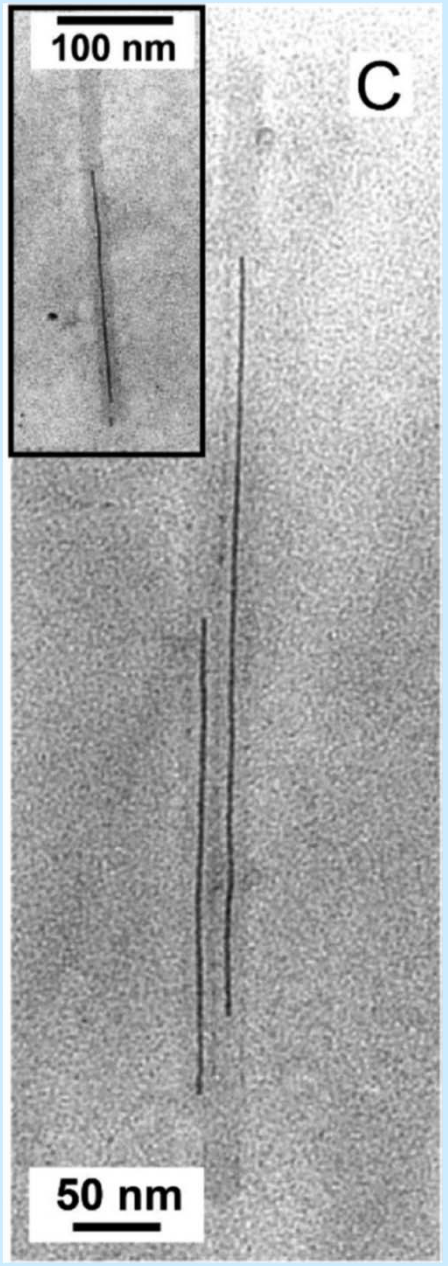

Chemical Vapor Transport

The chemical vapor transport of tungsten in the presence of oxygen onto substrates kept at temperatures higher than the tungsten oxide decomposition temperature (1450 °C)

Substrates were placed close to the filaments (0.5 mm diam) at a distance of 1 mm or less

O_2 flow rate was varied from 0.03 to 0.1 sccm in 90 sccm of either N_2 or Ar

Experiments were performed at different filament temperatures ranging from 1200 to 2000 °C and at a pressure of 150 mTorr

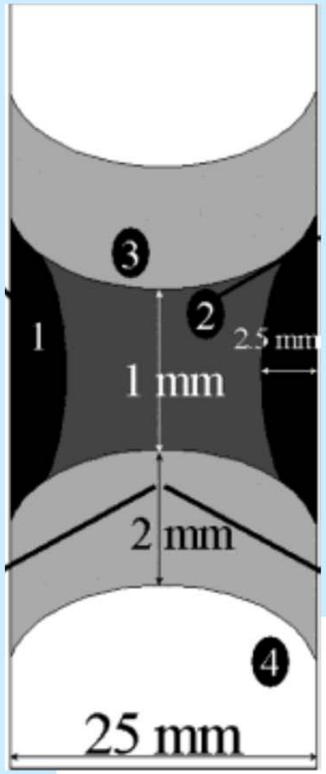

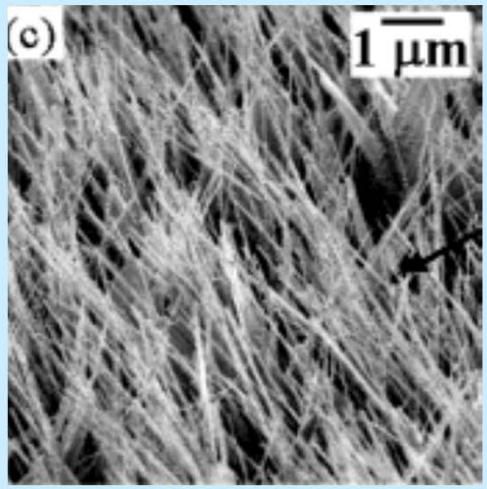

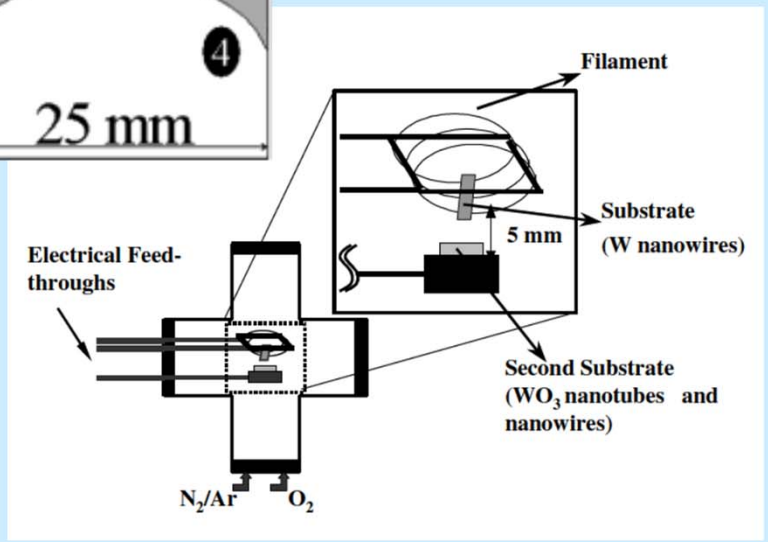

Chemical Vapor Transport

$W + O_2 \rightarrow WO_2\,(g)$

ΔG = -40.08 kJ/mol K (1450 °C)

$WO_2\,(g) \rightarrow W\,(s) + O_2$

ΔG = -267.33 kJ/mol K (1500 °C)

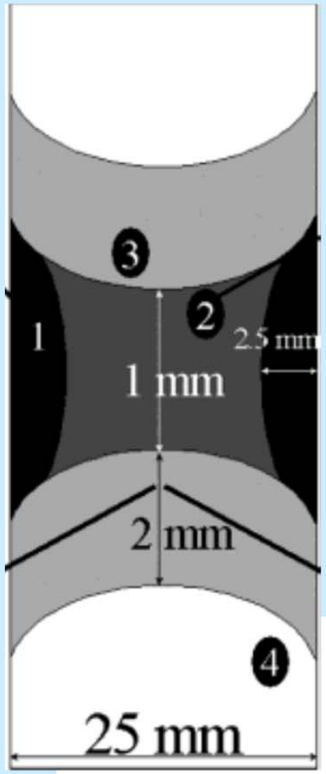

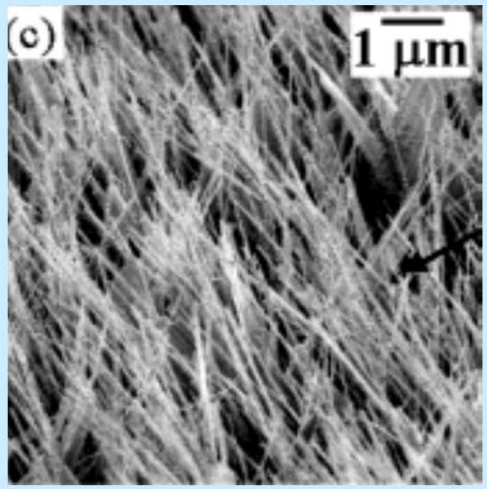

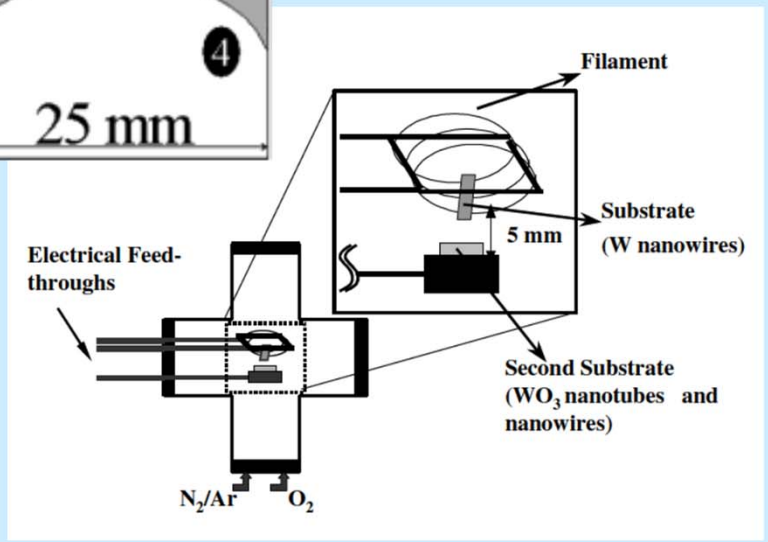

Chemical Vapor Deposition

$WO_3 + H_2O \rightarrow WO_2(OH)_2$

$WO_2(OH)_2 + 3\,H_2 \rightarrow W + 4\,H_2O$

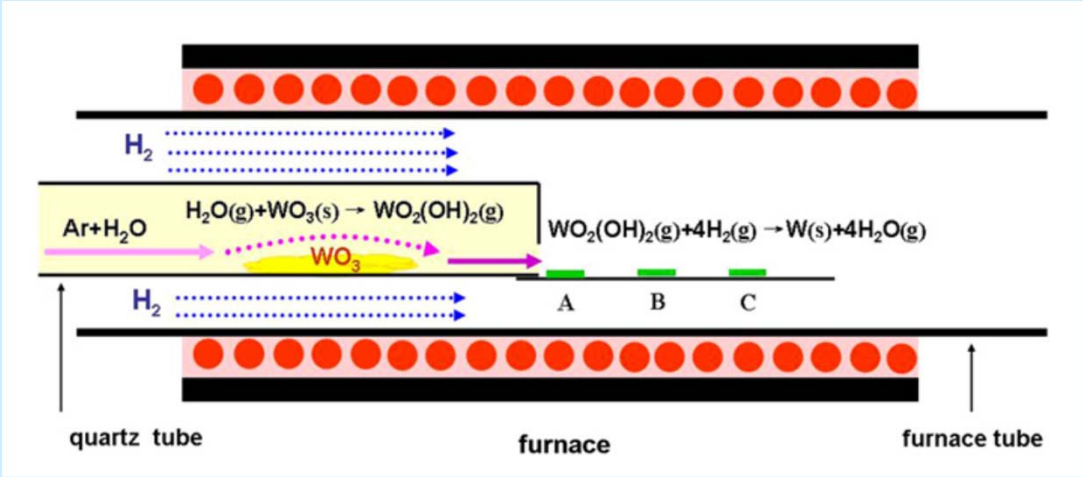

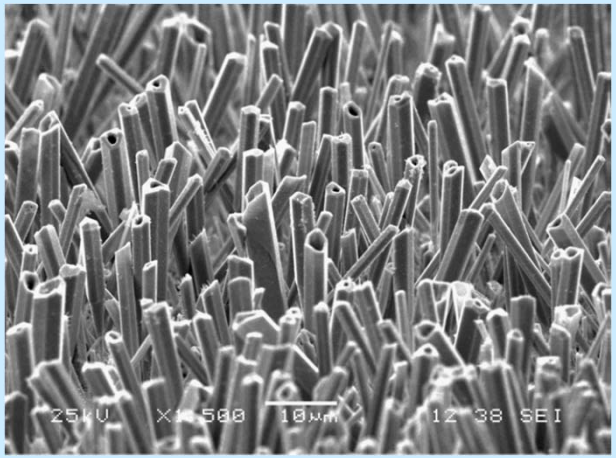

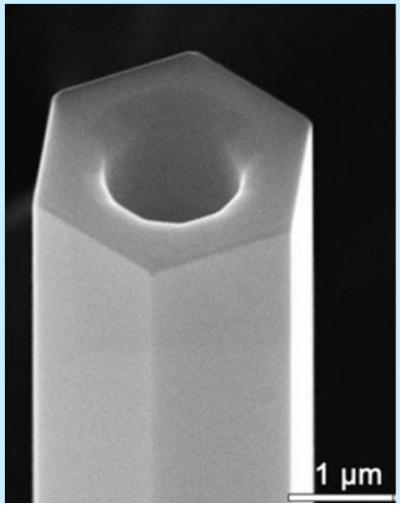

Directional Solidification of a Eutectic Alloy

Arrays of single crystalline wires embedded in a single crystalline matrix

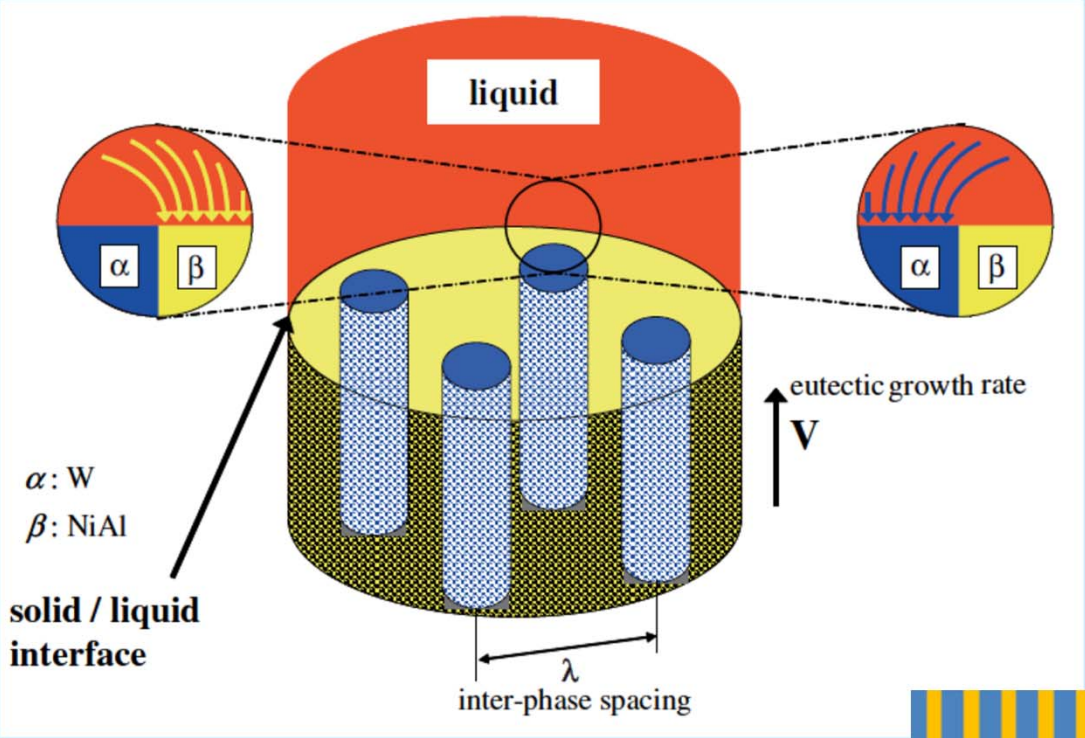

Ni-Al - W 1.5 at.% W
Directional solidification in a Bridgman type crystal growing facility
The crucible support, cooling ring and heating element (tungsten net)
The alumina crucible ~1700 ◦C for initial melting
thermal gradient 40 K cm^{-1}
a growth rate of 30 mm h^{-1}

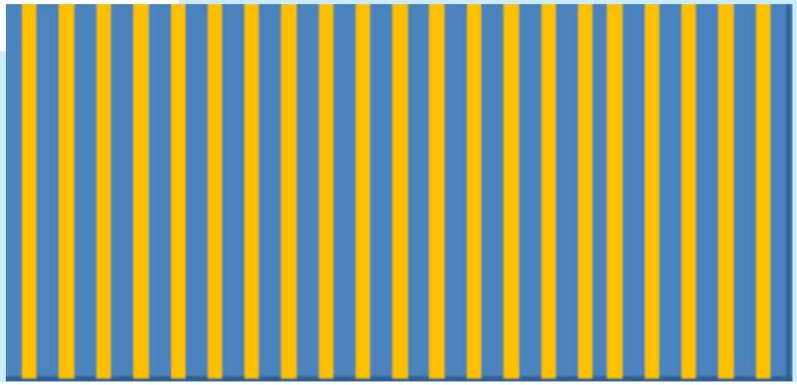

Directional Solidification of a Eutectic Alloy

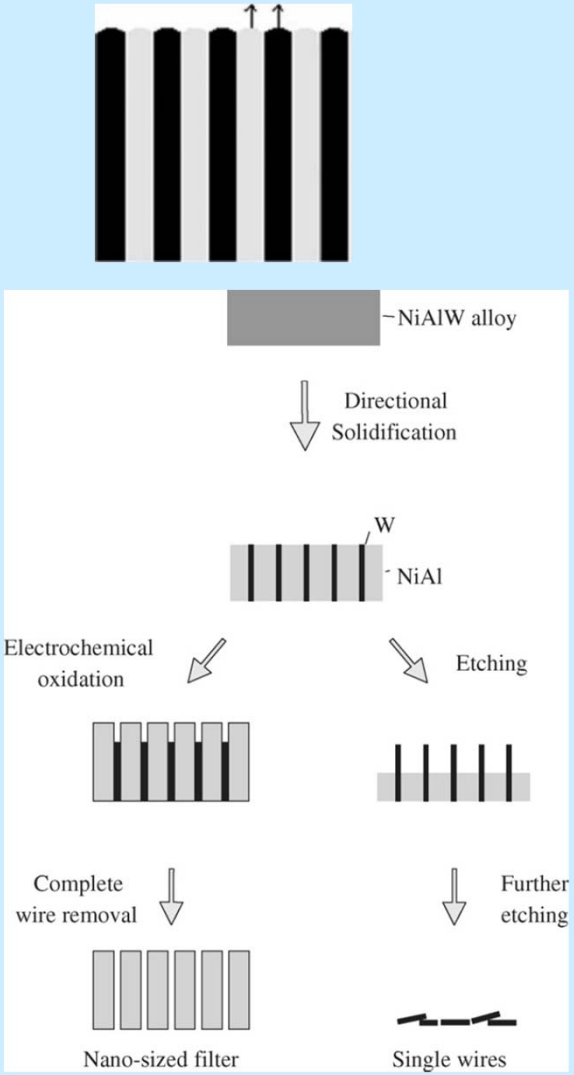

Digestion of the matrix
HCl (32%):H_2O_2 (30%):H_2O, 10:10:80

the potential oscillates between 0.150 and −0.025 V SHE reference electrode

The counter electrode - a strip of Pt foil
pH of 6.0

Directional Solidification of a Eutectic Alloy

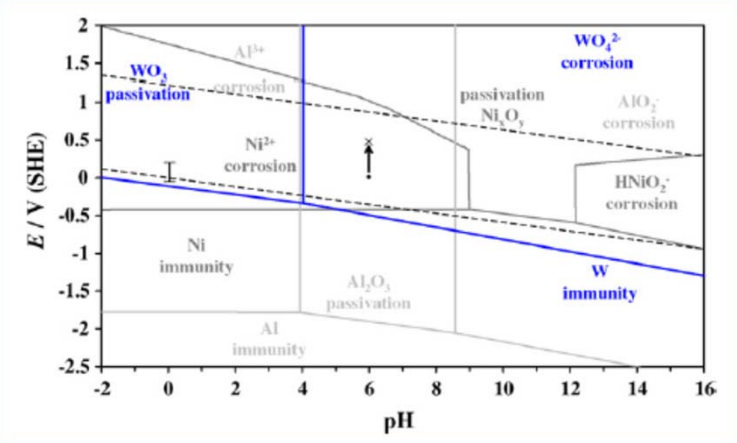

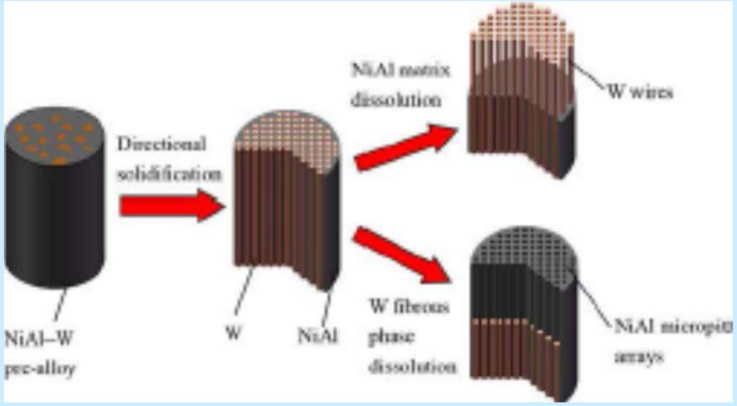

The tungsten wires
A diameter of 200 nm and the mean inter fibre spacing 3 µm

The fibre orientation was 100 referring to the rod axis

High aspect-ratios (>1000!)

Directional Solidification of a Eutectic Alloy

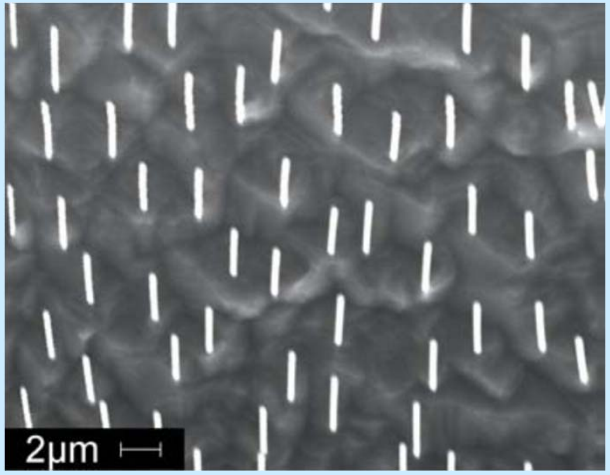

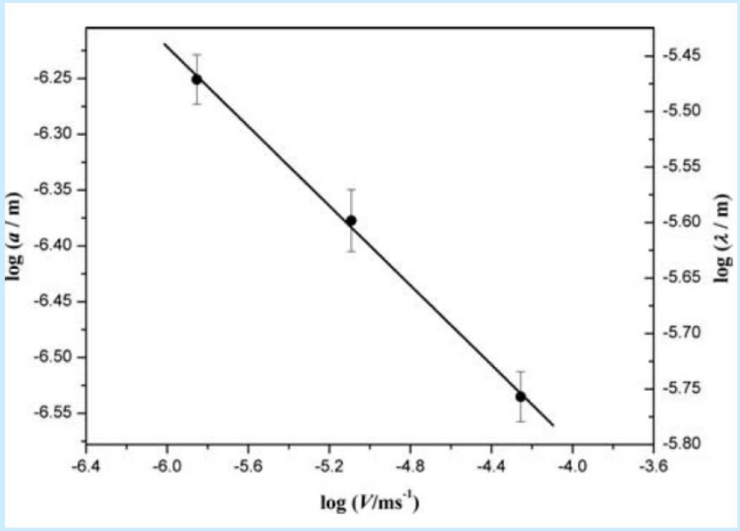

The growth rate V and the nanowire spacing λ

The increase in the growth rate results in the decrease of wire diameter and an increase in wire density $\lambda^2 V$ = const

The growth rate increases, the effect of the lateral diffusion flux along the solid/liquid interface diminishes and the boundary layer thickness increases

These changes in the growth conditions at the solid/liquid interface lead to a decrease in the fibre spacing

Directional Solidification of a Eutectic Alloy

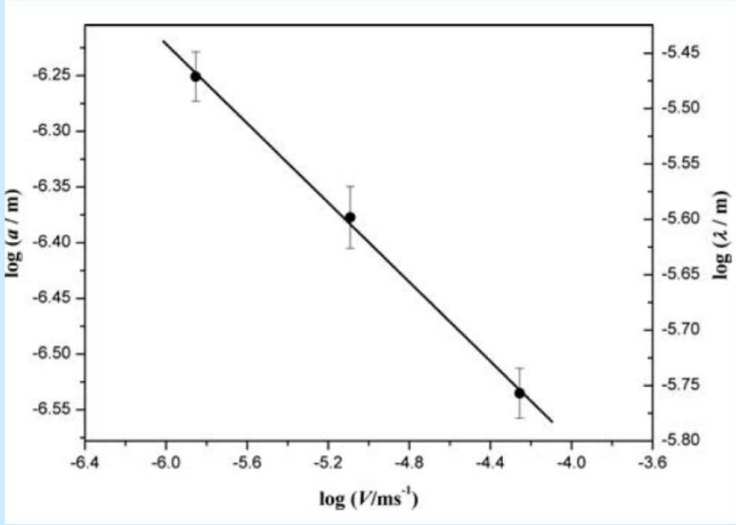

The nanowire diameter, a, is related to the spacing, λ, and the volume fraction of the wires, V_f :

$a^2 = gV_f \lambda^2$

g = the geometrical factor dependent on the fibre arrangement

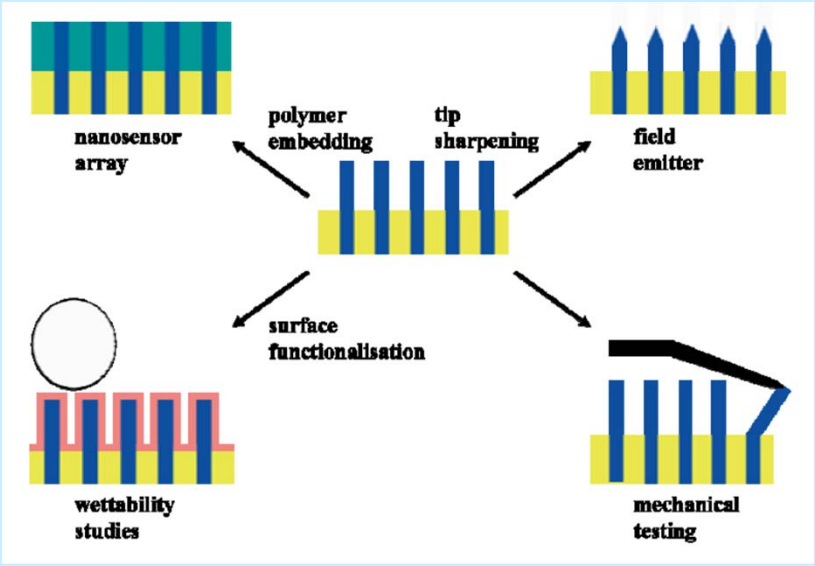

Cold-Field Electron Emission

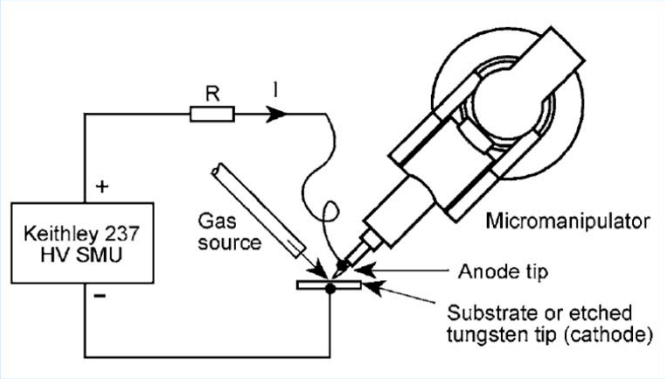

The ions are formed by direct electron impact from the field-emitted electrons

$M(CO)_n + e^- \rightarrow M(CO)_{n-x}^+ + x\ CO + 2e^-$
8.47 eV

$W(CO)_6$, $Fe(CO)_5$, $Co_2(CO)_8$, $Co(CO)_3NO$, benzene, naphthalene, acetylene, Tetramethyl silane

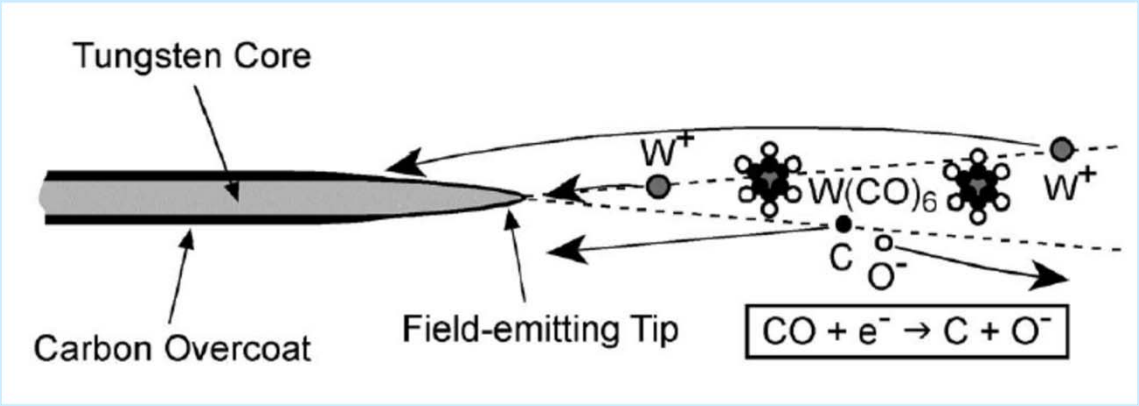

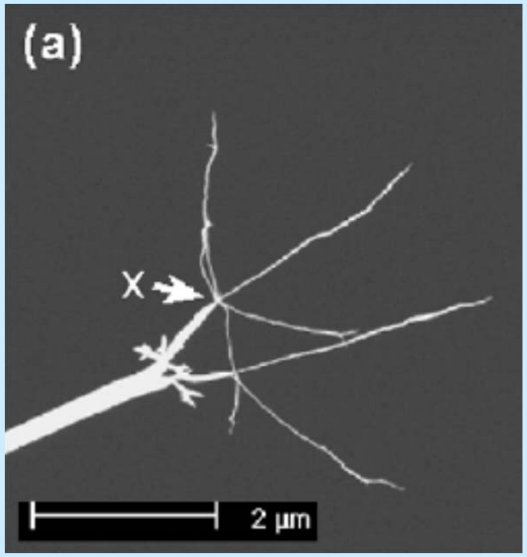

1D Metal Nanostructures

Electronic, plasmonic, magnetic, electrical, mechanical, and thermal properties

Optical transparency
Electrical conductivity
Mechanical flexibility
Magnetic anisotropy (Fe, Co, Ni)

- Touchscreens
- Flexible solar cells
- Optical sensors
- Contrast agents for biomedical imaging
- Therapeutic agents for cancer treatment
- Electrocatalysts
- Electrically and thermally conductive composites
- Wearable electronics

1D Metal Nanostructures

Monometallic
Multimetallic
Heterogeneously structured systems

(A) Alloyed
(B) Segmented
(C) Tadpole-like
(D) Dumbbell-like
(E) Core−shell
(F) Core−satellite
(G) Multiwalled nanotube

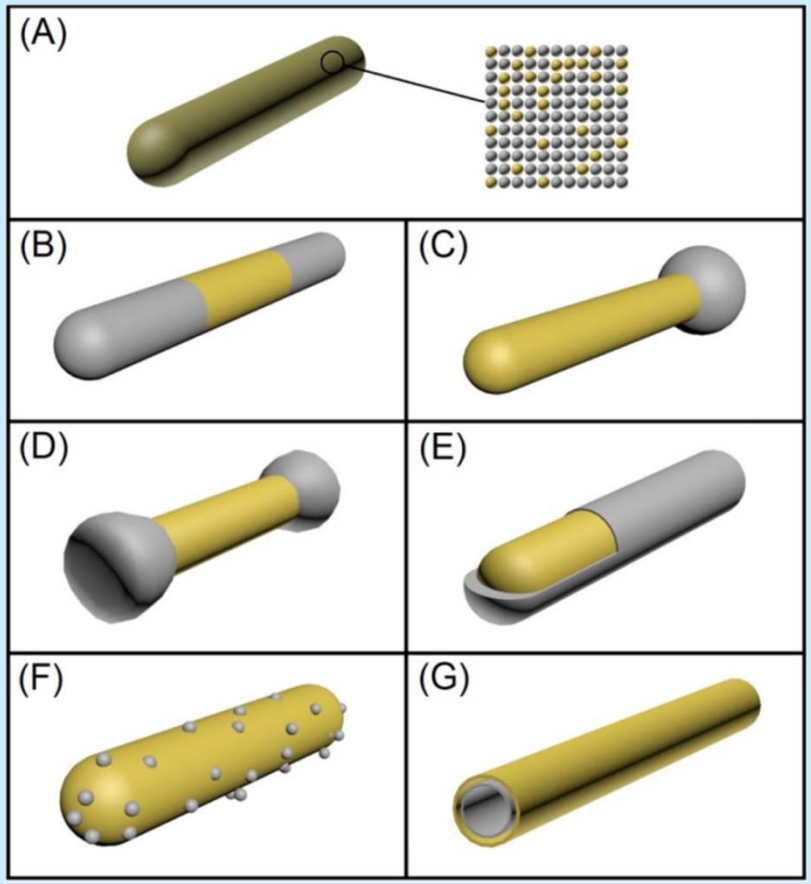

1D Metal Nanostructures

Localized Surface Plasmon Resonance
Anisotropic shape
Two LSPR modes - transverse and longitudinal directions